AD-A160 453 DEVELOPMENT OF A REDUCED MINDLIN HYBRID STRESS THIN MULTILAYER PLATE ELEM..(U) ILLINOIS UNIV AT CHICAGO CIRCLE DEPT OF CIVIL ENGINEERING MEC..

UNCLASSIFIED R L SPILKER ET AL. AUG 85 AMMRC-TR-85-23 F/G 4/2 NL

1/2

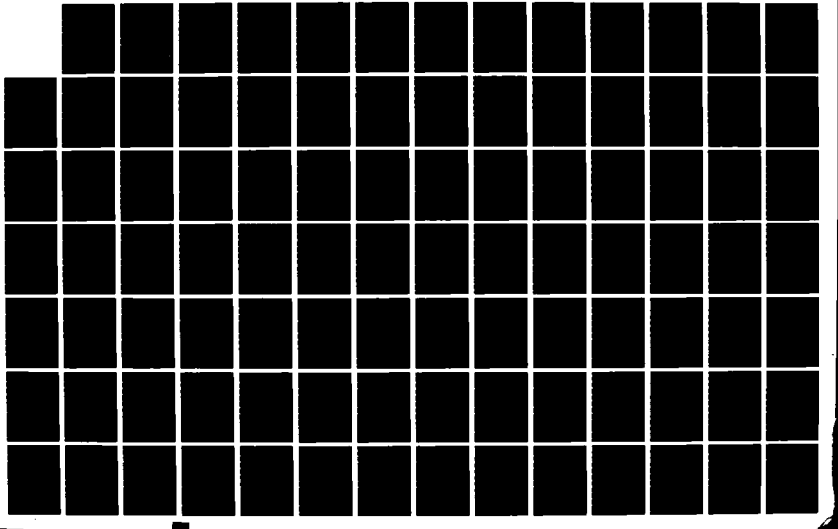

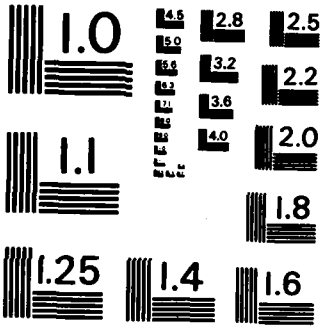

MICROCOPY RESOLUTION TEST CHART
NATIONAL BUREAU OF STANDARDS-1963-A

(2)

AD

AMMRC TR 85-23

DEVELOPMENT OF A REDUCED MINDLIN HYBRID STRESS THIN MULTILAYER PLATE ELEMENT WITH APPLICATION TO EDGE CONTACT PROBLEMS

August 1985

R. L. SPILKER and D. M. JAKOBS
University of Illinois at Chicago
Dept. of Civil Engineering, Mechanics, and Metallurgy
Chicago, Illinois 60680

FINAL REPORT

Contract No. DAAG46-82-K-0004

Prepared for

ARMY MATERIALS AND MECHANICS RESEARCH CENTER
Watertown, Massachusetts 02172-0001

The findings in this report are not to be construed as an official Department of the Army position, unless so designated by other authorized documents.

Mention of any trade names or manufacturers in this report shall not be construed as advertising nor as an official indorsement or approval of such products or companies by the United States Government.

DISPOSITION INSTRUCTIONS

Destroy this report when it is no longer needed.
Do not return it to the originator.

UNCLASSIFIED

SECURITY CLASSIFICATION OF THIS PAGE (When Data Entered)

REPORT DOCUMENTATION PAGE

READ INSTRUCTIONS BEFORE COMPLETING FORM

1. REPORT NUMBER: AMMRC TR 85-23	2. GOVT ACCESSION NO.: AD-A160 463
3. RECIPIENT'S CATALOG NUMBER:	
4. TITLE (and Subtitle): DEVELOPMENT OF A REDUCED MINDLIN HYBRID STRESS THIN MULTILAYER PLATE ELEMENT WITH APPLICATION TO EDGE CONTACT PROBLEMS	5. TYPE OF REPORT & PERIOD COVERED: Final Report 15 Aug 81 - 15 Jun 83
	6. PERFORMING ORG. REPORT NUMBER:
7. AUTHOR(s): R. L. Spilker and D. M Jakobs	8. CONTRACT OR GRANT NUMBER(s): DAAG46-82-K-0004
9. PERFORMING ORGANIZATION NAME AND ADDRESS: University of Illinois at Chicago, Dept. of Civil Engineering, Mechanics, and Metallurgy Chicago, Illinois 60680	10. PROGRAM ELEMENT, PROJECT, TASK AREA & WORK UNIT NUMBERS: D/A Project: 8X363304D215 AMCMS Code: 693000.2156
11. CONTROLLING OFFICE NAME AND ADDRESS: Army Materials and Mechanics Research Center ATTN: AMXMR-K Watertown, Massachusetts 02172-0001	12. REPORT DATE: August 1985
	13. NUMBER OF PAGES: 146
14. MONITORING AGENCY NAME & ADDRESS(if different from Controlling Office):	15. SECURITY CLASS. (of this report): Unclassified
	15a. DECLASSIFICATION/DOWNGRADING SCHEDULE:

16. DISTRIBUTION STATEMENT (of this Report)

Approved for public release; distribution unlimited.

17. DISTRIBUTION STATEMENT (of the abstract entered in Block 20, if different from Report)

18. SUPPLEMENTARY NOTES

19. KEY WORDS (Continue on reverse side if necessary and identify by block number)

Finite element analysis	Plates	Contact problem
Hybrid stress	Composite materials	Stress concentration
Multilayer plate	Elastic shells	

20. ABSTRACT (Continue on reverse side if necessary and identify by block number)

(SEE REVERSE SIDE)

DD FORM 1 JAN 73 1473 EDITION OF 1 NOV 65 IS OBSOLETE

UNCLASSIFIED

SECURITY CLASSIFICATION OF THIS PAGE (When Data Entered)

Block No. 20

ABSTRACT

A hybrid-stress formulation of isoparametric elements for the analysis of thin multilayer laminated composite plates is presented, and is applied to edge contact analyses. The element displacement behavior is characterized by laminate reference surface inplane and transverse displacements and laminate non-normal cross-section rotations; as a result, the number of degrees of freedom is independent of the number of layers. All components of stress are included and are related to a set of laminate stress parameters, the number of which is independent of the number of layers. Attention is restricted here to thin laminates: for thin laminates it is shown that the contributions of transverse shear stress and transverse normal stress to the internal complementary strain energy can be neglected. As a result, a modified stiffness-formation-algorithm can be used which provides a significant improvement in computation efficiency. The formulation is used to develop an 8-node isoparametric thin multilayer plate element. The resulting element is naturally invariant, of correct rank, and non-locking in the thin plate limit. Element performance is documented here for several illustrative examples. Keywords: finite element analysis, composite

The newly developed element is applied to the analysis of laminate edge contact. A hybrid-stress formulation for the incremental/iterative analysis of contact problems as well as the procedure to locate the surface of contact is presented. The assumed contact surface is divided into contact elements having unknown nodal contact tractions. The finite element equations are solved for the element nodal degrees of freedom as well as unknown nodal contact tractions. The assumed contact surface is checked to determine if it satisfies the contact conditions. If not a new contact surface is assumed and the (iterative) process is repeated. Attention is restricted here to symmetric laminates subject to contact in directions normal to the laminate edge, so that only inplane displacement occurs. Several examples involving elastic, non-frictional contracting bodies are presented to verify the formulation/algorithm. An example involving a laminated plate is also presented.

FOREWORD

This work was performed for the Army Materials and Mechanics Research Center, Watertown, Massachusetts, under Contract No. DAAG46-82-K-0004, with the University of Illinois at Chicago, Chicago, Illinois. Mr. J. F. Dignam of AMMRC was project manager and Dr. S. C. Chou as technical monitor. The support and encouragement of Mr. Dignam and Dr. Chou are gratefully acknowledged.

TABLE OF CONTENTS

ABSTRACT

Chapter page

I. INTRODUCTION 1

II. HYBRID STRESS REDUCED-MINDLIN ELEMENTS FOR THIN MULTILAYER PLATES 4

Introduction 4
Stiffness Matrix for a Moderately Thick Multilayer Plate Element 8
Stiffness Matrix for a Thin Multilayer Plate Element 20
Definition of the Reduced Functional 20
Definition of the Element Stiffness 24
Constraints in the Thin Plate Limit 33
Formation and Evaluation of an Invariant 8-node Thin Multilayer Plate Element 35
Element Displacement and Stress Interpolations 35
Element Stiffness Computation Time 41
Example Problems and Numerical Results 43
Cylindrical Bending of a 3-layer 90/0/90 Cross-ply . . 43
Angle ply Laminates under Transverse Loading 49
Concluding Remarks 57

III. FORMULATION OF THE CONTACT PROBLEM 59

Introduction 59
Hybrid Stress Functional for Contact 65
Variational Principle for the Contact Problem 65
Incremental Assumed Hybrid Stress Formulation 73
Matrix Equations 77
The Contact Element for Laminate Edge Contact 86
Solution Technique 91
Introduction 91
Extension of the Contact Surface 94
Release of Contact Nodes 97
Satisfaction of the Relationship between Normal and Tangential Contact Tractions 97
Convergence 100
Example Problems and Numerical Results 101
Contact between an Elastic Disk and an Elastic Half-space 104

Contact between a Nearly Rigid Disk and an Elastic Half-space 111
Contact between a Nearly Rigid Disk and a Symmetric Multilayer Composite Plate 118

IV. CONCLUSIONS AND SUGGESTIONS FOR FURTHER RESEARCH 131

Conclusions 131
Suggestions for Further Research 133

BIBLIOGRAPHY 134

Chapter I

INTRODUCTION

Multilayer fiber reinforced composites are of interest in a number of structural applications where high strength to weight ratios are required. An area of recent and continuing interest is the failure analysis of composite laminates. Composites are strongly anisotropic by nature and contain major microscopic inhomogeneities corresponding to the matrix/fiber nature of the materials. Therefore accurate and detailed stress distributions must be available in order to predict failure of laminated composite structures.

Most engineering devices are made up of assembled parts and many of these are mechanically joined. Even under small deformations nonlinearities often arise in these joints. The nonlinearities arise for instance in contact problems such as bolted connections, shrink fit, or roller bearings. Sometimes gaps separate various structural components presenting nonlinear problems which involve rigid body movement across a gap with subsequent contact of disconnected regions. In many situations structural components in contact slide relative to one another.

The complicating factor in these problems is the unknown surface of contact. In many cases, it is important to know the contact conditions in order to predict accurately the stresses and strength of the joint.

Analytic solutions of contact problems are limited to idealized simple configurations, loadings, and boundary conditions. These solu-

tions may be applied to design problems with varying degrees of success depending upon how closely the geometry and loading model the actual problem. Thus, numerical techniques are needed for solutions of realistic contact problems.

The finite element method will be used to develop an isoparametric multilayer plate element based on a hybrid-stress formulation. The displacement behavior will be characterized by laminate reference plane in-plane and transverse displacements and laminate non-normal cross-section rotations; as a result, the number of degrees of freedom will be independent of the number of layers. All components of stress will be included.

This multilayer plate element will be used to solve edge contact problems. A hybrid-stress formulation for the analysis of contact problems as well as the procedure to locate the surface of contact will be presented. The contact problem may be either frictional or frictionless and may involve extensive sliding between deformable bodies.

Chapter II is devoted to the development of the multilayer plate element. A review of recent work is included in section 2.1. A stiffness matrix is formulated for a moderately thick multilayer plate element in section 2.2. This stiffness is reduced to obtain a stiffness matrix for thin multilayer plate elements in section 2.3. Section 2.4 describes the formation and evaluation of a 8-node thin multilayer plate element.

Chapter III describes the hybrid-stress formulation for the analysis of contact problems as well as the solution technique and applications. A review of recent work is included in section 3.1. The hybrid

stress functional for contact is presented in section 3.2. The matrix equations are given in section 3.3. Section 3.4 describes the contact element and section 3.5 develops the solution technique. Application and evaluation are included in section 3.6.

Chapter IV is a statement of the summary and conclusions of this work. This chapter concludes with some suggestions for further work.

Chapter II

HYBRID STRESS REDUCED-MINDLIN ELEMENTS FOR THIN MULTILAYER PLATES

2.1 INTRODUCTION

Multilayer fiber reinforced composites are of interest in a number of structural applications where high strength to weight ratios are required. A number of multilayer plate elements have appeared in the literature, ranging in applicability from thin (lamination theory) to moderately thick (including transverse shear effects) laminated plates (e.g. [1-11]). These elements are based primarily on assumed-displacement or hybrid- stress formulations, although elements based on other variational principles have been proposed (e.g. [12-13]).

There are advantages to the use of the hybrid-stress model for multilayer plate elements. Hybrid-stress elements can be derived which include individual (independent) layer cross-section rotations (also possible in assumed-displacement elements) and individual(independent) layer stress fields. The layer stress fields can be selected such that interlayer surface traction continuity and laminate upper/lower surface-traction free conditions are exactly satisfied; examples of hybrid-stress elements of this type are found in References [6,10,11]. Elements in this category are applicable to moderately thick and thick laminates (i.e. typical thickness to span ratios as high as h/L=0.25).

Second, by proper choice of the spanwise distributions of the in-plane stresses, it is possible to derive single-layer hybrid-stress plate elements which are based on Mindlin-type through thickness displacements (i.e. independent non-normal cross-section rotations) and include all components of stress, and which are of correct rank and non-locking in the thin-plate limit [14-16]. ("Locking" refers here to excessively stiff solutions obtained with some moderately thick plate elements when applied to thin plate problems.) The characteristic of natural invariance can also be achieved for the 8-node plate element [17]. These attributes carry over to hybrid-stress multilayer plate elements [10,11]; the 8-node element of Reference [11], for example, is accurate for moderately thick to thick laminates, is of correct rank and naturally invariant, and is non-locking when used for thin laminated plates.

In many applications of laminated composites, the plate can be assumed to be thin and thus governed by lamination theory. Application of elements of the type in References [10,11], for example, to thin plates may be considered inefficient. In those elements the number of degrees of freedom and the number of stress parameters will grow in proportion to the number of layers, resulting in increased computation times and storage requirements for element stiffness formation. This generality at the expense of significantly increased computation cost is therefore not warranted. One approach used in References [10,11] was to kinematically constrain the through-thickness displacement field so that element nodal degrees of freedom corresponded to reference plane displacements and laminate cross-section rotations --- independent of the number of

layers. The elements produced accurate predictions for typical thickness ratios h/L =0.1 and lower. Those "restricted" elements [10,11] continued to be based on independent layer stress fields and thus computation time and storage requirements for the formation of an element stiffness continued to grow with the number of layers. Furthermore, the use of independent layer stress fields with a laminate displacement field seems inconsistent.

The formulation presented here rectifies this inconsistency by producing hybrid-stress multilayer plate elements for which the number of nodal degrees of freedom and the number of stress parameters is independent of the number of layers. In these elements, degrees of freedom at a node correspond to laminate reference surface inplane and transverse displacements and laminate cross-section rotations (i.e. a total of 5 dof per node independent of the number of layers). In order to produce stress fields in each layer related to a fixed set of laminate stress parameters, laminate inplane strains are first interpolated in terms of stress parameters. Layer inplane stress fields are related to these parameters via constitutive equations. Layer transverse shear and transverse normal stresses are obtained from the inplane stesses via integration of the homogeneous equilibrium equations; the constants of integration are selected to satisfy lower surface traction-free conditions and interlayer surface traction continuity.

This aproach was, in effect, used for the development of a 4-node hybrid-stress multilayer element in Reference [9]. Results in that study suggest that moderately-thick (i.e. $h/L \leq 0.1$) laminates can be accurately analyzed.

The multilayer element behavior, particularly in the thin plate limit, will depend on the form of the spanwise distribution of the stresses, just as in the single layer hybrid-stress Mindlin type elements. Thus, early phases of the present work aimed at the development of an 8-node multilayer element (with laminate degrees of freedom and stress parameters) having a spanwise stress distribution analogous to the single layer element QH3 of Reference [17]. The resulting multilayer element was of correct rank, non-locking, and naturally invariant. However computation times became excessive (as will be described later) when using the approach of Reference [9] for large numbers of layers; this motivated the search for an alternate approach for defining a hybrid-stress multilayer plate element.

In a recent study [18], Spilker has shown that the single-layer hybrid-stress elements of References [14-17] can be reduced to thin plate elements by neglecting the contributions of the transverse shear and transverse normal stresses to the internal complementary energy. Significant computational savings were found while maintaining the ease of formulating plate elements based on independent transverse displacement and cross-section rotations.

The present study extends the concepts of Reference [18] to multilayer plates. Described herein is a hybrid-stress formulation for thin multilayer laminated plates with nodal degrees of freedom corresponding to laminate reference surface inplane and transverse displacements and laminate cross-section rotations. All components of stress are included and are related to a set of laminate stress parameters, with contributions of transverse shear and normal stresses to the internal complemen-

tary energy neglected. Computation time for the resulting element stiffness matrix is shown to be essentially independent of the number of layers.

To illustrate the formulation, an 8-node multilayer plate element is presented which is analogous to the single layer element QH3T [18]. The 8-node element is naturally invariant, of correct rank, and non-locking. Results for several example problems show that the element converges to the thin plate (lamination theory) solution.

2.2 STIFFNESS MATRIX FOR A MODERATELY THICK MULTILAYER PLATE ELEMENT

The multilayer plate is assumed to lie in the x-y plane, with $z = 0$ corresponding to the laminate reference surface, located arbitrarily (e.g. geometric midsurface). The laminate consists of I perfectly-bonded layers numbered bottom to top, with $z = h_1, h_2 \ldots h_{I+1}$ locating the lower, interlayer, and upper surfaces, respectively (see Figure 1a). Displacement behavior is characterized by laminate reference surface displacements u_0, v_0, and w_0, in the x,y, and z directions, respectively, and laminate, cross-section rotations, θ_x and θ_y (which are assumed to be independent of w), about the x and y axes, respectively (see Figure 1b). Note that inplane displacements are included due to inherent material induced bending/stretching coupling in multilayer laminated plates.

The hybrid-stress functional for multilayer plates, assuming perfectly bonded layers and traction continuity on interlayer surfaces, is given by [10].

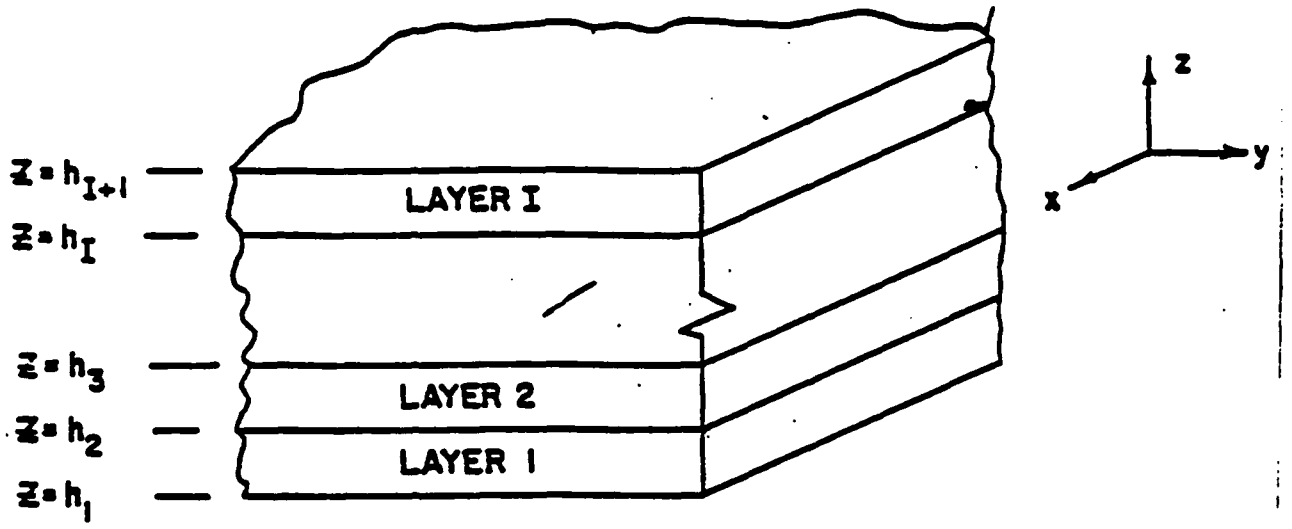

(a) layer numbering, interface coordinates

(b) through-thickness displacements

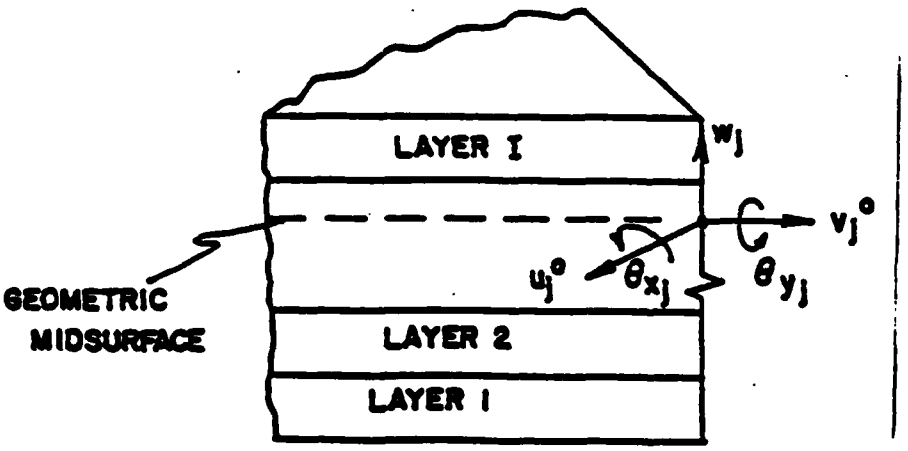

Figure 1 Nodal degrees of freedom for the through-thickness displacement field.

$$\pi_{mc} = \sum \sum \left\{ \frac{1}{2} \int_{V_{ni}} \underset{\sim}{\sigma}^{iT} \underset{\sim}{S}^{i} \underset{\sim}{\sigma}^{i} \, dV - \int \sigma^{iT} \hat{\varepsilon} \, dV \right\} \tag{2.1}$$

$$+ \int_{A_n} wp \, dA$$

where $\underset{\sim}{\sigma}^T = [\sigma_x \ \sigma_y \ \sigma_z \ \sigma_{xz} \ \sigma_{xz} \ \sigma_{yz}]$ are components of stress, $\hat{\underset{\sim}{\varepsilon}}^T = [\epsilon_x \ \epsilon_y \ \epsilon_z \ \epsilon_{xy} \ \epsilon_{xz} \ \epsilon_{yz}]$ are components of "strain" as computed from displacements via the linear strain- displacement relations. Subscripts/superscripts i and n refer to layer i and element n, so that V_{ni} is the volume of layer i for element n. The $\underset{\sim}{S}^i$ matrix relates stresses and strains in the xyz coordinate system and is given in detail in Reference [10]. The last term in equation (2.1) is a load term corresponding to transverse distributed load, p(x,y), acting over the spanwise area, A_n, of element n.

The purpose of the present section is to define the form of the displacement and stress interpolations for a thin-to-moderately-thick multilayer plate element for which the number of nodal degrees of freedom and the number of stress parameters is independent of the number of layers. Intermediate element matrices and the element stiffness matrix will also be defined. However, the present formulation serves as the basis for the development of efficient thin multilayer plate elements via a reduction scheme analogous to Reference [18]. The reduction scheme and corresponding elements are discussed in subsequent subsections.

The displacements u, v, and w at any x,y,z location of the laminate are given by

$$\begin{aligned} u(x,y,z) &= u_o(x,y) + z\,\theta_y(x,y) \\ v(x,y,z) &= v_o(x,y) - z\,\theta_x(x,y) \\ w(x,y,z) &= -w_o(x,y) \end{aligned} \tag{2.2}$$

Using the linear strain-displacement relations, the inplane strains, $\hat{\underset{\sim}{\varepsilon}}_p^{\,i}$, for layer i are given by

$$\hat{\underset{\sim}{\varepsilon}}_p^{\,i} = \begin{Bmatrix} \hat{\varepsilon}_x^{\,i} \\ \hat{\varepsilon}_y^{\,i} \\ \hat{\gamma}_{xy}^{\,i} \end{Bmatrix} = \begin{Bmatrix} \partial u_o/\partial x \\ \partial v_o/\partial y \\ \partial u_o/\partial y + \partial v_o/\partial x \end{Bmatrix} + z \begin{Bmatrix} \partial \theta_y/\partial x \\ -\partial \theta_x/\partial y \\ \partial \theta_y/\partial x - \partial \theta_x/\partial y \end{Bmatrix} \tag{2.3}$$

The transverse shear strains, $\hat{\underset{\sim}{\varepsilon}}_t^{\,i}$, are given by

$$\hat{\underset{\sim}{\varepsilon}}_t^{\,i} = \begin{Bmatrix} \hat{\gamma}_{xz}^{\,i} \\ \hat{\gamma}_{yz}^{\,i} \end{Bmatrix} = \begin{Bmatrix} \partial w/\partial x + \theta_y \\ \partial w/\partial y - \theta_x \end{Bmatrix} \tag{2.4}$$

and the transverse normal strain, $\hat{\underset{\sim}{\varepsilon}}_z^{\,i}$, is zero. It is understood that strains in layer i for equations (2.3) and (2.4) are obtained by evaluating z between h_i and h_{i+1}.

Denote the nodal degrees of freedom corresponding to u_o by $\underset{\sim}{u}$, those corresponding to v_o by $\underset{\sim}{v}_o$, those corresponding to w_o by $\underset{\sim}{w}_o$, etc. The spanwise distributions of u_o, v_o, w_o, θ_x, and θ_y can be interpolated in terms of nodal degrees of freedom by using any of the families of 2-D C^o continuity shape functions. As the present multilayer elements will be of isoparametric planform, the x,y coordinates are related to coordinates ξ,η by the relation

$$x = \sum_j N_j(\xi,\eta)\, x_j$$
$$y = \sum_j N_j(\xi,\eta)\, y_j \qquad (2.5)$$

where the sum extends over element nodes, $(x_j,\ y_j)$ are the coordinates of element node j, and the $N_j(\xi,\eta)$ correspond to the appropriate Serendipity shape functions.

We assume here that the shape functions used for the displacements and rotations are the same and are indentical to those used in the geometric mapping of equation (2.5). Then

$$\begin{Bmatrix} u_o \\ v_o \\ w_o \\ \theta_x \\ \theta_y \end{Bmatrix} = \sum_j N_j(\xi,\eta) \begin{Bmatrix} u_o \\ v_o \\ w_o \\ \theta_x \\ \theta_y \end{Bmatrix}_j \qquad (2.6)$$

represent the displacement/rotation interpolations, with u_{o_j}, v_{o_j}, etc. corresponding to degrees of freedom at node j. For convenience, we define the interpolation vector $\underset{\sim}{N}$ and element nodal degrees of freedom, $\underset{\sim}{q}$, as

$$\underset{\sim}{N} = \begin{bmatrix} N_1 & N_2 & N_3 & \cdots \end{bmatrix}$$

$$\underset{\sim}{q}^T = \begin{bmatrix} \underset{\sim}{u}_o^T & \underset{\sim}{v}_o^T & \underset{\sim}{w}_o^T & \underset{\sim}{\theta}_x^T & \underset{\sim}{\theta}_y^T \end{bmatrix} \tag{2.7}$$

Substituting equation (2.6) into equations (2.3) and (2.4) produces

$$\underset{\sim}{\hat{\varepsilon}}^i = \begin{Bmatrix} \hat{\varepsilon}_x \\ \hat{\varepsilon}_y \\ \hat{\varepsilon}_z \\ \hat{\gamma}_{xy} \\ \hat{\gamma}_{xz} \\ \hat{\gamma}_{yz} \end{Bmatrix} = \begin{bmatrix} \partial\underset{\sim}{N}/\partial x & 0 & 0 & 0 & z\,\partial\underset{\sim}{N}/\partial x \\ 0 & \partial\underset{\sim}{N}/\partial y & 0 & -z\,\partial\underset{\sim}{N}/\partial y & 0 \\ 0 & 0 & 0 & 0 & 0 \\ \partial\underset{\sim}{N}/\partial y & 0 & 0 & -z\,\partial\underset{\sim}{N}/\partial x & z\,\partial\underset{\sim}{N}/\partial y \\ 0 & \partial\underset{\sim}{N}/\partial x & \partial\underset{\sim}{N}/\partial x & 0 & \underset{\sim}{N} \\ 0 & \partial\underset{\sim}{N}/\partial y & \partial\underset{\sim}{N}/\partial y & -\underset{\sim}{N} & 0 \end{bmatrix} \underset{\sim}{q} \tag{2.8}$$

or

$$\underset{\sim}{\hat{\varepsilon}}^i = \underset{\sim}{B}^i \underset{\sim}{q} \tag{2.9}$$

Note that $\underset{\sim}{N} = \underset{\sim}{N}(\xi,\eta)$ and thus derivatives in equation (2.8) will incorporate the mapping of equation (2.5) as in all isoparametric elements.

The stresses $\underset{\sim}{\sigma}^i$ in each layer are to be expressed in terms of a set of laminate stress parameters, $\underset{\sim}{\beta}$, the total number of which is independent of the number of layers (i.e. consistent with a multilayer element having laminate degrees of freedom independent of the number of layers). This can be accomplished by using a scheme similar to that used by Spilker et al [9] for a 4-node hybrid-stress multilayer element.

The laminate inplane strains are assumed to vary linearly through the laminate thickness and are expressed in terms of laminate "stress parameters", $\underset{\sim}{\beta}$, in the form

$$\begin{Bmatrix} \varepsilon_x \\ \varepsilon_y \\ \gamma_{xy} \end{Bmatrix} = \underset{\sim}{\tilde{P}}\underset{\sim}{\beta} = \left[\underset{\sim}{\tilde{P}}_s \;\vdots\; z\,\underset{\sim}{\tilde{P}}_b \right] \begin{Bmatrix} \underset{\sim}{\beta}_s \\ \underset{\sim}{\beta}_b \end{Bmatrix} \tag{2.10}$$

In equation (2.10), the subscripts s and b refer to stretching and bending contributions, respectively. The interpolation matrices $\underset{\sim}{\tilde{P}}_s$ and $\underset{\sim}{\tilde{P}}_b$ are functions (usually polynomials) of x and y. The assumption of linear z variation of inplane strains is consistent with the displacement distribution of equations (2.2). However, note that the strains in equations (2.10) are not directly related to the displacement derivatives (i.e. not related to $\underset{\sim}{\hat{\varepsilon}}_p{}^i$ in equation (2.3)).

The inplane stresses in layer i can be related to $\underset{\sim}{\beta}$ via substituting equation (2.10) into the inplane stress-strain (plane stress) relation; i.e.

$$\begin{Bmatrix} \sigma_x \\ \sigma_y \\ \sigma_{xy} \end{Bmatrix}^i = \underset{\sim}{Q}^i \begin{Bmatrix} \varepsilon_x \\ \varepsilon_y \\ \gamma_{xy} \end{Bmatrix} - \underset{\sim}{Q}^i \underset{\sim}{\bar{P}} \underset{\sim}{\beta} \tag{2.11}$$

The matrix $\underset{\sim}{Q}^i$ is the inverse of the inplane portion of $\underset{\sim}{S}^i$ as will be discussed in more detail later. Note that the inplane stresses in equation (2.11) vary linearly in z. The transverse shear stresses and transverse normal stress in layer i can be related to $\underset{\sim}{\beta}$ by integrating the homogeneous equilibrium equations; i.e.

$$\sigma_{xz}^i = -\int_z \left(\frac{\partial \sigma_x^i}{\partial x}\right) + \left(\frac{\partial \sigma_{xy}^i}{\partial y}\right) dz \tag{2.12a}$$

$$\sigma_{yz}^i = -\int_z \left(\frac{\partial \sigma_{xy}^i}{\partial x}\right) + \left(\frac{\partial \sigma_y^i}{\partial y}\right) dz \tag{2.12b}$$

$$\sigma_z^i = -\int_z \left(\frac{\partial \sigma_{xz}^i}{\partial x} + \left(\frac{\partial \sigma_{yz}^i}{\partial y}\right)\right) dz \tag{2.12c}$$

In general, stresses from equation (2.11) are substituted into equations (2.12). The constants of integration for each layer in equations (2.12) are used to satisfy traction-free conditions on the lower surface (con-

stants for layer 1), and continuity of σ_{xz}, σ_{yz}, and σ_z at interlayer surfaces (i.e. at $z = h_i$ using the constants of layer i for i = 2,3...I). Details of these calculations are involved and will be presented later in conjunction with an 8-node element.

Using equations (2.11) and (2.12), and the general procedure just outlined, it will be possible to relate the stresses in layer i to β in the form

$$\underset{\sim}{\sigma}^i = \underset{\sim}{P}^i \underset{\sim}{\beta} \tag{2.13}$$

Note that the stresses satisfy equilibrium as required in a hybrid-stress element.

Equations (2.9), (2.13), and the interpolation for w_0 are substituted into the hybrid-stress functional of equation (2.1), and the following <u>laminate</u> matrices are defined

$$\underset{\sim}{H} = \sum_i H_i \tag{2.14a}$$

$$\underset{\sim}{G} = \sum_i \underset{\sim}{G}_i \tag{2.14b}$$

where, invoking the mapping of equation (2.5) to the ξ,η system

$$\underset{\sim}{H}_i = \int_{-1}^{1}\int_{-1}^{1} \underset{\sim}{P}^{iT}\,\underset{\sim}{S}^{i}\,\underset{\sim}{P}^{i}\,|J|\,d\xi\,d\eta \tag{2.15a}$$

$$\underset{\sim}{G}_i = \int_{-1}^{1}\int_{-1}^{1} \underset{\sim}{P}^{iT}\,\underset{\sim}{B}^{i}\,|J|\,d\xi\,d\eta \tag{2.15b}$$

$$\underset{\sim}{F} = \int_{-1}^{1}\int_{-1}^{1} \underset{\sim}{N}^{T}\,p\,|J|\,d\xi\,d\eta \tag{2.15c}$$

In equations (2.15), it is assumed that the layer stress interpolation matrix, $\underset{\sim}{P}^{i}$, and the prescribed distributed load, p, are expressed as functions of ξ and η using equations (2.5). Also, $|J|$ is the Jacobian of the coordinate transformation. Equation (2.1) then becomes

$$\pi_{mc} = \sum_{n} \left\{ \frac{1}{2}\,\underset{\sim}{\beta}^{T}\,\underset{\sim}{H}\,\underset{\sim}{\beta} - \underset{\sim}{\beta}^{T}\,\underset{\sim}{G}\,\underset{\sim}{q} + \underset{\sim}{q}^{T}\,\underset{\sim}{F} \right\} \tag{2.16}$$

where $\underset{\sim}{F}$ is the element nodal force vector. Equation (2.16) is in the standard form for hybrid-stress elements.

We also consider the possiblity that additional interrelations among the $\underset{\sim}{\beta}$ may exist which can be expressed in the general form

$$\underset{\sim}{R}\underset{\sim}{\beta} = 0 \tag{2.17}$$

Inter-relations of this form were first used for hybrid-stress elements by Mau and Pian [6] to enforce interlayer traction continuities in multilayer elements. They have been used more recently as an alternate scheme to enforce equilibrium in hybrid-stress elements [19-21], and to reduce stress fields in single layer hybrid-stress Mindlin-type plate elements [18]. They could also be used to enforce, for example, partial equilibrium. In the present multilayer elements, the inter-relations among β, expressed by equation (2.17), will be used to reduce the stress field to a desirable form and to satisfy the zero transverse shear stress conditions at the upper laminate surface.

Following Reference [6], equation (2.17) is introduced into equation (2.16) via the Lagrange Multiplier method. From the stationary condition of the functional it can be shown that the stress parameters are related to nodal degrees of freedom by

$$\underset{\sim}{\beta} = \underset{\sim}{\hat{H}}^{-1}\underset{\sim}{G}\underset{\sim}{q} \tag{2.18}$$

and the element stiffness matrix is given by

$$\underset{\sim}{k} = \underset{\sim}{G}^{T}\underset{\sim}{\hat{H}}^{-1}\underset{\sim}{G} \tag{2.19}$$

where $\underset{\sim}{\hat{H}}^{-1}$ is the augmented matrix

$$\hat{\underset{\sim}{H}}^{-1} = \underset{\sim}{H}^{-1} - \underset{\sim}{H}^{-1}\underset{\sim}{R}^{T}\left(\underset{\sim}{R}\,\underset{\sim}{H}^{-1}\underset{\sim}{R}^{T}\right)^{-1}\underset{\sim}{R}\,\underset{\sim}{H}^{-1} \tag{2.20}$$

The formulation just presented produces a multilayer plate element having nodal degrees of freedom and stress parameters which are, in number, independent of the number of layers. Per the studies of References [9, 10], a multilayer element of this type should provide reasonable predictions for thin to moderately thick laminates; i.e. for typical thickness to span ratios of h/L = 0.1 and lower.

In early phases of the present effort, 8-node elements of this type were formulated. Despite the fixed number of stress parameters and nodal degrees of freedom, it was found that computation times to form k grew excessively with increasing numbers of layers. This was found to be due, to a large extent, to the complexity of $\sigma_{xz}{}^{i}$, $\sigma_{yz}{}^{i}$, and $\sigma_{z}{}^{i}$ from equations (2.12) and their contributions to $\underset{\sim}{H}$ and $\underset{\sim}{G}$ (equations (2.15)). As a result, it was decided to restrict attention to thin multilyer laminates (i.e. h/L ≤ .05), for which most applications were intended, and to pursue a reduced formulation similar to that recently used for single layer plates by Spilker [18] which allowed for significant savings in computation times for $\underset{\sim}{k}$. The reduction scheme and corresponding element matrices are described in the next subsection.

2.3 STIFFNESS MATRIX FOR A THIN MULTILAYER PLATE ELEMENT

In a recent study [18], Spilker has shown that a hybrid-stress formulation for single layer Mindlin-type isoparametric plate bending elements can be reduced to provide computationally efficient isoparametric thin plate elements. The elements utilize independent interpolations for transverse displacement and cross-section rotations, and include all components of stress. It was shown that the contributions of transverse shear stress and transverse normal stress to the internal complementary energy (i.e. the $\underset{\sim}{H}$ matrix) could be neglected for thin plates. The resulting elements were found to converge to classical thin plate theory solutions. This reduction also allowed use of an alternate algorithm for stiffness matrix calculation which produced significant savings in computation time. This reduction is developed for thin multilayer plates in this section, and an efficient implementation for stiffness matrix calculation is given.

2.3.1 Definition of the Reduced Functional

In order to define a reduced hybrid-stress functional for thin multilayer plates, it is necessary to consider the functional of equation (2.1) along with the assumptions/ interpolations of the previous section. Of particular interest are the through-thickness distributions of stresses $\underset{\sim}{\sigma}^i$ and strains from displacements, $\hat{\underset{\sim}{\varepsilon}}^i$, and contributions to each term in equation (2.1) which might be neglected for thin plates. A functional will then be defined which is valid for thin multilayer plates and a computationally efficient implementation of this functional will be presented.

Recall that inplane strains $\hat{\underset{\sim}{\epsilon}}_p^i$ of equation (2.3) are of order z, that the transverse shear strains $\hat{\underset{\sim}{\epsilon}}_t^i$ of equation (2.4) are constant in z, and that the transverse normal strain $\hat{\epsilon}_z^i = 0$ for all layers. Per equations (2.10) and (2.11), the inplane stresses σ_p^i (i.e. $\underset{\sim}{\sigma}_p^{iT}=[\sigma_x^i \ \sigma_y^i \ \sigma_{xy}^i]$) are of order z. Then via equations (2.12), the transverse shear stresses (i.e. $\underset{\sim}{\sigma}_t^{iT} = [\sigma_{xz}^i \ \sigma_{yz}^i]$) will be of order z^2, and the transverse normal stress, σ_z^i, will be of order z^3.

Now consider each term in equation (2.1) as plate thickness is made small. The final term corresponds to nodal loads due to distributed applied loads and is not affected by plate thickness. Consider the second term in equation (2.1). Contributions of the product $\underset{\sim}{\sigma}_p^{iT}\hat{\underset{\sim}{\epsilon}}_p^i$, integrated through the thickness will be of order h^3 (for present purposes, h may be considered as a normalized thickness; i.e. plate thickness divided by a typical spanwise dimension). Likewise the contributions to the second term in equation (2.1) of the product $\underset{\sim}{\sigma}_t^{iT}\hat{\underset{\sim}{\epsilon}}_t^i$ (transverse shear stresses/strains) will be of order h^3. The product $\underset{\sim}{\sigma}_z^{iT}\hat{\underset{\sim}{\epsilon}}_z^i$ does not contribute since $\hat{\epsilon}_z^i=0$.
In view of the above contributions, no reduction of the second integral in equation (2.1) is possible when h is small.

Reductions of the first integral of equation (2.1) are possible for small h. For a layer having a general fiber orientation, the material property matrix will have the following form:

$$\begin{Bmatrix} \varepsilon_x \\ \varepsilon_y \\ \varepsilon_z \\ \gamma_{xz} \\ \gamma_{yz} \\ \gamma_{xy} \end{Bmatrix}^i = \begin{bmatrix} S_{11} & S_{12} & S_{13} & 0 & 0 & S_{16} \\ S_{12} & S_{22} & S_{23} & 0 & 0 & S_{26} \\ S_{13} & S_{23} & S_{33} & 0 & 0 & S_{36} \\ 0 & 0 & 0 & S_{44} & S_{45} & 0 \\ 0 & 0 & 0 & S_{45} & S_{55} & 0 \\ S_{16} & S_{26} & S_{36} & 0 & 0 & S_{66} \end{bmatrix}^i \begin{Bmatrix} \sigma_x \\ \sigma_y \\ \sigma_z \\ \sigma_{xz} \\ \sigma_{yz} \\ \sigma_{xy} \end{Bmatrix} \tag{2.21}$$

Expressions for the $S_{kl}{}^i$ are given, for example, in Reference [10].

To examine the effects of h, it is convenient to expand the first term in equation (2.1) as follows:

$$\frac{1}{2}\int_{V_{n^i}} \underset{\sim}{\sigma}^{iT} \underset{\sim}{S}^i \underset{\sim}{\sigma}^i \, dV = \frac{1}{2}\int_{V_{n^i}} \Big[\underset{\sim}{\sigma}_p{}^{iT} \underset{\sim}{S}_p{}^i \underset{\sim}{\sigma}_p{}^i + \underset{\sim}{\sigma}_p{}^{iT} \begin{Bmatrix} S_{13} \\ S_{23} \\ S_{36} \end{Bmatrix}^i \sigma_z{}^i$$

$$+ \sigma_z{}^i \lfloor S_{13} \quad S_{23} \quad S_{36} \rfloor^i \underset{\sim}{\sigma}_p{}^i + S_{33} \left(\sigma_z{}^i\right)^2 \tag{2.22}$$

$$+ \underset{\sim}{\sigma}_t{}^{iT} \underset{\sim}{S}_t{}^i \underset{\sim}{\sigma}_t{}^i \Big] \, dV$$

where

$$\underset{\sim}{S}_p^i = \begin{bmatrix} S_{11} & S_{12} & S_{16} \\ S_{12} & S_{22} & S_{26} \\ S_{16} & S_{26} & S_{66} \end{bmatrix}^i \tag{2.23a}$$

$$\underset{\sim}{S}_t^i = \begin{bmatrix} S_{44} & S_{45} \\ S_{45} & S_{55} \end{bmatrix}^i \tag{2.23b}$$

Referring to the orders of h in equation (2.22), the first term is of order h^3, the second and third terms are of order h^5, the fourth term is of order h^7, and the fifth term is of order h^5. In addition, each of the second through fifth terms is related to the same set (or a subset) of β as the first term. Thus, for small h the second through fifth terms in equation (2.22) can be neglected compared with the first term.

It should be noted that it is possible to further divide the preceeding discussion into contributions due to stretching and those due to bending. Although the contributions of stretching and bending differ by a factor h^2, the relative contributions from each of the terms in equation (2.22) is as described above and the conclusions drawn above are valid.

With the reductions described above, the hybrid functional of equation (2.1) can be rewritten for thin multilayer plates in the following form:

$$\Pi_{mc} = \sum_n \sum_i \left\{ \frac{1}{2} \int_{V_n^i} \underset{\sim}{\sigma}_p^{iT} \underset{\sim}{S}_p^i \underset{\sim}{\sigma}_p^i \, dV - \int_{V_n^i} \lfloor \underset{\sim}{\sigma}_p^{iT} \; \underset{\sim}{\sigma}_t^{iT} \rfloor \begin{Bmatrix} \underset{\sim}{\varepsilon}_p^i \\ \underset{\sim}{\varepsilon}_t^i \end{Bmatrix} dV + \int_{A_n} w\, p \, dA \right. \qquad (2.24)$$

In summary, the functional of equation (2.24) for thin multilayer laminates differs from the general laminated plate functional in equation (2.1) in that contributions of transverse shear stresses and transverse normal stress to the internal complementary energy have been neglected. This is analogous to the reduction performed for single layer plate elements in Reference [18]. Of significance in practice is the fact that it is exactly those eliminated terms which contributed significantly to stiffness computation time in the non-reduced element. As a result of this reduction, a modified, more efficient algorithm for stiffness calculation can be used. This algorithm is described next.

2.3.2 Definition of the Element Stiffness

An efficient algorithm can be defined for stiffness formation for a thin multilayer plate element based on the reduced functional in equation (2.24). We begin by assuming that the same order polynomial is used to interpolate each component of inplane strain, both stretching and bending contributions (see equation (2.10)); i.e.

$$\begin{aligned} \underset{\sim}{\varepsilon_x} &= \underset{\sim}{a}\,\underset{\sim}{\beta_1} + z\,\underset{\sim}{a}\,\underset{\sim}{\beta_2} \\ \underset{\sim}{\varepsilon_y} &= \underset{\sim}{a}\,\underset{\sim}{\beta_3} + z\,\underset{\sim}{a}\,\underset{\sim}{\beta_4} \\ \underset{\sim}{\varepsilon_{xy}} &= \underset{\sim}{a}\,\underset{\sim}{\beta_5} + z\,\underset{\sim}{a}\,\underset{\sim}{\beta_6} \end{aligned} \tag{2.25}$$

where $\underset{\sim}{a}$ is a vector of polynomials, e.g.

$$\underset{\sim}{a} = \begin{bmatrix} 1 & x & y & x^2 & xy & y^2 & \cdots \end{bmatrix} \tag{2.26}$$

Using the notation of equation (2.10)

$$\underset{\sim}{P} = \begin{bmatrix} \underset{\sim}{a} & \underset{\sim}{3a} & \underset{\sim}{0} & \underset{\sim}{0} & \underset{\sim}{0} & \underset{\sim}{0} \\ \underset{\sim}{0} & \underset{\sim}{0} & \underset{\sim}{a} & \underset{\sim}{3a} & \underset{\sim}{0} & \underset{\sim}{0} \\ \underset{\sim}{0} & \underset{\sim}{0} & \underset{\sim}{0} & \underset{\sim}{0} & \underset{\sim}{a} & \underset{\sim}{3a} \end{bmatrix} \tag{2.27a}$$

and

$$\underset{\sim}{\beta}^T = \begin{bmatrix} \underset{\sim}{\beta_1}^T & \underset{\sim}{\beta_2}^T & \underset{\sim}{\beta_3}^T & \underset{\sim}{\beta_4}^T & \underset{\sim}{\beta_5}^T & \underset{\sim}{\beta_6}^T \end{bmatrix} \tag{2.27b}$$

The inplane stresses in layer i, $\underset{\sim}{\sigma}_p{}^i$, can be related to $\underset{\sim}{\beta}$ through equation (2.11). Note that modifications to the strain distribution in equations (2.25) can be achieved by introducing the necessary interrelations in the form of equation (2.17).

The transverse shear stresses do not contribute to the first integral in equation (2.24) (which will lead to the H matrix), but do contribute to the second integral in equation (2.24) (which will lead to the $\underset{\sim}{G}$ matrix). To define $\underset{\sim}{\sigma}_t{}^i$ for layer i, equations (2.25) are substituted into equation (2.11), and the result substituted into equations (2.12a) and (2.12b). The constants of integration for layer 1 are used to enforce the zero traction condition at the lower surface; the constants of integration for layer i are used to satisfy the traction con-

tinuity at $z = h_i$ between layers i and i-1 (i>1). After some manipulation, it can be shown that σ_{xz}^i and σ_{yz}^i are given by

$$\sigma_{xz}^i = T_{1113}^i \underset{\sim}{\beta}_1 + T_{1223}^i \underset{\sim}{\beta}_3 + T_{1333}^i \underset{\sim}{\beta}_5 + F_{1113}^i \underset{\sim}{\beta}_2 + F_{1223}^i \underset{\sim}{\beta}_4 + F_{1333}^i \underset{\sim}{\beta}_6 \tag{2.28a}$$

$$\sigma_{yz}^i = T_{2312}^i \underset{\sim}{\beta}_1 + T_{2322}^i \underset{\sim}{\beta}_3 + T_{2323}^i \underset{\sim}{\beta}_5 + F_{2312}^i \underset{\sim}{\beta}_2 + F_{2322}^i \underset{\sim}{\beta}_4 + F_{2323}^i \underset{\sim}{\beta}_6 \tag{2.28b}$$

where the coefficient vectors are functions of x,y, and z, and are given by

$$\begin{aligned} T_{jklm}^i = {} & [(h_i - z) Q_{jk}^i + (h_{i-1} - h_i) Q_{jk}^{i-1} + (h_{i-2} - h_{i-1}) Q_{jk}^{i-2} \\ & + \ldots + (h_1 - h_2) Q_{jk}^1] \partial g / \partial x \\ & + [(h_i - z) Q_{lm}^i + (h_{i-1} - h_i) Q_{lm}^{i-1} + (h_{i-2} - h_{i-1}) Q_{lm}^{i-2} \\ & + \ldots + (h_1 - h_2) Q_{lm}^1] \partial g / \partial y \end{aligned} \tag{2.29}$$

$$\begin{aligned} F_{jklm}^i = {} & \tfrac{1}{2}[(h_i^2 - z^2) Q_{jk}^i + (h_{i-1}^2 - h_i^2) Q_{jk}^{i-1} + (h_{i-2}^2 - h_{i-1}^2) Q_{jk}^{i-2} \\ & + \ldots + (h_1^2 - h_2^2) Q_{jk}^1] \partial g / \partial x \\ & + \tfrac{1}{2}[(h_i^2 - z^2) Q_{lm}^i + (h_{i-1}^2 - h_i^2) Q_{lm}^{i-1} + (h_{i-2}^2 - h_{i-1}^2) Q_{lm}^{i-2} \\ & + \ldots + (h_1^2 - h_2^2) Q_{lm}^1] \partial g / \partial y \end{aligned}$$

Inplane stresses $\underset{\sim}{\sigma}_p^i$ and transverse shear stresses $\underset{\sim}{\sigma}_t^i$ are substituted into the functional of equation (2.24). Also, $\hat{\underset{\sim}{\varepsilon}}_p^i$ and

$\hat{\underset{\sim}{\xi}}_t^i$ can be related to nodal degrees of freedom, $\underset{\sim}{q}$, as described earlier, and substituted into equation (2.24). With these substitutions, Π_{mc} of equation (2.24) can be put in the form

$$\Pi_{mc} = \sum_{\eta} \left\{ \frac{1}{2} \underset{\sim}{\beta}^T \underset{\sim}{H} \underset{\sim}{\beta} - \underset{\sim}{\beta}^T \underset{\sim}{G} \underset{\sim}{q} + \underset{\sim}{q}^T \underset{\sim}{F} \right\} \tag{2.30}$$

as in equation (2.16).

For the present thin multialyer plate element, however, the matrices $\underset{\sim}{H}$ and $\underset{\sim}{G}$ can be defined in a more convenient fashion. To facilitate these definitions, we assume $\underset{\sim}{\beta}$ are ordered as in equation (2.27b) and $\underset{\sim}{q}$ are ordered as in equation (2.7). We then define the following integrated vector products (note that the integrals are performed in ξ, η and $dA = |J| d\xi d\eta$):

$$\underset{\sim}{\Phi} = \int_{A_n} \underset{\sim}{a}^T \underset{\sim}{a} \, dA \tag{2.31}$$

and

$$\underset{\sim}{\alpha}_1 = \int_{A_n} \underset{\sim}{a}^T \underset{\sim}{N} \, dA \qquad \underset{\sim}{\alpha}_2 = \int_{A_n} \underset{\sim}{a}^T \frac{\partial \underset{\sim}{N}}{\partial x} \, dA \qquad \underset{\sim}{\alpha}_3 = \int_{A_n} \underset{\sim}{a}^T \frac{\partial \underset{\sim}{N}}{\partial y} \, dA$$

$$\underset{\sim}{\alpha}_4 = \int_{A_n} \frac{\partial \underset{\sim}{a}^T}{\partial x} N \, dA \qquad \underset{\sim}{\alpha}_5 = \int_{A_n} \frac{\partial \underset{\sim}{a}^T}{\partial x} \frac{\partial \underset{\sim}{N}}{\partial x} \, dA \qquad \underset{\sim}{\alpha}_6 = \int_{A_n} \frac{\partial \underset{\sim}{a}^T}{\partial x} \frac{\partial \underset{\sim}{N}}{\partial y} \, dA \tag{2.32}$$

$$\underset{\sim}{\alpha}_7 = \int_{A_n} \frac{\partial \underset{\sim}{a}^T}{\partial y} N \, dA \qquad \underset{\sim}{\alpha}_8 = \int_{A_n} \frac{\partial \underset{\sim}{a}^T}{\partial y} \frac{\partial \underset{\sim}{N}}{\partial x} \, dA \qquad \underset{\sim}{\alpha}_9 = \int_{A_n} \frac{\partial \underset{\sim}{a}^T}{\partial y} \frac{\partial \underset{\sim}{N}}{\partial y} \, dA$$

In addition, we define the following "material parameters" which come about in the through-thickness integrations, summed over all layers:

$$A_{kl} = \sum_{i=1}^{I} (h_{i+1} - h_i) Q^i_{kl} \tag{2.33a}$$

$$B_{kl} = \sum_{i=1}^{I} \tfrac{1}{2}(h_{i+1}^2 - h_i^2) Q^i_{kl} \tag{2.33b}$$

$$D_{kl} = \sum_{i=1}^{I} \tfrac{1}{3} (h_{i+1}^3 - h_i^3) Q^i_{kl} \tag{2.33c}$$

$$\hat{B}_{kl} = \sum_{i=1}^{I} (h_{i+1} - h_i) \left[\tfrac{1}{2} (h_{i+1} + h_i) - h_{I+1}\right] Q^i_{kl} \tag{2.33d}$$

$$\hat{D}_{kl} = \sum_{i=1}^{I} \tfrac{1}{2}(h_{i+1} - h_i) \left[\tfrac{2}{3} (h_{i+1}^2 + h_{i+1} h_i + h_i^2) - (h_{i+1} + h_i) h_{I+1}\right] Q^i_{kl} \tag{2.33e}$$

With these definitions, $\underset{\sim}{H}$ is given by

$$\underset{\sim}{H} = \begin{bmatrix} E_{11}\underset{\sim}{\phi} & & & & & \\ E_{12}\underset{\sim}{\phi} & E_{22}\underset{\sim}{\phi} & & & \text{symmetric} & \\ E_{13}\underset{\sim}{\phi} & E_{23}\underset{\sim}{\phi} & E_{33}\underset{\sim}{\phi} & & & \\ E_{14}\underset{\sim}{\phi} & E_{24}\underset{\sim}{\phi} & E_{34}\underset{\sim}{\phi} & E_{44}\underset{\sim}{\phi} & & \\ E_{15}\underset{\sim}{\phi} & E_{25}\underset{\sim}{\phi} & E_{35}\underset{\sim}{\phi} & E_{45}\underset{\sim}{\phi} & E_{55}\underset{\sim}{\phi} & \\ E_{16}\underset{\sim}{\phi} & E_{26}\underset{\sim}{\phi} & E_{36}\underset{\sim}{\phi} & E_{46}\underset{\sim}{\phi} & E_{66}\underset{\sim}{\phi} & E_{66}\underset{\sim}{\phi} \end{bmatrix} \tag{2.34}$$

where E_{ij} are terms in the symmetric, positive definite matrix E given by

$$\underset{\sim}{E} = \begin{bmatrix} A_{11} & & & & & \\ B_{11} & D_{11} & & & \text{symmetric} & \\ A_{12} & B_{12} & A_{22} & & & \\ B_{12} & D_{12} & B_{22} & D_{22} & & \\ A_{13} & B_{13} & A_{23} & B_{23} & A_{33} & \\ B_{13} & D_{13} & B_{23} & D_{23} & B_{33} & D_{33} \end{bmatrix} \tag{2.35}$$

The inverse of $\underset{\sim}{H}$ (needed for $\underset{\sim}{k}$) is then given by [23]:

$$\underset{\sim}{H}^{-1} = \begin{bmatrix} E_{11}^{-1}\underset{\sim}{\Phi}^{-1} & & & \text{symmetric} & & \\ E_{12}^{-1}\underset{\sim}{\Phi}^{-1} & E_{22}^{-1}\underset{\sim}{\Phi}^{-1} & & & & \\ E_{13}^{-1}\underset{\sim}{\Phi}^{-1} & E_{23}^{-1}\underset{\sim}{\Phi}^{-1} & E_{33}^{-1}\underset{\sim}{\Phi}^{-1} & & & \\ E_{14}^{-1}\underset{\sim}{\Phi}^{-1} & E_{24}^{-1}\underset{\sim}{\Phi}^{-1} & E_{34}^{-1}\underset{\sim}{\Phi}^{-1} & E_{44}^{-1}\underset{\sim}{\Phi}^{-1} & & \\ E_{15}^{-1}\underset{\sim}{\Phi}^{-1} & E_{25}^{-1}\underset{\sim}{\Phi}^{-1} & E_{35}^{-1}\underset{\sim}{\Phi}^{-1} & E_{45}^{-1}\underset{\sim}{\Phi}^{-1} & E_{55}^{-1}\underset{\sim}{\Phi}^{-1} & \\ E_{16}^{-1}\underset{\sim}{\Phi}^{-1} & E_{26}^{-1}\underset{\sim}{\Phi}^{-1} & E_{36}^{-1}\underset{\sim}{\Phi}^{-1} & E_{46}^{-1}\underset{\sim}{\Phi}^{-1} & E_{56}^{-1}\underset{\sim}{\Phi}^{-1} & E_{66}^{-1}\underset{\sim}{\Phi}^{-1} \end{bmatrix} \tag{2.36}$$

where E_{ij}^{-1} are terms in the matrix $\underset{\sim}{E}^{-1}$.

The matrix G can be defined as

$$\underset{\sim}{G} = \begin{bmatrix} (A_{11}\underset{\sim}{\alpha}_2 + A_{13}\underset{\sim}{\alpha}_3) & (A_{12}\underset{\sim}{\alpha}_3 + A_{13}\underset{\sim}{\alpha}_2) \\ (B_{11}\underset{\sim}{\alpha}_2 + B_{13}\underset{\sim}{\alpha}_3) & (B_{12}\underset{\sim}{\alpha}_3 + B_{13}\underset{\sim}{\alpha}_2) \\ (A_{12}\underset{\sim}{\alpha}_2 + A_{23}\underset{\sim}{\alpha}_3) & (A_{22}\underset{\sim}{\alpha}_3 + A_{23}\underset{\sim}{\alpha}_2) \\ (B_{12}\underset{\sim}{\alpha}_2 + B_{23}\underset{\sim}{\alpha}_3) & (B_{22}\underset{\sim}{\alpha}_3 + B_{23}\underset{\sim}{\alpha}_2) \\ (A_{13}\underset{\sim}{\alpha}_2 + A_{33}\underset{\sim}{\alpha}_3) & (A_{23}\underset{\sim}{\alpha}_3 + A_{33}\underset{\sim}{\alpha}_2) \\ (B_{13}\underset{\sim}{\alpha}_2 + B_{33}\underset{\sim}{\alpha}_3) & (B_{23}\underset{\sim}{\alpha}_3 + B_{33}\underset{\sim}{\alpha}_2) \end{bmatrix}$$

$$\begin{array}{l} (\hat{B}_{11}\underset{\sim}{\alpha}_5 + \hat{B}_{13}\underset{\sim}{\alpha}_8 + \hat{B}_{12}\underset{\sim}{\alpha}_9 + \hat{B}_{13}\underset{\sim}{\alpha}_6) \\ (\hat{D}_{11}\underset{\sim}{\alpha}_5 + \hat{D}_{13}\underset{\sim}{\alpha}_8 + \hat{D}_{12}\underset{\sim}{\alpha}_9 + \hat{D}_{13}\underset{\sim}{\alpha}_6) \\ (\hat{B}_{12}\underset{\sim}{\alpha}_5 + \hat{B}_{23}\underset{\sim}{\alpha}_8 + \hat{B}_{22}\underset{\sim}{\alpha}_9 + \hat{B}_{23}\underset{\sim}{\alpha}_6) \\ (\hat{D}_{12}\underset{\sim}{\alpha}_5 + \hat{D}_{23}\underset{\sim}{\alpha}_8 + \hat{D}_{22}\underset{\sim}{\alpha}_9 + \hat{D}_{23}\underset{\sim}{\alpha}_6) \\ (\hat{B}_{13}\underset{\sim}{\alpha}_5 + \hat{B}_{33}\underset{\sim}{\alpha}_8 + \hat{B}_{23}\underset{\sim}{\alpha}_9 + \hat{B}_{33}\underset{\sim}{\alpha}_6) \\ (\hat{D}_{13}\underset{\sim}{\alpha}_5 + \hat{D}_{33}\underset{\sim}{\alpha}_8 + \hat{D}_{23}\underset{\sim}{\alpha}_9 + \hat{D}_{33}\underset{\sim}{\alpha}_6) \end{array} \tag{2.37}$$

$$\begin{array}{l} -(B_{12}\underset{\sim}{\alpha}_3 + B_{13}\underset{\sim}{\alpha}_2 + \hat{B}_{12}\underset{\sim}{\alpha}_7 + \hat{B}_{13}\underset{\sim}{\alpha}_4) \\ -(D_{12}\underset{\sim}{\alpha}_3 + D_{13}\underset{\sim}{\alpha}_2 + \hat{D}_{12}\underset{\sim}{\alpha}_7 + \hat{D}_{13}\underset{\sim}{\alpha}_4) \end{array}$$

$$
\begin{aligned}
&-(B_{22}\underset{\sim}{\alpha}_3 + B_{23}\underset{\sim}{\alpha}_2 + \hat{B}_{22}\underset{\sim}{\alpha}_7 + \hat{B}_{23}\underset{\sim}{\alpha}_4)\\
&-(D_{22}\underset{\sim}{\alpha}_3 + D_{23}\underset{\sim}{\alpha}_2 + \hat{D}_{22}\underset{\sim}{\alpha}_7 + \hat{D}_{23}\underset{\sim}{\alpha}_4)\\
&-(B_{23}\underset{\sim}{\alpha}_3 + B_{33}\underset{\sim}{\alpha}_2 + \hat{B}_{23}\underset{\sim}{\alpha}_7 + \hat{B}_{33}\underset{\sim}{\alpha}_4)\\
&-(D_{23}\underset{\sim}{\alpha}_3 + D_{33}\underset{\sim}{\alpha}_2 + \hat{D}_{23}\underset{\sim}{\alpha}_7 + \hat{D}_{33}\underset{\sim}{\alpha}_4)
\end{aligned}
$$

$$
\left.
\begin{aligned}
&(B_{11}\underset{\sim}{\alpha}_2 + B_{13}\underset{\sim}{\alpha}_3 + \hat{B}_{11}\underset{\sim}{\alpha}_4 + \hat{B}_{12}\underset{\sim}{\alpha}_7)\\
&(D_{11}\underset{\sim}{\alpha}_2 + D_{13}\underset{\sim}{\alpha}_3 + \hat{D}_{11}\underset{\sim}{\alpha}_4 + \hat{D}_{12}\underset{\sim}{\alpha}_7)\\
&(B_{12}\underset{\sim}{\alpha}_2 + B_{23}\underset{\sim}{\alpha}_3 + \hat{B}_{12}\underset{\sim}{\alpha}_4 + \hat{B}_{23}\underset{\sim}{\alpha}_7)\\
&(D_{12}\underset{\sim}{\alpha}_2 + D_{23}\underset{\sim}{\alpha}_3 + \hat{D}_{12}\underset{\sim}{\alpha}_4 + \hat{D}_{23}\underset{\sim}{\alpha}_7)\\
&(B_{13}\underset{\sim}{\alpha}_2 + B_{33}\underset{\sim}{\alpha}_3 + \hat{B}_{13}\underset{\sim}{\alpha}_4 + \hat{B}_{33}\underset{\sim}{\alpha}_7)\\
&(D_{13}\underset{\sim}{\alpha}_2 + D_{33}\underset{\sim}{\alpha}_3 + \hat{D}_{13}\underset{\sim}{\alpha}_4 + \hat{D}_{33}\underset{\sim}{\alpha}_7)
\end{aligned}
\right]
$$

Note that the ordering of $\underset{\sim}{q}$ (equation (2.7)) used to define $\underset{\sim}{G}$ is convenient but not conventional. In practice, $\underset{\sim}{q}$ will be ordered

$$
\underset{\sim}{q}^T = [u_{o1}\ v_{o1}\ w_{o1}\ \theta_{x1}\ \theta_{y1}\ u_{o2}\ v_{o2}\ w_{o2}\ \theta_{x2}\ \ldots] \tag{2.38}
$$

and terms in $\underset{\sim}{G}$ from equation (2.37) will be assigned to the proper column location corresponding to equation (2.38).

In most applications of the present thin multilayer plate formulation, additional interrelations among the $\underset{\sim}{\beta}$ in the form of equation (2.17) will be needed. For example, the stress field resulting from the strain field of equations (2.25) will contain complete polynomials in order to preserve natural invariance [24]. The resulting thin plate

constraints (to be discussed in the next section) may be excessive, and thus a reduction of the stress field (which preserves invariance) may be necessary. Such a reduction could be put in the form of equation (2.17). As a second example, it is noted that the stress field used for the present thin multilayer plate elements satisfies equilibrium, satisfies lower laminate surface traction-free conditions, and satisfies traction continuity on interlayer surfaces. Recall that the preceeding traction conditions were satisfied using the constants of integration in equations (2.12a) and (2.12b). If the inplane tractions on the upper laminate surface (i.e. σ_{xz} and σ_{yz}) are to be set to zero, this upper surface condition must be enforced by introducing interrelations among the $\underset{\sim}{\beta}$ in the form of equation (2.17). These two kinds of stress field reductions will be illustrated later in the development of an 8-node element.

With $\underset{\sim}{H}$, $\underset{\sim}{G}$, and $\underset{\sim}{R}$ defined as just described, the element stiffness can be defined by equation (2.19). The major computational advantages brought about by the reduced formulation are summarized in the following:

(a) Perhaps the most significant computational saving results because the only layer dependent operations in the formation of $\underset{\sim}{k}$ are the definitions of the constants in equations (2.33). These operations are so insignificant that there is no real increase in computation time from 1 to 100 layers. In effect, computation time is independent of the number of layers.

(b) The area integrals in equations (2.31) and (2.32) can be efficiently evaluated numerically. Only the lower triangle of $\underset{\sim}{\phi}$ (equations (2.31)) need be evaluated. Also, if desired, the integrals could be evaluated analytically since no $|J|$ will occcur in the denominator.

(c) The calculation of $\underset{\sim}{H}^{-1}$ would normally involve a system of the order of the number of β. Instead, the definition of $\underset{\sim}{H}^{-1}$ by equation (2.36) requires inversion of a symmetric 6x6 matrix ($\underset{\sim}{E}$) and inversion of a symmetric matrix ($\underset{\sim}{\phi}$) which involves approximately one-sixth the number of β s.

(d) The "cost" of items (b) and (c) is the more complicated stiffness expression in equations (2.19) and (2.20). Since the constraints in equation (2.17) do not involve equilibrium, they are generally few in number compared with the number of β's. Thus $\underset{\sim}{R}$ contains many zeroes, and operations involving $\underset{\sim}{R}$ can be streamlined to avoid most multiplications by zero.

Illustrative comparisons of stiffness computation times for an 8-node element will be given later.

2.3.3 Constraints in the Thin Plate Limit

In the earlier study of single layer hybrid-stress plate elements [19], it was shown that the reduced thin plate element was identical to the nonreduced (moderately thick) plate element in the thin plate limit. Thus, the performance of the thin plate reduced element will be guided by the thin-plate-limit constraints of the nonreduced element.

The same holds for the present multilayer elements: the reduced thin multilayer plate element will be identical to the nonreduced multilayer element in the thin plate limit. The thin-plate-limit constraints on the nonreduced element are enforced for all plate thickneses on the reduced thin plate element. If we denote by $\overline{\underset{\sim}{\sigma}}_t$ the transverse shear stresses integrated through the thickness and summed over all layers, then the thin-plate-limit constraints of the nonreduced formulation are

$$\int_{A_n} \delta\overline{\underset{\sim}{\sigma}}_t^T \underset{\sim}{\gamma}_t \, dA = 0 \qquad \text{for } \delta\underset{\sim}{\sigma}_t \neq 0 \tag{2.39}$$

Equation (2.39) represents weighted, integrated, Kirchhoff-type constraints. The form is analogous to the constraints for the single layers elements of References [15-18]. Thus, by analogy with the single layer elements, multilayer elements of the present type which are based on a fixed set of (laminate) stress parameters should have spanwise distributions of $\overline{\sigma_{xz}}$ and $\overline{\sigma_{yz}}$ which are identical to those of the corresponding non-locking single layer hybrid-stress plate elements [19].

In the reduced multilayer thin plate element, the constraints of equation (2.39) are imposed for all plate thicknesses. If the nonreduced element is nonlocking in the thin plate limit, the reduced element will converge to the lamination (thin plate) theory solution regardless of plate thickness.

2.4 FORMATION AND EVALUATION OF AN INVARIANT 8-NODE THIN MULTILAYER PLATE ELEMENT

2.4.1 Element Displacement and Stress Interpolations

To illustrate the formulation of a thin multilayer plate element based on the reduced formulation of the preceeding section, we consider an 8-node multilayer plate element as shown in Figure 2. The 8-node element has been selected in view of studies of single layer hybrid-stess (Mindlin-type) plate elements, wherein it is shown that a nonlocking, naturally invariant 8-node element of correct rank can be developed [18]. That element, denoted QH3 in Reference [18], has served as the guide for a multilayer element with independent layer displacement and stress fields [11] and a reduced thin single layer element [19], and will guide the development of the present 8-node thin multilayer plate element.

The displacement/rotation interpolation, and the geometric mapping (since the element is isoparametric) used for the 8-node element is the standard 8-node biquadratic Serendipity shape functions (expressed in the ξ,η system). The shape functions $N_i(\xi,\eta)$, $i = 1,2...8$ for equations (2.5) through (2.7) can be found in most texts on finite element methods. With five degrees of freedom per node, the present element has 40 dof, independent of the number of layers.

The stress field for our model single layer plate element, QH3, was obtained by starting with complete cubic polynomials in x,y for each of the inplane stresses. The stress field was then subjected to the constraint that σ_z be independent of x,y.

To produce the analog multilayer thin plate element, the strain interpolation vector, $\underset{\sim}{a}$, in equations (2.25) should be a complete cubic polynomial, i.e.

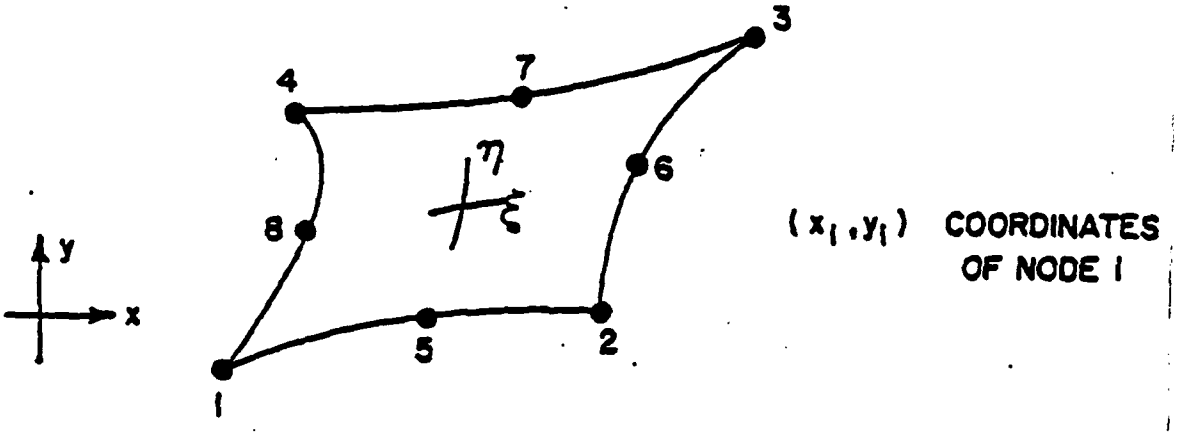

Figure 2 Geometry and numbering conventions for the 8-node multilayer element.

$$\underset{\sim}{1} = \begin{bmatrix} 1 & x & y & x^2 & xy & y^2 & x^3 & x^2y & xy^2 & y^3 \end{bmatrix} \tag{2.40}$$

As a result, the unconstrained stress field contains a total of 60 β 's, with

$$\begin{aligned} \underset{\sim}{\beta}_1^T &= \begin{bmatrix} \beta_1 & \beta_2 & \cdots & \beta_{10} \end{bmatrix} \\ \underset{\sim}{\beta}_2^T &= \begin{bmatrix} \beta_{11} & \beta_{12} & \cdots & \beta_{20} \end{bmatrix} \\ &\vdots \\ \underset{\sim}{\beta}_6^T &= \begin{bmatrix} \beta_{51} & \beta_{52} & \cdots & \beta_{60} \end{bmatrix} \end{aligned} \tag{2.41}$$

Given the $\underset{\sim}{N}_j(\xi,\eta)$ and $\underset{\sim}{a}$, the $\underset{\sim}{H}$ and $\underset{\sim}{G}$ matrices can be formed. The 60 β stress field resulting from substituting equation (2.40) into equation (2.25) must be reduced to correspond to QH3. In particular, the distribution of $\bar{\sigma}_z$ given by

$$\bar{\sigma}_z = -\frac{\partial \bar{\sigma}_x}{\partial x} z - \frac{\partial \bar{\sigma}_y}{\partial y} z \tag{2.42}$$

must be independent of x and y. Since σ_z is linear in x and y, this produces two constraints as follows:

$$\sum_{i=1}^{I} \left[(h_{i+1} - h_i) \qquad \left[\tfrac{1}{2} (h_{i+1} + h_i) - h_{I+1} \right] \right.$$

$$\left\{ 3Q_{11}^i \beta_7 + 2Q_{13}^i \beta_8 + 3Q_{12}^i \beta_{27} + 2Q_{23}^i \beta_{28} + 3Q_{13}^i \beta_{47} \right.$$

$$\left. + 2Q_{33}^i \beta_{48} + Q_{12}^i \beta_9 + Q_{22}^i \beta_{29} + Q_{23}^i \beta_{49} \right\}$$

$$+\left[\tfrac{1}{2}(h_{i+1}-h_i)\left[\tfrac{2}{3}(h_{i+1}^2+h_{i+1}h_i+h_i^2)-(h_{i+1}+h_i)h_{I+1}\right]\right.$$

$$\left\{3Q_{11}^{i}\beta_{17}+2Q_{13}^{i}\beta_{18}+3Q_{12}\beta_{37}+2Q_{32}\beta_{38}+3Q_{13}\beta_{57}\right.$$

$$\left.\left.+2Q_{33}\beta_{58}+Q_{12}\beta_{19}+Q_{22}\beta_{39}+Q_{23}\beta_{59}\right\}\right]=0$$

$$\sum_{i=1}^{I}\left[(h_{i+1}+h_i)\qquad\left[\tfrac{1}{2}(h_{i+1}-h_i)-h_{I+1}\right]\right. \tag{2.43}$$

$$\left\{Q_{11}^{i}\beta_8+2Q_{13}^{i}\beta_9+Q_{12}^{i}\beta_{28}+2Q_{23}^{i}\beta_{29}+Q_{13}^{i}\beta_{48}\right.$$

$$+2Q_{33}^{i}\beta_{49}+3Q_{12}^{i}\beta_{10}+3Q_{22}^{i}\beta_{30}+3Q_{23}^{i}\beta_{50}\Big\}$$

$$+\left[\tfrac{1}{2}(h_{i+1}-h_i)\left[\tfrac{2}{3}(h_{i+1}^2+h_{i+1}h_i+h_i^2)-(h_{i+1}+h_i)h_{I+1}\right]\right.$$

$$\left\{Q_{11}\beta_{18}+2Q_{13}\beta_{19}+Q_{12}\beta_{38}+2Q_{23}\beta_{37}+Q_{13}\beta_{58}\right.$$

$$\left.\left.+2Q_{33}\beta_{59}+3Q_{12}\beta_{20}+3Q_{22}\beta_{40}+3Q_{23}\beta_{60}\right\}\right]=0$$

In addition, we require that σ_{xz} and σ_{yz} be zero at the upper laminate surface. Since σ_{xz} and σ_{yz} are complete quadratic polynomials, this produces a total of 12 constraints, as follows:

$$\sum_i \left[\left\{ Q'_{11}\beta_2 + Q'_{13}\beta_3 + Q'_{12}\beta_{22} + Q'_{23}\beta_{23} + Q'_{13}\beta_{42} + Q'_{33}\beta_{43} \right\} + \tfrac{1}{2}(h_{i+1}+h_i)\left\{ Q'_{11}\beta_{12} + Q'_{13}\beta_{13} + Q'_{12}\beta_{32} + Q'_{23}\beta_{33} + Q'_{13}\beta_{52} + Q'_{33}\beta_{53} \right\} \right] = 0$$

$$\sum_i \left[\left\{ 2Q'_{11}\beta_4 + Q'_{13}\beta_5 + 2Q'_{12}\beta_{24} + Q'_{23}\beta_{25} + 2Q'_{13}\beta_{44} + Q'_{33}\beta_{45} \right\} + \tfrac{1}{2}(h_{i+1}+h_i)\left\{ 2Q'_{11}\beta_{14} + Q'_{31}\beta_{15} + 2Q'_{12}\beta_{34} + Q'_{32}\beta_{35} + 2Q'_{13}\beta_{54} + Q'_{33}\beta_{55} \right\} \right] = 0$$

$$\sum_i \left[\left\{ Q'_{11}\beta_5 + 2Q'_{13}\beta_6 + Q'_{12}\beta_{25} + 2Q'_{23}\beta_{26} + Q'_{13}\beta_{45} + 2Q'_{33}\beta_{46} \right\} + \tfrac{1}{2}(h_{i+1}+h_i)\left\{ Q'_{11}\beta_{15} + 2Q'_{13}\beta_{16} + Q'_{12}\beta_{35} + 2Q'_{23}\beta_{36} + Q'_{13}\beta_{55} + 2Q'_{33}\beta_{56} \right\} \right] = 0$$

$$\sum_i \left[\left\{ Q'_{11}\beta_7 + Q'_{13}\beta_9 + Q'_{12}\beta_{27} + Q'_{23}\beta_{29} + Q'_{13}\beta_{48} + Q'_{33}\beta_{49} \right\} + \tfrac{1}{2}(h_{i+1}+h_i)\left\{ Q'_{11}\beta_{18} + Q'_{13}\beta_{19} + Q'_{12}\beta_{38} + Q'_{23}\beta_{39} + Q'_{13}\beta_{58} + Q'_{33}\beta_{59} \right\} \right] = 0$$

$$\sum_i \left[\left\{ Q'_{11}\beta_9 + 3Q'_{13}\beta_{10} + Q'_{12}\beta_{29} + 3Q'_{23}\beta_{30} + Q'_{13}\beta_{49} + 3Q'_{33}\beta_{50} \right\} + \tfrac{1}{2}(h_{i+1}+h_i)\left\{ Q'_{11}\beta_{19} + 3Q'_{13}\beta_{20} + Q'_{12}\beta_{39} + 3Q'_{32}\beta_{40} + Q'_{13}\beta_{59} + 3Q'_{33}\beta_{60} \right\} \right] = 0$$

$$\sum_i \left[\left\{ Q'_{13}\beta_2 + Q'_{23}\beta_{22} + Q'_{33}\beta_{42} + Q'_{12}\beta_3 + Q'_{22}\beta_{23} + Q'_{23}\beta_{43} \right\} + \tfrac{1}{2}(h_{i+1}+h_i)\left\{ Q'_{13}\beta_{12} + Q'_{23}\beta_{32} + Q'_{33}\beta_{52} + Q'_{12}\beta_{13} + Q'_{22}\beta_{33} + Q'_{23}\beta_{53} \right\} \right] = 0$$

$$\sum_i \Big[\{3Q'_{11}\beta_7 + Q'_{13}\beta_8 + 3Q'_{12}\beta_{27} + Q'_{23}\beta_{28} + 3Q'_{13}\beta_{47} + Q'_{33}\beta_{48} + \tfrac{1}{2}(h_{i+1}+h_i)\{3Q'_{11}\beta_{17} + Q'_{13}\beta_{18} + 3Q'_{12}\beta_{37} + Q'_{23}\beta_{38} + 3Q'_{13}\beta_{57} + Q'_{33}\beta_{58}\}\Big] = 0 \tag{2.44}$$

$$\sum_i \Big[\{2Q'_{13}\beta_4 + 2Q'_{23}\beta_{24} + 2Q'_{33}\beta_{44} + Q'_{12}\beta_5 + Q'_{22}\beta_{25} + Q'_{23}\beta_{45}\} + \tfrac{1}{2}(h_{i+1}+h_i)\{2Q'_{13}\beta_{14} + 2Q'_{23}\beta_{34} + 2Q'_{33}\beta_{54} + Q'_{12}\beta_{15} + Q'_{22}\beta_{35} + Q'_{23}\beta_{55}\}\Big] = 0$$

$$\sum_i \Big[\{Q'_{13}\beta_5 + Q'_{23}\beta_{25} + Q'_{33}\beta_{45} + 2Q'_{12}\beta_6 + 2Q'_{22}\beta_{26} + 2Q'_{23}\beta_{46}\} + \tfrac{1}{2}(h_{i+1}+h_i)\{Q'_{13}\beta_{15} + Q'_{23}\beta_{35} + Q'_{33}\beta_{55} + 2Q'_{12}\beta_{16} + 2Q'_{22}\beta_{36} + 2Q'_{23}\beta_{56}\}\Big] = 0$$

$$\sum_i \Big[\{3Q'_{13}\beta_7 + 3Q'_{23}\beta_{27} + 3Q'_{33}\beta_{47} + Q'_{12}\beta_8 + Q'_{22}\beta_{28} + Q'_{23}\beta_{48}\} + \tfrac{1}{2}(h_{i+1}+h_i)\{3Q'_{13}\beta_{17} + 3Q'_{23}\beta_{37} + 3Q'_{33}\beta_{57} + Q'_{12}\beta_{18} + Q'_{22}\beta_{38} + Q'_{23}\beta_{58}\}\Big] = 0$$

$$\sum_i \Big[\{Q'_{13}\beta_8 + Q'_{23}\beta_{28} + Q'_{33}\beta_{48} + Q'_{12}\beta_9 + Q'_{22}\beta_{29} + Q'_{23}\beta_{49}\} + \tfrac{1}{2}(h_{i+1}+h_i)\{Q'_{13}\beta_{18} + Q'_{23}\beta_{38} + Q'_{33}\beta_{58} + Q'_{12}\beta_{19} + Q'_{22}\beta_{39} + Q'_{23}\beta_{59}\}\Big] = 0$$

$$\sum_i \left[\left\{ Q_{13}^i \beta_{19} + Q_{23}^i \beta_{24} + Q_{33}^i \beta_{49} + 3Q_{12}^i \beta_{10} + 3Q_{22}^i \beta_{30} + 3Q_{23}^i \beta_{50} \right\} + (h_{i+1} + h_i) \left\{ Q_{13}^i \beta_{14} + Q_{23}^i \beta_{29} + Q_{33}^i \beta_{59} + 3Q_{12}^i \beta_{20} + 3Q_{22}^i \beta_{40} + 3Q_{23}^i \beta_{60} \right\} \right] = 0$$

Equations (2.43) and (2.44) represent 14 interrelations among the β's which can be put in the form of equation (2.17) and thus define the R matrix. If we consider these interrelations as reducing the effective number of β's, we can say that the present element has a total of 46 β's. In future discussions, we will refer to this 8-node thin multilayer plate element as MQH3T.

Element MQH3T possesses correct rank, independent of the number of layers. It is also naturally invariant. As it is based on the reduced formulation of the previous section, it should be expected that MQH3T will converge to lamination theory solutions, and that convergence behavior will be like the single layer element QH3 [18].

2.4.2 Element Stiffness Computation Time

Computation time (on an IBM 370/168 using double precision) for the stiffness matrix of MQH3T is 3.38 seconds, essentially independent of the number of layers. A breakdown of that time is given in Table 1. The largest single block of time is for the final matrix multiplications. The next largest block is the time to compute H^{-1}.

TABLE 1

Computation Time for the Stiffness Matrix of Element MQH3T

OPERATION	CPU (secs)
Zero/Initialize Matrices	0.034
Evaluate area Integrals in eqns. (2.31) and (2.32) (Needed for $\hat{H}^{-1}$ and G) Using a 4x4 Gauss Rule	0.124
Form ϕ^{-1} (eqn.(2.31) and E^{-1} (eqn.(2.35))	0.012
Form $\hat{H}^{-1}$ (eqn.(2.20))	0.843
Form G (eqn.(2.37))	0.559
Compute $k=G^T H^{-1} G$	1.810
TOTAL	3.382

Some comparisons with computation times for other element stiffnesses are useful. Early attempts to produce a non-reduced 8-node multilayer element, hereafter denoted MQH3, having fixed β's and degrees of freedom resulted in stiffness computation times of 27.9 secs for 1 layer, and 109.4 secs for 3 layers. This is what motivated the study of a reduced formulation. The 8-node multilayer element MLPQH3 of Reference [11] having independent layer stress fields and independent layer displacement fields requires 30.4 secs for 3 layers (note--less CPU time than MQH3). Finally, the single layer hybrid-stress 8-node plate element (bending only) based on a reduced formulation, QH3T, of Reference [18] requires 1.8 secs. These comparisons illustrate the computational advantages of MQH3T.

2.4.3 Example Problems and Numerical Results

2.4.3.1 Cylindrical Bending of a 3-layer 90/0/90 Cross-ply

The problem considered is a 3 layer 90/0/90 cross-ply (θ measured from the x-axis) plate of infinite length in the x-direction, length L in the y-direction, simply supported at y=0,L and subject to a sinusoidal distributed transverse load (uniform versus x). Mesh and boundary conditions are given in Figure 3. Each layer is of equal thickness, h/3, and layer material properties are E_{11}=25x10^6 psi., E_{22}=10^{6}psi., ν_{12}=.25, ν_{23}=.25, G_{12}=.5x10^6 psi., G_{23}=.2x10^6 psi. This problem has been selected because an elasticity solution exists which is valid for all laminate thickness ratios [24].

Quantities of interest are the transverse displacement w, the through thickness distribution of in-plane normal stress σ_y at the plate center (y=L/2), and transverse shear stress, σ_{yz}, at the boundary (y=0).

Results will be presented in terms of the following normalized quantities.

$$\bar{w} = \frac{100\, E_{22}\, h^3\, w}{q_0 L^4}$$

$$\bar{\sigma}_y = \frac{\sigma_y}{q_0} \qquad \bar{\sigma}_{yz} = \frac{\sigma_{yz}}{q_0} \tag{2.45}$$

The quantity q_0 is the magnitude of the distributed sinusoidal load.

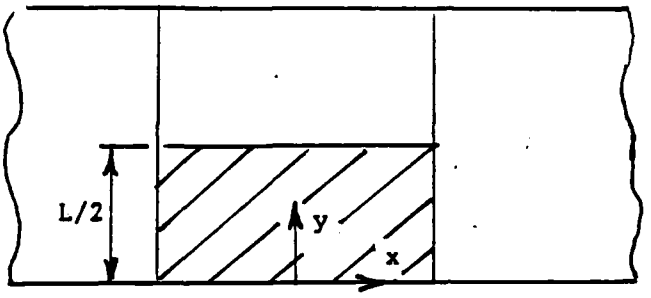

(a) top view

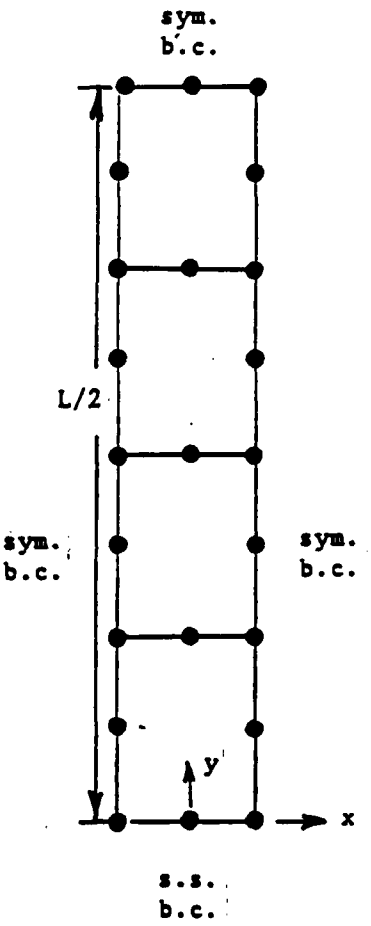

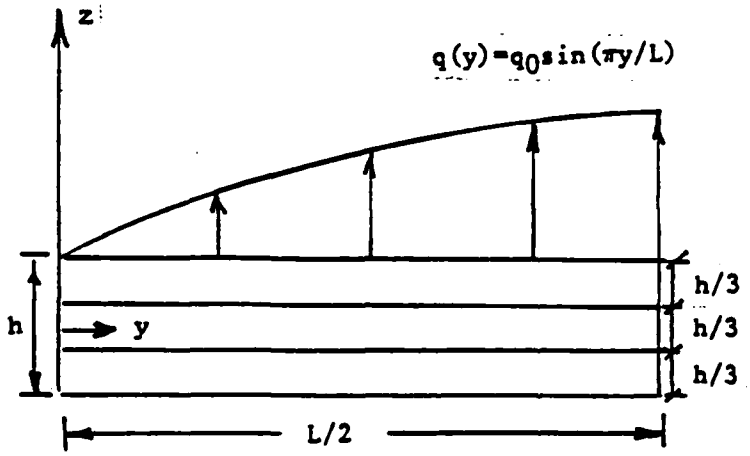

(b) side view

Figure 3 Problem definition and mesh for the cylindrical bending of a semi-infinite plate under sinusoidal loading.

For a thin laminate the linear through thickness inplane displacement field assumed in MQH3T is adequate. Convergence of the center transverse displacement normalized by the exact value, [24] for a thin (h/L=0.01) laminate is shown in Figure 4. The behavior of the multilayer composite plate element with complete stress contributions (MQH3) is compared with the reduced thin multilayer plate element (MQH3T) which excludes the contributions of transverse shear stresses and transverse normal stress to the internal complementary energy (i.e. the $\underline{H}$ matrix). The two elements converge in a similar manner and both give very good results with element MQH3 converging only slightly more quickly than MQH3T: this is because the results are normalized by the exact solution, rather than by lamination theory.

For thin laminates, the performance of element MQH3T is essentially identical to the element MQH3. As thickness ratio, h/L, increases the more general element MQH3 is necessary to produce accurate predictions. To compare the range of applicability of MQH3T and MQH3, plates having thickness ratios in the range h/L=0.01 to h/L=0.25 have been analyzed using a three element mesh (converged per Figure 2). The results obtained for the center transverse displacement, $\overline{w}_c$ are given in Table 2 for element MQH3 and in Table 3 for element MQH3T. Element MQH3 produces accurate predictions of w over a wide range of thickness ratios from thin (h/L=0.01) to thick (h/L=0.25) laminates. In Table 3, the predicted $\overline{w}_c$ using element MQH3T does not increase with increasing h/L. This is consistent with lamination theory (as expected), which gives poor predictions of center transverse displacement for values of h/L>.01. Note that lamination theory produces a value of $\overline{w}$=.50966 for this problem, in essential agreement with the MQH3T results.

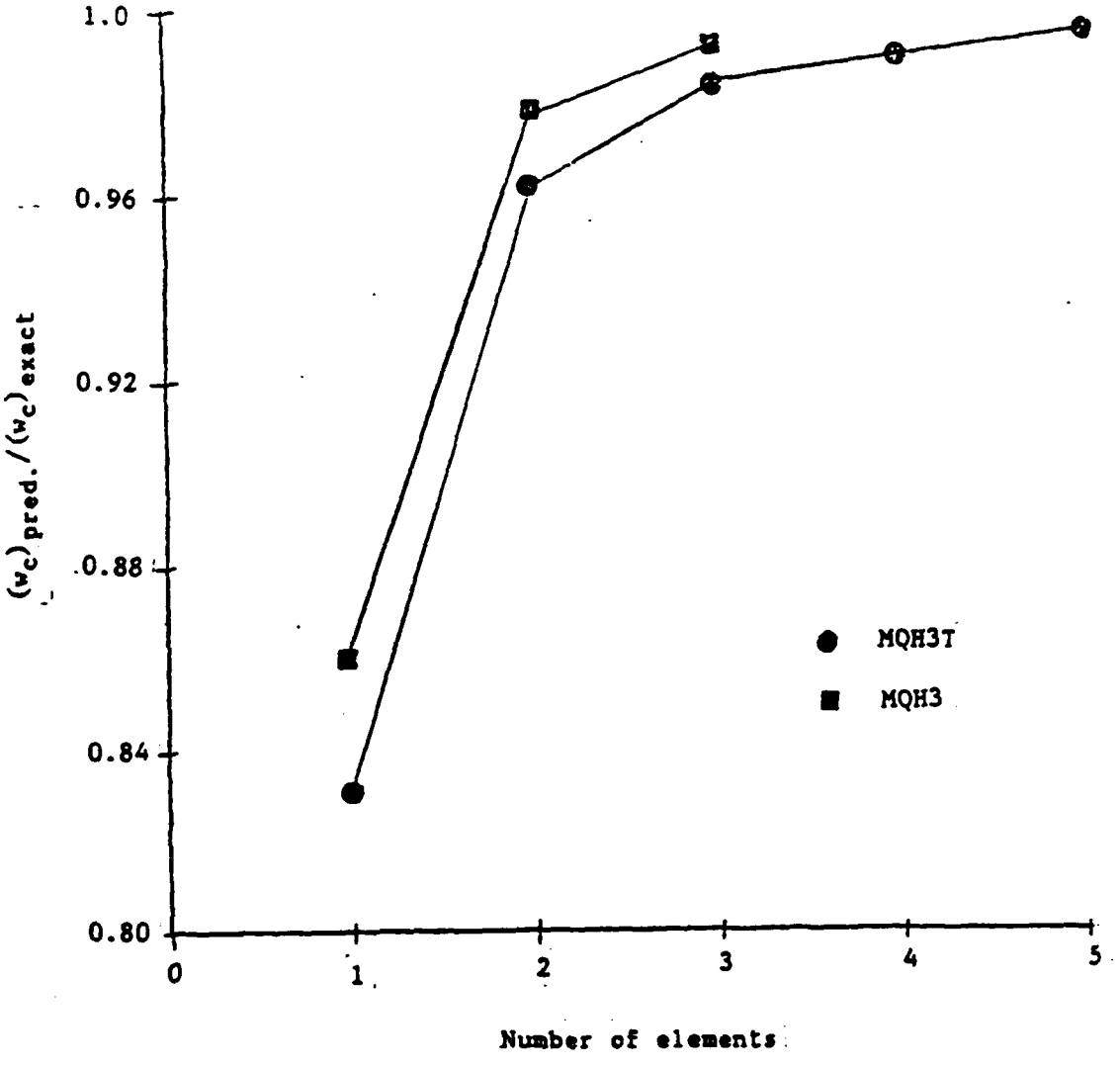

Figure 4 Convergence of the center transverse displacement normalized by the elasticity solution for the cylindrical bending of a plate for which h/L=0.01.

TABLE 2

Effects of thickness ratio, h/L, on the predicted center transverse displacement of element MQH3 for the cylindrical bending of a 90/0/90 cross-ply for a 3 element mesh

h/L	$(w_c)_{exact}$	$(w_c)_{predicted}$	predicted/exact
0.25	3.0233	2.8872	1.047
0.10	0.9278	0.9333	0.994
0.05	0.6160	0.6167	0.999
0.0375	0.5689	0.5702	0.998
0.01	0.50906	0.5133	0.992

TABLE 3

Effects of thickness ratio, h/L, on the predicted transverse displacement of element MQH3T for the cylindrical bending of a 90/0/90 cross-ply using a 3 element mesh

h/L	$(w_c)_{exact}$	$(w_c)_{predicted}$	predicted/exact
0.25	3.0233	0.50104	0.1657
0.10	0.9278	0.50123	0.5402
0.05	0.616	0.50123	0.8137
0.0375	0.5689	0.50122	0.8811
0.01	0.50906	0.50123	0.9846

In the range h/L>.01, MQH3 is clearly the more accurate element since the contribution of transverse shear stresses and transverse normal stresses to the internal complementary energy have been retained. However, as illustrated earlier, computation time for $\underset{\sim}{k}$ of MQH3 grows

excessively with increasing numbers of layers. Thus, use of MQH3 for thin plates is not appropriate. The reduced element is clearly the better element for h/L<.01 because of the significant savings in CPU time and the fact that there is no loss of accuracy within the range of h/L to be considered here (thin plates). Therefore only the reduced element will be used for subsequent tests.

The prediction of spanwise distributions of stresses can be illustrated using the 90/0/90 example problem. Spilker et al. [23] established the existence of optimal sampling points for hybrid-stress elements. Briefly, approximate strains $\underset{\sim}{S}\underset{\sim}{q}$ approach the exact strains $\underset{\sim}{D}\underset{\sim}{u}$ (where $\underset{\sim}{u}$ are the exact displacements and $\underset{\sim}{D}$ is the differential operator matrix corresponding to the linear strain-displacement equations) in a weighted least squares sense. Owing to a property of Gauss quadrature, the Gauss stations corresponding to the Gauss rule which just integrates the stress field $\underset{\sim}{\sigma}=\underset{\sim}{P}\underset{\sim}{\beta}$ are the optimal sampling points.

To examine the predicted spanwise distributions, it is convenient to consider the (normalized) moment (from σ_y) and shear force (from σ_{xz}) distributions given by:

$$\bar{M} = \frac{\pi^2}{g_o L^2} M = \frac{\pi^2}{g_o L^2} \int_{-\frac{h}{2}}^{h/2} \sigma_y z \, dz \tag{2.46}$$

$$\bar{Q} = \frac{\pi}{g_o L} Q = \frac{\pi}{g_o L} \int_{-\frac{h}{2}}^{\frac{h}{2}} \sigma_{yz} dz$$

The present element MQH3T is based on a single layer element QH3 [17]. Evaluation of the single layer element determined that convergence of $\overline{M}$ at nodes is in general somewhat better than at the 2x2 Gauss stations while the results obtained for $\overline{Q}$ at the 2x2 Gauss stations are extremely accurate. Using element QH3 as a guide, results are plotted in Figures 5 and 6 for $\overline{M}$ and $\overline{Q}$ for a thin 90/0/90 plate, h/L=.01 and using 3 elements. Results for $\overline{M}$ are plotted versus y along the left edge of the mesh. The prediction of $\overline{M}$ is reasonably accurate at the nodes and center of each element. Results for $\overline{Q}$ are plotted versus y along a line which passes through the 2x2 Gauss stations. The predicted distribution of $\overline{Q}$ is poor on a pointwise basis but the optimal sampling points corresponding to the 2 point Gauss rule are evident.

The through thickness distributions of σ_y at y=L/2 and transverse shear stress σ_{yz} near y=0 for thin laminated (h/L=0.01) are shown in Figures (7a-7b). A 3 element mesh is used and the lamination theory solution is also shown. The predicted distribution of σ_y at y/L=0.5 agrees exactly with the lamination theory solution (Figure 7a). The predicted distribution of σ_{yz} calculated at the 2x2 Gauss station nearest to y=0 agrees very closely with lamination theory, Figure 7b.

2.4.3.2 Angle ply Laminates under Transverse Loading

The final example problem considered is a 2 layer laminate of angle ply ($\pm\theta$) contruction, subject to a uniformly distributed transverse load (see Figure 8). For present purposes, only square plates are considered so that a=b and a uniform NxN mesh is used; note that the entire plate must be modeled since fiber-orientation induced stretching/bending

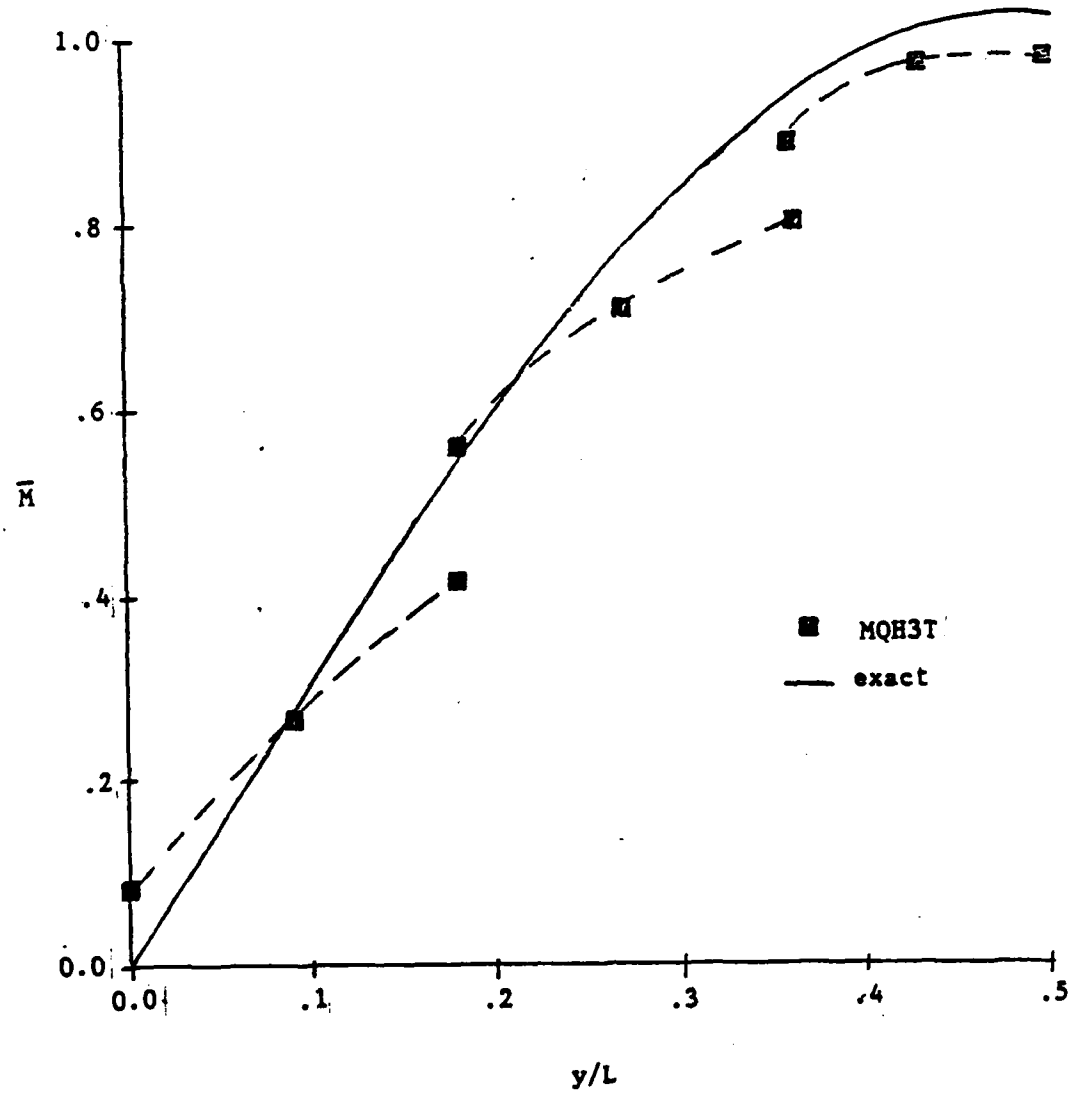

Figure 5 Normalized moment $\bar{M}$ distribution vs y for a thin (h/L=0.01) 90/0/90 cross-ply in cylindrical bending using a 3 element mesh.

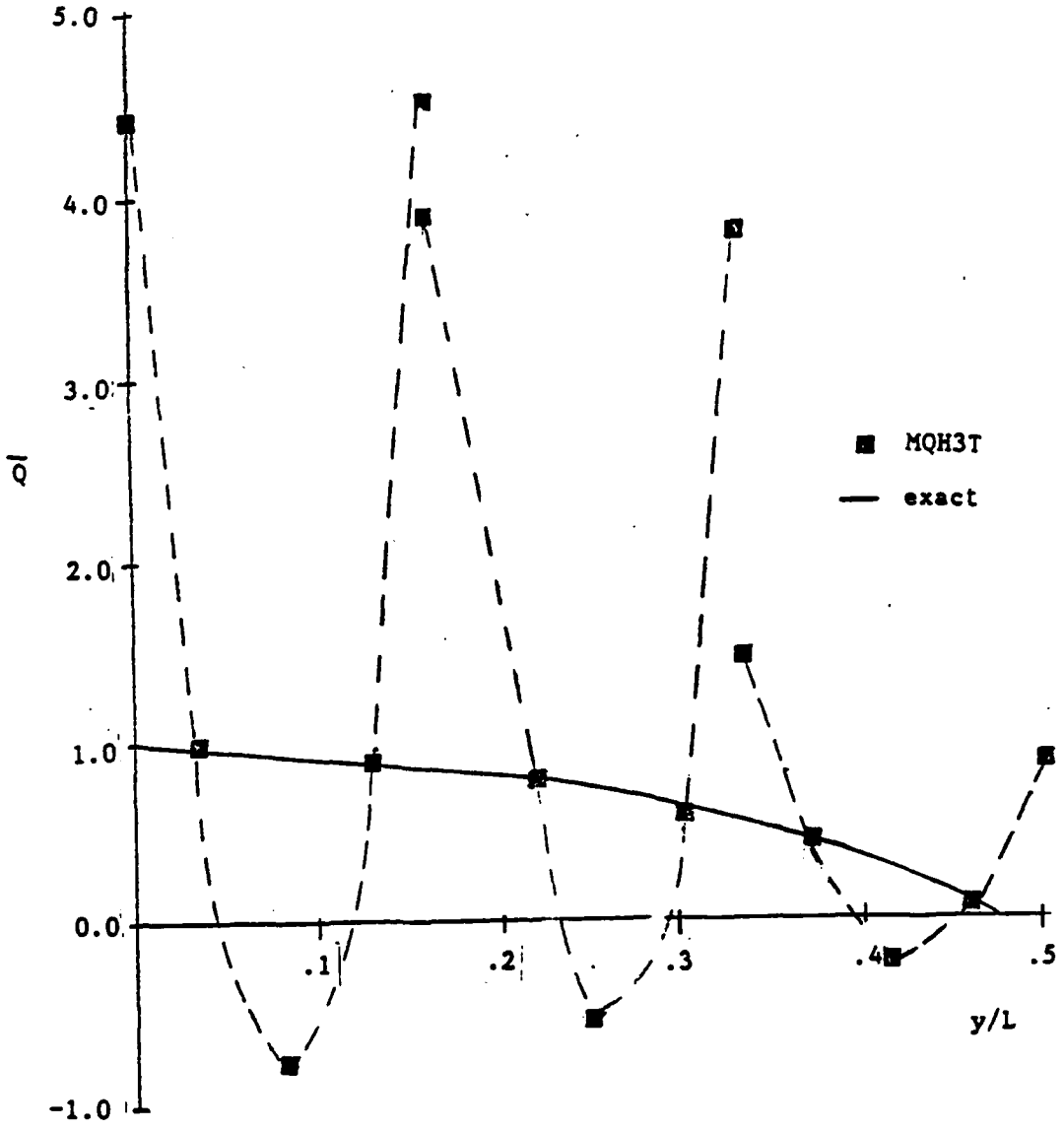

Figure 6 Normalized transverse shear force $\bar{Q}$ distribution vs y for a thin (h/L=0.01) 90/0/90 cross-ply in cylindrical bending using a 3 element mesh.

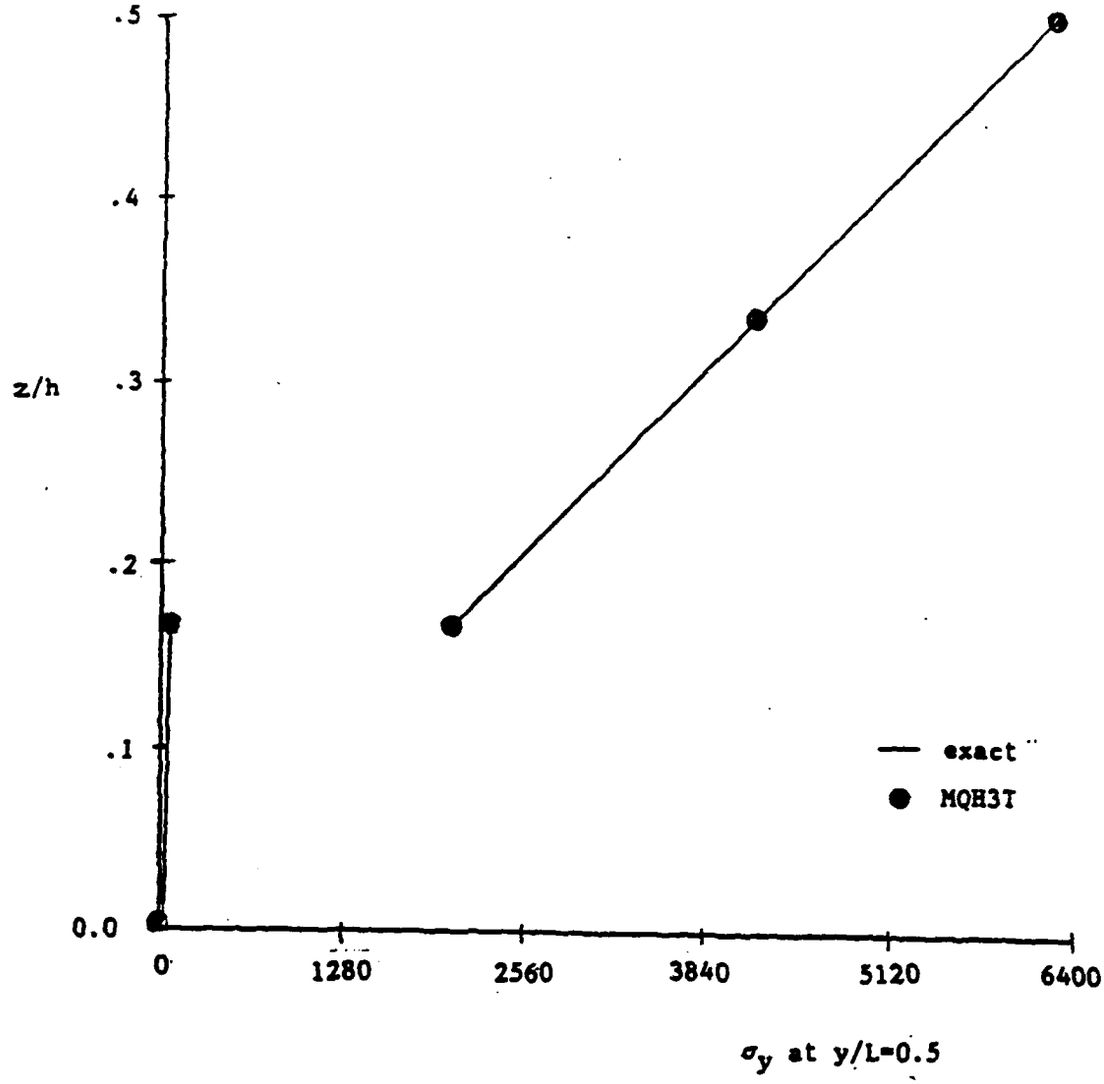

Figure 7a Through thickness stress distribution for thin (h/L=0.01) 90/0/90 cross-ply laminates in cylindrical bending using a 3 element mesh.

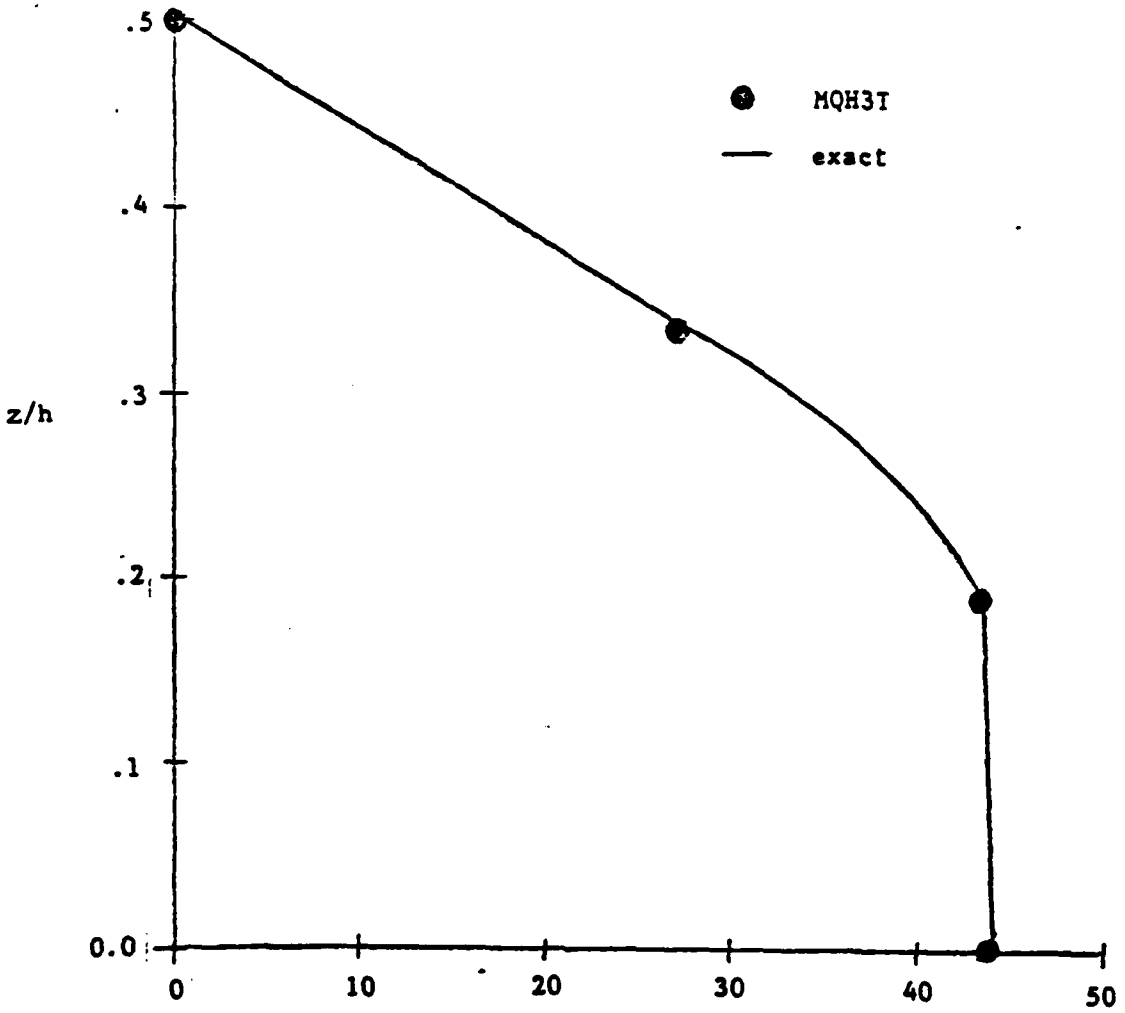

Figure 7b Through thickness stress distribution for thin (h/L=0.01) 90/0/90 cross-ply laminates in cylindrical bending using a 3 element mesh.

coupling exists which eliminates the usual (i.e. single layer) x-y plane symmetries. Results will be compared with a series solution (20 terms used here) given by Whitney [25] since that solution is based on lamination theory.

All results are obtained for a=b=10, h=0.02, so that h/L=.002. Layer material properties are $E_{11}=40x10^6$ psi., $E_{22}=10^6$ psi., $\nu_{12}=\nu_{23}=.25$, $G_{12}=G_{23}=.5x10^6$ psi.

For all cases, a uniformly distributed transverse load is applied. Plates are considered for which all sides are simply supported and for which all sides are ideally clamped. Quantities of interest to assess element performance are transverse displacement, w_c and moments, M_x and M_y at the center of the plate. As well as inplane displacements u and v along the edge of the plate.

Results are presented first for simply supported plates. Limited convergence results for the case $\theta = 15°$ are given in Table 4. Table 4 shows all quantities of interest to be within 2.5 per cent of the exact value for a 6x6 mesh of the entire plate.

Using the 6x6 mesh of the whole square plate, the effect of θ on the prediction of w, is shown in Table 5. Typically, θ has little effect on the accuracy of the predictions.

The second example problem is a plate clamped on all sides. Convergence results for θ = 15°, 25°, and 45° are given in Table 6. The results are poor for small θ, i.e. $\theta = 15°$ and good for $\theta = 45°$. Table 6 shows the transverse displacement for the case $\theta = 45°$ to be within 7 per cent of the exact value for a 6x6 mesh.

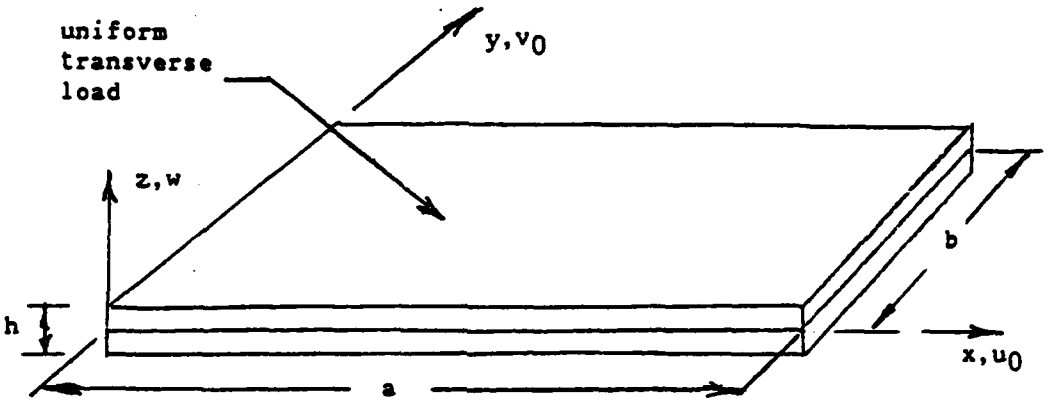

(a) geometry

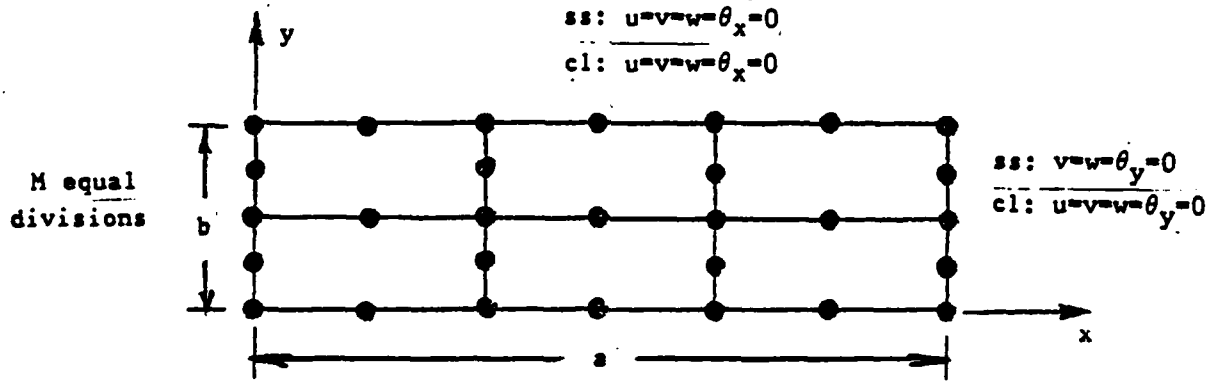

(b) mesh and boundary conditions (top view)

Figure 8 Problem definition and mesh for a 2 layer rectangular plate of angle-ply ($\pm\theta$) contstruction under uniform transverse loading.

TABLE 4

Convergence of a simply supported square angle ply plate under uniform transverse load $\theta = 45°$

		Mesh (whole plate) 2x2	4x4	6x6
u_0 at (a/2,0)	pred.	0.009	0.0079	0.0078
exact=.00771	pred./ex.	1.171	1.0295	1.013
w_0 at (a/2,b/2)	pred.	8.113	8.9883	8.9486
exact=8.927	pred./ex.	.9088	1.007	1.0024
M_x at (a/2,b/2)	pred.	8.6127	11.8877	11.6890
exact=10.42	pred./ex.	0.754	1.041	1.0236
v_0 at (0,b/2)	pred.	0.03356	0.03279	0.03279
exact=0.03281	pred./ex.	1.0228	0.996	0.9994
M_y at (a/2,b/2)	pred.	1.1193	1.241	1.2332
exact=1.234	pred./ex.	.907	1.006	0.9994

TABLE 5

Results for a thin simply supported square plate of angle ply construction under transverse load for a 6x6 mesh.

Fiber Orientation	w_c	w_{exact}	predicted/exact
±5°	595.5	592.0	1.006
±15°	894.9	892.7	1.002
±25°	983.3	983.8	1.000
±35°	944.3	945.1	0.999
±45°	914.4	915.2	0.999

Using the 6x6 mesh of the whole square plate, the effect of θ on the prediction of the transverse displacement is shown in Table 7. The

TABLE 6

Convergence of the transverse displacement at the center of a clamped square angle-ply plate under uniform transverse load

Fiber Orientation	Mesh 2x2 w_c	pred./ex.	4x4 w_c	pred./ex.	6x6 w_c	pred./ex.
±15°	2.5378	1.2006	2.4057	1.138	2.5109	1.1879
±25°	3.3457	1.1365	3.0768	1.045	3.2143	1.0920
±45°	3.6611	1.0130	3.5004	0.970	3.8569	1.0680

problems occur when the length of an element is much greater in one direction than the other. As has been stated earlier the element we are now considering is analogous to a single layer element QH3 of Reference [17]. In the single layer element study [17], these effects were most apparent for aspect ratios of a/b= 2 and 3 in the case of clamped boundaries, where as much a 5 per cent was found. Considering the present problem of laminated plates when theta is small and the fibers nearly line up with the x-axis, the element is much stronger in the x-direction than in the y-direction. This may be causing a "material aspect ratio" effect analogous to the "geometric aspect ratio" effect observed in isotropic single layer plate elements--- further study to the phenomenon is needed.

2.4.4 Concluding Remarks

This chapter has dealt with a hybrid formulation of an isoparametric element for the analysis of thin multilayer laminated composite plates. The principal objective was the development and evaluation of an element in which the displacement behavior is characterized by lami-

nate reference plane inplane and transverse displacements and laminate non-normal cross section rotations and in which the components of stress are related to a set of laminate stress parameters; i.e. so that there is no increase in the number of degrees of freedom or the number of stress parameters as the number of layers increases. For thin multilayer laminates, a reduced formulation was defined which allows for a significantly more efficient stiffness-generating algorithm. The results of this sudy have been applied to the development of element MQH3T.

In summary, element MQH3T gave good convergence performance. The element retains a high degree of accuracy for thin plates having a thickness ratio less than h/L=0.01. The spanwise distribution of M pointed out that the best points to calculate σ_y are at the sides and center of each element. The spanwise distribution of Q indicated that the best points to calcuated σ_{yz} are at the 2x2 Gauss stations. The poor results displayed for small θ in the case of an angle-ply plate which has been clamped on all edges are thought to be due to a type of "material" aspect ratio problem. For the case of an angle-ply plate which is simply supported on all edges the results are very good and θ has little effect on the accuracy of the predictions.

Chapter III

FORMULATION OF THE CONTACT PROBLEM

3.1 INTRODUCTION

The finite element method is now widely recognized as a powerful tool in solving problems in structural and continuum mechanics. The finite element method owes its popularity largely to its generality. It permits easy modeling of arbitrary shapes, with arbitrary loads, boundary conditions and can include the effects of material and/or geometrical nonlinearities. The unique characteristics of the contact problem make an analysis difficult even by the finite element method. As the load varies, the region of contact between bodies changes and sliding relative to each other occurs. This sliding may be accompanied by frictional forces which act to oppose the sliding motion.

The work done thus far in the area of finite element analysis of contact problems can be differentiated in the following areas. First, the formulation is based on either the displacement model or on various hybrid and mixed models. Second, the models are capable of considering contact problems in which there may be node to element side contact or they are capable of handling only problems in which there is node to node contact. The last distinguishing characteristic is that the effect of friction along the contact surface may or may not be included. The largest portion of the work done has utilized the displacement model formulation and can only account for moderate sliding between contacting bodies (i.e. node to node contact).

This method was first applied by Yamada, et.al. [26] to the Hertz contact problem of two identical cylinders pressed together. The meshes were divided so that nodes of one cylinder were in contact with the nodes of the opposing cylinder.

White and Enderby [27] applied the finite element analysis to the problem of a connecting rod eye loaded by means of a pin. They used linear triangular elements to model the two deformable bodies and special overlapping connecting elements, which were assigned stiffness to model the surface of contact. Iterations were required to obtain the correct displacements.

Gaertner [28] investigated plane elastic contact of solids subject to small strains with friction. Linear triangular displacement finite elements were used. Node to node contact was considered and an iterative method was utilized to find the equilibrium state.

Fredriksson [29] introduced a 2-dimensional contact constitutive relation; a general slip criterion with associated slip rule was included. The contact surface was limited to extending in the node to node configuration. In order to reduce the size of the problem, degrees of freedom not related to the nonlinearities were eliminated using the super element technique. A Coulomb type of slip criterion with an associated slip hardening rule was assumed.

Gap elements were utilized by Stadter and Weiss [30] to model the gap process. The solution was achieved through a iterative procedure which adjusts the modulus of the gap elements. The procedure was applied to the thermostructural analysis of the heat shield of a radioisotope thermoelectric generator design.

The method presented by Okamoto and Nakazawa [31] dealt with the irreversibility resulting from stick-slip phenomenon. The loading was incremental where the magnitude of each increment of load was calculated to cause a change in one node pair along the contact surface. The contact conditions were additional conditions independent of stiffness equations.

Sachdeva and Ramakrishnan [32] generalized a procedure developed by Francaville and Zienkiewicz [33] to include frictional effects under proportional loading. The method uses the flexibility matrix which was obtained by inversion of the condensed stiffness matrix in which all nodes were eliminated except those where contact was likely to take place.

A direct automated procedure for frictionless contact problems is presented by Mahmoud et.al. [34]. This method circumvents the need for the inclusions of interface elements and does not calculate contact pressure. Simplicity seems to be the primary goal of its authors. The method applies only to contact problems in which there is no tangential motion relative to the contact surface and to contact problems which are purely advancing or receding. The direct incremental method used here means the applied load was scaled so that it would just close the respective gap yet not induce the interpenetration to the contact surfaces.

Displacement models have also been developed to account for extensive sliding contact, i.e. nodes of one body may come in contact with the side of the element on the boundary of the opposing body. Therefore these models also account for friction along the contact surface.

Chan and Tuba [35] solved the problem of contact using linear triangular elements derived by an assumed displacement model. The model allowed for node to node and node to element boundary contact and coulomb friction betweed the two bodies. The effects of clearance, friction, and load on stresses in turbine blade fastenings were studied and compared with photoelastic experimental results.

Large displacement contact-impact problems has been studied by Hughes et.al. [36]. The theory includes frictional effects and allows for geometrically complicated contact surfaces. Contact is not limited to node to node configurations.

Hybrid and mixed models have also been used to solve contact problems in as attempt to obtain more accurate results. Kubomura [37] developed a method for analyzing contact problems which may be either frictional or frictionless and may involve extensive sliding between deformable bodies. It consists of a hybrid formulation including the conditions of contact, and a scheme to determine the place of contact.

The work of Hung and Saxce [38] assumes that no friction between solid bodies exists so that the contact condition may be expressed in terms of displacements alone. The superelement technique was used to reduce the number of degrees of freedom. Hybrid triangles with 12 degrees of freedom were used to model the deformable bodies.

The mixed finite element method was applied to two dimensional elastic contact problems by Tseng and Olson [39]. Some of the displacement variables were treated as natural boundary conditions in the contact region. The procedure includes sliding and adhering of contact node pairs.

The representation of the surface of contact has been a subject of special concern. A special bond element was utilized by Schafer [40] to represent mathematically the disipative processes which occur during contact. A relationship between the shear stress and the frictional deformation is assumed to be known, and an element stiffness matrix is derived with the aid of the principle of virtual work.

Oden and Piries [41] propose nonclassical friction laws in an attempt to overcome physical and mathemetical difficulties which arise through use for the classical Coulomb law of friction. Variational principles for boundary-value problems in elasticity in which such nonlinear nonlocal laws hold were then developed.

The problems of elastic beams or plates supported on a foundation have been examined. An iterative technique was presented by Svec [42] for determination of contact area between a plate and its supporting elastic foundation.

Mohr [43] modelled an elastic supporting beam or plate. The method is not iterative. A contact stiffness matrix is calculated to simulate adhesion to rigid surfaces.

Westbrook [44] solved contact problems for the elastic beam. Variational inequalities and finite elements were used to obtain approximate solutions to bending problems for elastic beams in the presence of a rigid barrier.

Solutions of the problem of wheel contact have been reported. Tielking and Schapery [45] presented a method of shell contact using discrete Fourier transform for analysis for linear and certain types of nonlinear problems. The method is used to calculated the road contact

pressure predicted by a finite element toroidal shell model of a pneumatic tire.

A numerical method was developed by Paul and Hashemi [46] for the determination of contact pressure which arises when two elastic bodies with closely conforming non-Hertzian frictionless surfaces are pressed together. The method included a technique for automatically altering meshes that overlay the changing contact patches. Problems of wheel and rail contact were examined.

Mathematical techniques have also been applied to contact problems. Singh and Paul [47] showed how to solve antiformal non-Hertzian problems using the so-called simply discretized method. The problems solved involved frictionless surfaces.

Conry and Seireg [48] used optimization techniques to develop a mathematical programming method which utilized a simplex-type algorithm. The technique is applied to contact of beams of elastic foundations.

The present work is an extension of the work done by Kubomura [37]. The hybrid stress model is used to solve edge contact problems involving thin multilayer laminated composite plates, modeled using the newly developed multilayer elements. The model can analyze problems in which there may or may not be friction along the contact surface. There may be extensive sliding between the two contacting bodies. "Contact elements" having unknown nodal contact tractions are used to model the contact surface.

In general, the contact of an elastic body with the edge of a laminated plate could produce complicated three-dimensional effects. There might include, for example, introduction of bending forces and bending

displacements even in symmetric laminates, severe warping in the zone of contact, and a contact surface which varies through the thickness of the laminate. In principle, such a 3-D contact analysis could be developed. However, such an analysis was felt to be impractical at this stage of investigation because of the excessive computer core and CPU requirements needed to model these effects (i.e. a more general multilayer plate element, and an arbitrary 3-D contact surface inspection and correction scheme). Therefore, attention is restricted here to thin symmetric laminates subject to edge contact which does not vary in the thickness direction and for which the contactor moves only in the plane of the laminate. In effect, only inplane laminate displacements will occur even though the bending/stretching multilayer element MQH3T will be used.

3.2 HYBRID STRESS FUNCTIONAL FOR CONTACT

3.2.1 Variational Principle for the Contact Problem

Let us consider two elastic bodies --- body A and body B. Body A and body B are in contact along the contact surface S_c. The boundary of body A and the boundary of body B along the contact surface, S_c occupy the same space, but the two bodies do not overlap.

As can be seen in Figure 9, each body is under its own system of prescribed tractions and prescribed displacements. Tractions along the contact surface are resolved into normal and shear components.

Using equilibrium we can relate these tractions.

$$T_s^A + T_s^B = 0$$

$$T_n^A + T_n^B = 0 \qquad (3.1)$$

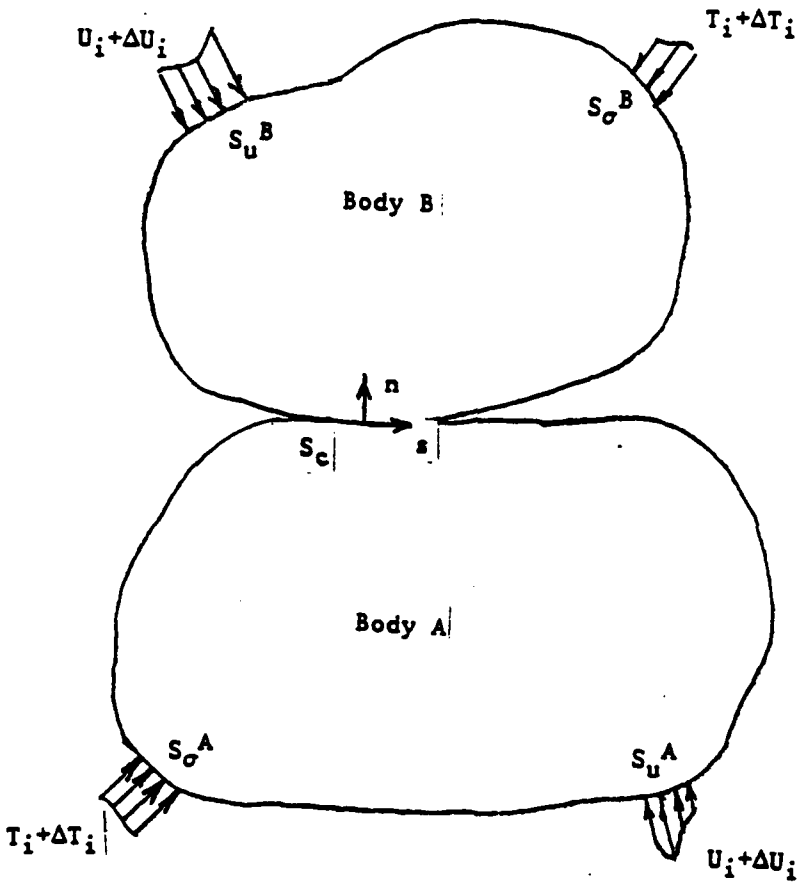

Figure 9 Definition of the problem of contact between two deformable bodies.

Sliding between the two elastic bodies relative to one another is allowed. When sliding occurs the following contact conditions must be satisfied for each of the contacting bodies along the contact zone.

$$T_s = \pm \mu T_n \tag{3.2}$$

Where T_n is the normal traction on the surface of contact, T_s is the tangential traction of the surface of contact, and μ is the coefficient of friction. Note that $(\,)^a$ and $(\,)^b$ (or A and B) denote quantities pertaining to body A and body B respectively.

The location of the contact surface is assumed between the two elastic bodies as illustrated in Figure 10. At times during contact, the bodies may undergo extensive sliding relative to one another. Other studies assumed that nodes of one body remain in contact with nodes of the other. This may not be adequate because when two bodies come into contact it is likely that the surface of one body will move relative to the other body. In the formulation used here, one contacting body is allowed to slide relative to the opposing contacting body. This motion of the contacting bodies causes unknown nodal forces to be applied to the contacting nodes. The nodal forces of one contacting body are in equilibrium with the nodal forces applied to the opposing body; the procedure used here results in coupled matrix equations with nodal forces within the zone of contact as additional unknown quantities.

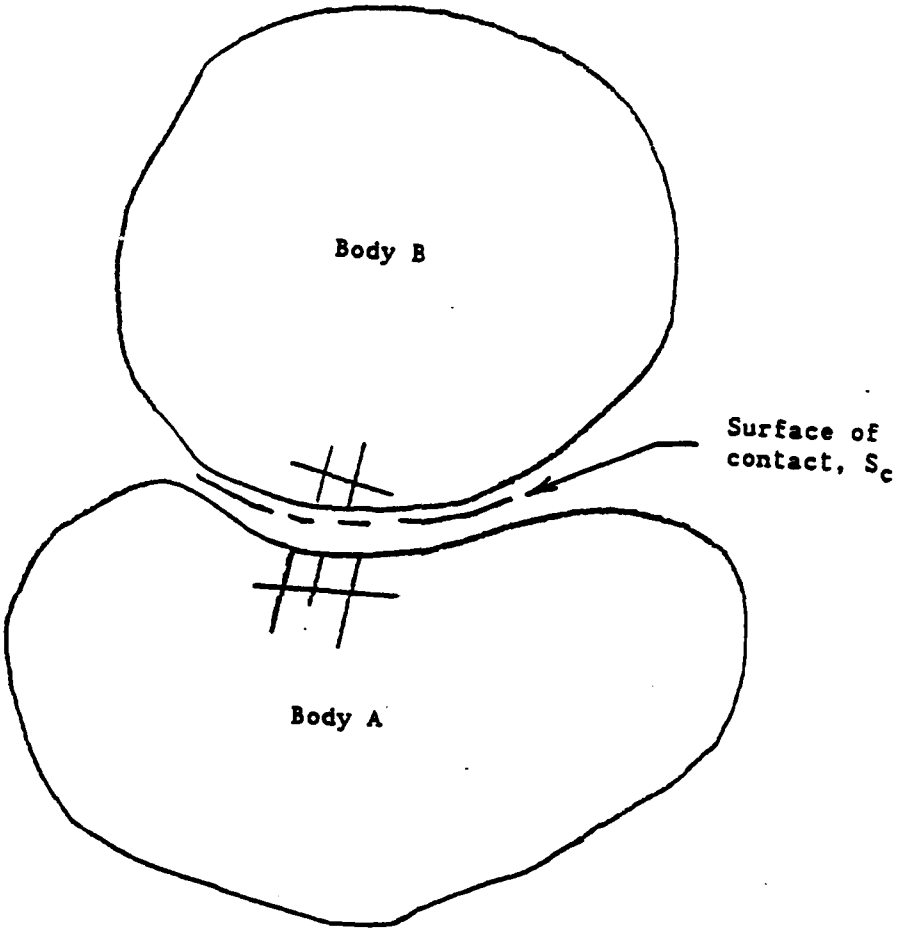

Figure 10 Definition of contact surface, S_c.

From the theory of elasticity certain conditions must be satisfied if two elastic bodies are in contact. First, in the region of contact the tractions are equal in magnitude and opposite in direction. Second, the normal tractions are compressive and the shear tractions oppose the direction of motion. Coulomb's law of friction is satisfied. Third, there are no gaps and no penetration in the region of contact.

The conditions above are imposed upon stresses and displacements in the region of contact as follows:

Displacements

$$X_i^A + U_i^A = X_i^B + U_i^B$$

Stresses

$$\begin{aligned} T_n^A + T_n^B &= 0 \\ T_s^A + T_s^B &= 0 \\ T_s^A &\leq \pm \mu T_n^A \\ T_s^B &\leq \pm \mu T_s^B \end{aligned} \tag{3.3}$$

where X_i are the coordinates before deformation, U_i are the displacements, T_n are the normal tractions on the surface of contact, T_s are the tangential tractions on the surface of contact, and μ is the coefficient of friction. The convention of the last of equations

(3.3) is such that tangential tractions counteract relative movement. The equality holds when there is sliding; otherwise the inequality holds.

The hybrid stress functional [38] is based on a modified complementary energy principle in which interelement traction continuity and mechanical boundary conditions have been released via the Lagrange Multiplier technique, and is given by

$$\Pi_{mc} = \sum_n \left\{ \int_{\nabla_n} S_{ijkl}\,\sigma_{ij}\,\sigma_{kl}\,d\nabla - \int_{S_n} U_i T_i\,dS + \int_{S_{\sigma_n}} \bar{T}_i U_i\,dS \right\} \tag{3.4}$$

where, S_{ijkl} is the elastic compliance tensor, T_i are tractions, $\bar{T}_i$ are prescribed tractions, σ_{ij} are stresses, ∇_n is the volume of the nth element. S_n is the interelement boundary of the nth element, and S_{σ_n} is the portion of the boundary of the nth element on which stresses are prescribed. $T_i = \sigma_{ij}\nu_j$ where ν_j are the outward unit normal components, and $\sigma_{ij,j} = 0$ from equilibrium. Note the second term of equation (2.1) is equivalent to the second term of equation (3.4). This is seen by applying the divergence theorem to the second term of equation (2.1) and requiring that stresses satisfy the homogeneous equilibrium equations (as required by the hybrid stress model).

The conditions of contact, equations (3.3), are introduced into the hybrid stress functional Π_{mc}, equation (3.4), using the Lagrange multiplier technique, where $\tilde{T}_n$ and $\tilde{T}_s$ are the Lagrange multipliers. The hybrid stress functional $\Pi_{mc}{}^c$, which includes the conditions of contact imposed upon the two contacting bodies within the zone of contact is stated in the form [38]:

$$\Pi_{mc}^{e} = \int_{V^{A+B}} S_{ijkl}\,\sigma_{ij}\,\sigma_{kl}\,dV - \int_{S_n^{A+B}} U_i T_i\,dS$$

$$+ \int_{S_{\sigma_n}^{A+B}} \bar{T}_i U_i\,dS - \int_{S_{cn}} \left\{ \tilde{T}_n \left[(U_n^A + X_n^A) - (U_n^B + X_n^B) \right] \right. \tag{3.5}$$

$$\left. + \tilde{T}_s \left[(U_s^A + X_s^A) - (U_s^B + X_s^B) \right] \right\} dS$$

To find the stationary value of the functional, we take the variation with respect to displacements, U_i, stress, σ_{ij}, and the Lagrange multipliers, $\tilde{T}_s$ and $\tilde{T}_n$. The resulting Euler equations which deal with the surface of contact are given by:

Displacements

$$(U_n^A + X_n^A) - (U_n^B + X_n^B) = 0$$
$$(U_s^A + X_s^B) - (U_s^B + X_s^B) = 0$$

Stresses

$$(\tilde{T}_n + T_n^A) = 0 \tag{3.6}$$
$$(\tilde{T}_n - T_n^B) = 0$$
$$(\tilde{T}_s + T_s^A) = 0$$
$$(\tilde{T}_s - T_s^B) = 0$$

Coulomb's law of friction is also one of the conditions of contact which must be satisfied. A constraint is therefore added to satisfy the condition dealing with the friction which occurs when the opposing bodies slide relative to one another; i.e:

$$\tilde{T}_s = \pm \mu \tilde{T}_n \quad . \tag{3.7}$$

Substituting equation (3.7) into the Euler equations which deal with the surface of contact, equation (3.6), yields

$$\begin{aligned}
&(U_n^A + X_n^A) - (U_n^B + X_n^B) = 0 \\
&(U_s^A + X_s^A) - (U_s^B + X_s^B) = 0 \\
&(T_n^A + T_n^B) = 0 \\
&(T_s^A + T_s^B) = 0 \\
&T_s^A \leq \mu T_n^A \\
&T_s^B \leq \mu T_n^B
\end{aligned} \tag{3.8}$$

These conditions on the field variables in the zone of contact are exactly the same as the conditions of contact. Thus, the functional Π_{mc}^{c}, equation (3.5), will satisfy the conditions of contact (within the zone of contact) necessary to solve the problem of two bodies in contact.

3.2.2 Incremental Assumed Hybrid Stress Formulation

Geometric nonlinearities in the relationship between load and displacement complicate the general contact problem; i.e. as loading conditions change, the surface of contact also changes in a nonlinear fashion. The best method to approach such a problem is with an incremental formulation. As the loading condition changes incrementally from state to state, the place of contact changes.

It is difficult to treat the contact surface as an unknown in the formulation because we are unable to compute the necessary integrals over the surface of contact. The method used to solve the contact problem involves assuming a contact surface and computing the field variables which render the functional stationary. It is then determined whether the field variables satisfy the conditions of contact within the contact zone. If the conditions of contact are not satisfied, another contact surface is assumed. This process (iteration) is repeated until all conditions are satisfied.

The nonlinear analysis becomes a step-by-step solution which has been decomposed into a series of linear incremental problems with initial conditions. For instance, a displacement u may be expressed in terms of an initial value, u^0, and and incremental value, Δu.

$$u = u^{\circ} + \Delta u \tag{3.9}$$

At the beginning of each step, the initial value of the field variables are, in general, not exact. Hence they may not satisfy stress equilibrium conditions or the compatibility requirements. Correction

terms for equilibrium and compatibility can be included in a finite element formulation based on an incremental variational principle. The incremental hybrid-stress functional for contact as developed by Kubomura [38] may be stated as:

$$\Pi_{mc}^{c} = \sum_{n} \left\{ \int_{\nabla_n^{A+B}} \frac{1}{2} \Delta\sigma_{ij} S_{ijkl} \Delta\sigma_{kl} \, d\nabla - \int_{\partial\nabla_n^{A+B}} \Delta T_i \Delta\tilde{U}_i \, dS \right.$$

$$- \int_{S_{\sigma_n}^{A+B}} \Delta\bar{T}_i \Delta\tilde{U}_i \, dS - \int_{S_{\sigma_n}+S_{cn}} T_i \Delta\tilde{U}_i \, dS + \int_{S_{\sigma_n}^{A+B}} \bar{T}_i \Delta\tilde{U}_i \, dS$$

(3.10)

$$\left. - \int_{S_n} (\tilde{T}_i + \Delta\tilde{T}_i) \left[(\tilde{U}_i^{A} + \Delta\tilde{U}_i^{A} + X_i^{A}) - (\tilde{U}_i^{B} + \Delta\tilde{U}_i^{B} + X_i^{B}) \right] dS \right\}$$

where:

$\Delta\sigma_{ij}$ is the incremental stress tensor.

ΔT_i are the incremental tractions.

$\Delta\tilde{U}_i$ are the incremental displacements on the boundary.

$\Delta\bar{T}_i$ are the incremental applied tractions.

$(\tilde{T}_i+\Delta\tilde{T}_i)$ are the nodal contact forces within the zone of contact.

$\tilde{U}_i$ are the displacements on the boundary, $\partial\nabla_n$.

∇_n is the volume of the n^{th} element.

$\partial\nabla_n$ is the boundary of the n^{th} element.

S_{σ_n} is the portion of the boundary surface on which tractions are prescribed.

S_{u_n} is the portion of the boundary surface on which displacements are prescribed.

S_{c_n} is the portion of the boundary surface the two bodies have in common, known as the contact zone.

When using the functional $\Pi_{mc}{}^{c}$ the following conditions must be exactly satisfied:

$$\Delta\sigma_{ij,j} = 0$$

$$\sigma_{ij,j} = 0$$

$$\Delta T_i = \Delta\sigma_{ij}\nu_j \qquad (3.11)$$

$$T_i = \sigma_{ij}\nu_j$$

$$\Delta\tilde{U} = \Delta\bar{U} \quad \text{on} \quad S_{u_n}$$

where $\overline{\Delta U}$ is the incremental form of the prescribed displacements.

The conditions of contact within the zone of contact, previously stated in equation (3.3), are stated now in an incremental form:

$$(T_n{}^A + \Delta T_n{}^A) + (T_n{}^B + \Delta T_n{}^B) = 0$$
$$(T_s{}^A + \Delta T_s{}^A) + (T_s{}^B + \Delta T_s{}^B) = 0$$

$$(T_s^A + \Delta T_s^A) \leq \pm\mu\,(T_n^A + \Delta T_n^A) \qquad (3.12)$$
$$(T_s^B + \Delta T_s^B) \leq \pm\mu\,(T_n^B + \Delta T_n^B)$$

$$(U_n^A + \Delta U_n^A + X_n^A) - (U_n^B + \Delta U_n^B + X_n^B) = 0$$
$$(U_s^A + \Delta U_s^A + X_s^A) - (U_s^B + \Delta U_s^B + X_s^B) = 0$$

where

T_n, ΔT_n are the initial and incremental tractions, respectively, normal to the contact surface.

T_s, ΔT_s are the initial and incremental tractions tangential to the contact surface respectively.

U_n, ΔU_n are the initial and incremental displacements normal to the contact surface, respectively.

U_s, ΔU_s are the initial and incremental displacements tangential to the contact surface, respectively.

X_n, X_s are the normal and shear components respectively of the coordinates before deformation.

One important feature of incremental solutions is that at the beginning of a loading increment the solution is, in general, not exact, hence it may not satisfy stress equilibrium conditions and it may also violate the compatibility conditions. The formulation of the functional $\Pi_{mc}{}^c$ takes into consideration the effect of initial equilibrium imbalance and leads to a system of matrix equations for the incremental solution with equilibrium correction Violation of displacement compati-

bility leads to an incremental solution which also contains corrections for the compatibility mismatch.

3.3 MATRIX EQUATIONS

The hybrid stress functional $\Pi_{mc}{}^{c}$, equation (3.10), for contact problems is stated below in matrix form:

$$
\begin{aligned}
\Pi_{mc}^{c} = \sum_{n} \Bigg\{ & \int_{\forall_n} \frac{1}{2} \Delta\underset{\sim}{\sigma}^{T} \underset{\sim}{f} \Delta\underset{\sim}{\sigma} \, d\forall \\
& - \int_{\partial\forall_n} \Delta T^{T} \Delta\tilde{U} \, ds \\
& + \int_{S_{\sigma n}} (\bar{T} + \Delta\bar{T})^{T} \Delta\tilde{U} \, ds \\
& - \int_{S_{\sigma n} + S_{cn}} \underset{\sim}{T}^{T} \Delta\underset{\sim}{\tilde{U}} \, ds \\
& - \int_{S_{cn}} (\tilde{T} + \Delta\tilde{T})^{T} (\Delta\tilde{U}^{A} - \Delta\tilde{U}^{B}) \, ds \\
& - \int_{S_{cn}} (\tilde{T} + \Delta\tilde{T})^{T} \left[(\tilde{U}^{A} + X^{A}) - (\tilde{U}^{B} + X^{B}) \right] ds
\end{aligned}
\tag{3.13}
$$

where $(\,)^T$ is the transpose of $(\,)$. The vectors and matrices are designated by underscoring with a tilde. The functional $\Pi_{mc}{}^{c}$, equation (3.13), includes equivalent nodal forces for the corrections of (a) initial material overlapping, (b) separation and (c) initial force imbalance at the surface of contact.

In the hybrid stress model $\Delta\sigma$ is interpolated in terms of a set of stress parameters such that the homogeneous equilibrium equations are satisfied.

$$\underset{\sim}{\Delta\sigma} = \underset{\sim}{P}\ \underset{\sim}{\Delta\beta} \tag{3.14}$$

The boundary tractions are related to the same stress parameters (using Cauchy's formula):

$$\underset{\sim}{\Delta T} = \underset{\sim}{R}\ \underset{\sim}{\Delta\beta} \tag{3.15}$$

The displacements are interpolated in terms of nodal displacements q and Δq:

$$\underset{\sim}{\Delta\tilde{U}} = \underset{\sim}{N}\ \underset{\sim}{\Delta q}$$

$$\underset{\sim}{\tilde{U}} = \underset{\sim}{N}\ \underset{\sim}{q} \tag{3.16}$$

Coordinates are interpolated in terms of their nodal values,

$$\underset{\sim}{X} = \underset{\sim}{N}\ \underset{\sim}{x} \tag{3.17}$$

The contact surface is also discretized into finite elements called contact elements having contact nodes. The contact tractions are interpolated in the contact element in terms of their nodal values, t in the form:

$$(\tilde{T} + \Delta\tilde{T}) = \underset{\sim}{M}\,\underset{\sim}{t} \tag{3.18}$$

We substitute equations (3.14-3.18) into equation (3.13) to obtain:

$$\begin{aligned}
\pi_{mc}^{c} = \sum^{n} \Bigg\{ & \int_{\nabla_n} \frac{1}{2}\Delta\underset{\sim}{\beta}^T \underset{\sim}{P}^T \underset{\sim}{S}\, \underset{\sim}{P}\, \Delta\underset{\sim}{\beta}\, d\nabla \\
& - \int_{\partial\nabla_n} \Delta\underset{\sim}{\beta}^T \underset{\sim}{R}^T \underset{\sim}{N}\, \Delta\underset{\sim}{q}\, d\nabla \\
& + \int_{S_{\sigma n}} \Delta\underset{\sim}{q}^T \underset{\sim}{N}^T \underset{\sim}{\bar{T}}\, dS \\
& + \int_{S_{\sigma n}} \Delta\underset{\sim}{\rho}^T \underset{\sim}{N}^T \underset{\sim}{L}\bar{T}\, dS \\
& - \int_{S_{\sigma n}+S_{cn}} \Delta\underset{\sim}{q}^T \underset{\sim}{N}^T \underset{\sim}{T}\, dS \\
& - \int_{S_{cn}} \underset{\sim}{t}^T \underset{\sim}{m}^T \underset{\sim}{N}\, (\Delta\underset{\sim}{q}^A - \Delta\underset{\sim}{q}^B)\, dS \\
& - \int_{S_{cn}} \underset{\sim}{t}^T \underset{\sim}{m}^T \underset{\sim}{N}\, \left[(\underset{\sim}{q}^A + \underset{\sim}{x}^A) - (\underset{\sim}{q}^B + \underset{\sim}{x}^B) \right] dS \Bigg\}
\end{aligned} \tag{3.19}$$

The following matrices are then defined

$$\underset{\sim}{H}_n = \int_{\nabla_n} \underset{\sim}{P}^T \underset{\sim}{S} \underset{\sim}{P} \, d\nabla$$

$$\underset{\sim}{G}_n = \int_{\partial V_n} \underset{\sim}{R}^T \underset{\sim}{N} \, ds$$

$$\Delta \underset{\sim}{Q}_n = \int_{S_{\sigma n}} \underset{\sim}{N}^T \Delta \underset{\sim}{\bar{T}} \, ds$$

$$\underset{\sim}{Q}_n = \int_{S_{\sigma n}} \underset{\sim}{N}^T \underset{\sim}{\bar{T}} \, ds \qquad (3.20)$$

$$\underset{\sim}{R}_{En}^{\circ} = \int_{S_{\sigma n} + S_{cn}} \underset{\sim}{N}^T \underset{\sim}{T} \, ds$$

$$\underset{\sim}{R}_{cn}^{\circ} = \int_{S_{cn}} \underset{\sim}{M}^T \underset{\sim}{N} \left[(\underset{\sim}{q}^A + \underset{\sim}{\chi}^A) - (\underset{\sim}{q}^B + \underset{\sim}{\chi}^B) \right] ds$$

$$\underset{\sim}{F}_n = \int_{S_{cn}} \underset{\sim}{M}^T \underset{\sim}{N} \, ds$$

where $\underset{\sim}{Q}_n$ and $\underset{\sim}{R}_{En}^{\circ}$ are stress equilibrium checks on S_{σ_n} and S_{cn}, respectively, and $\underset{\sim}{R}_{cn}$ is an initial mismatch check on S_{cn}.

Upon substitution of equations (3.20) the hybrid stress functional for contact problems becomes:

$$
\begin{aligned}
\Pi_{mc}^{e} = \sum \tfrac{1}{2}\, & \Delta\underline{\beta}^{A}\, \underline{H}_n^{A}\, \Delta\underline{\beta}^{A} - \Delta\underline{\beta}^{AT}\, \underline{G}_n^{A}\, \Delta\underline{q}^{A} \\
& + \Delta\underline{q}^{AT}\, \Delta\underline{Q}_n^{A} + \Delta\underline{q}^{AT}\, \underline{Q}_n^{A} - \Delta\underline{q}^{AT}\, \underline{R}_{En}^{A} \\
& + \tfrac{1}{2}\, \Delta\underline{\beta}^{BT}\, \underline{H}_n^{B}\, \Delta\underline{\beta}^{B} - \Delta\underline{\beta}^{BT}\, \underline{G}_n^{B}\, \Delta\underline{q}^{B} \\
& + \Delta\underline{q}^{BT}\, \Delta\underline{Q}_n^{B} + \Delta\underline{q}^{BT}\, \underline{Q}_n^{B} - \Delta\underline{q}^{BT}\, \underline{R}_{En}^{B} \\
& - \Delta\underline{q}^{A}\, \underline{F}_n^{AT}\, \underline{t} + \Delta\underline{q}^{B}\, \underline{F}_n^{BT}\, \underline{t} - \underline{t}^{T}\, \underline{R}_{cn}^{o}
\end{aligned}
\tag{3.21}
$$

The element nodal displacements and contact element nodal tractions are not independent from element to element. The element variables, (), can be related to their counterpart assembled structure variables, denoted here by ()*, by Boolean matrices, L_n^A, L_n^B, and L_n^t:

$$
\begin{aligned}
\underline{t} &= \underline{L}_n^{t}\, \underline{t}^{*} \\
\Delta\underline{q}^{A} &= \underline{L}_n^{A}\, \Delta\underline{q}^{A*} \\
\Delta\underline{q}^{B} &= \underline{L}_n^{B}\, \Delta\underline{q}^{B*} \\
\underline{q}^{A} &= \underline{L}_n^{A}\, \underline{q}^{A*} \\
\underline{q}^{B} &= \underline{L}_n^{B}\, \underline{q}^{B*}
\end{aligned}
\tag{3.22}
$$

Note that the element stress parameters, $\Delta\beta$, are independent from element to element. It is therefore not necessary to define a set of "structure" stress paramenters.

Equations (3.22) are substituted into equation (3.21) to yield:

$$\begin{aligned}\Pi_{mc}^{c} = \sum_n \Big\{ & \tfrac{1}{2}\,\Delta\underset{\sim}{\beta}^{AT} \underset{\sim}{H}_n^{A}\,\Delta\underset{\sim}{\beta}^{A} - \Delta\underset{\sim}{\beta}^{AT}\underset{\sim}{G}_n^{A}\underset{\sim}{L}_n^{A}\,\Delta\underset{\sim}{f}^{A*} \\ & + \underset{\sim}{f}^{*AT}\underset{\sim}{L}_n^{AT}\Delta\underset{\sim}{Q}^{A} + \Delta\underset{\sim}{f}^{A*T}\underset{\sim}{L}_n^{AT}\underset{\sim}{Q}_n^{A} - \underset{\sim}{f}^{A*T}\underset{\sim}{L}_n^{AT}\underset{\sim}{R}_{EN}^{A\circ} \\ & + \tfrac{1}{2}\Delta\underset{\sim}{\beta}^{BT}\underset{\sim}{H}_n^{B}\Delta\underset{\sim}{\beta}^{B} - \Delta\underset{\sim}{\beta}^{BT}\underset{\sim}{G}_n^{B}\underset{\sim}{L}_n^{B}\,\Delta\underset{\sim}{f}^{B*} \\ & + \underset{\sim}{f}^{*BT}\underset{\sim}{L}_n^{BT}\,\Delta\underset{\sim}{Q}_n^{B} + \Delta\underset{\sim}{f}^{B*T}\underset{\sim}{L}_n^{T}\underset{\sim}{Q}_n^{B} \\ & - \Delta\underset{\sim}{f}^{B*T}\underset{\sim}{L}_n^{BT}\underset{\sim}{R}_{EN}^{B\circ} - \underset{\sim}{t}^{*}\underset{\sim}{L}_n^{tT}\underset{\sim}{R}_{Gn}^{\circ} \\ & - \Delta\underset{\sim}{f}^{*AT}\underset{\sim}{L}_n^{AT}\underset{\sim}{F}_n^{AT}\underset{\sim}{L}_n^{t}\underset{\sim}{t}^{*} + \Delta\underset{\sim}{f}^{*BT}\underset{\sim}{L}_n^{BT}\underset{\sim}{F}_n^{B}\underset{\sim}{L}_n^{t}\underset{\sim}{t}^{*} \Big\}\end{aligned} \tag{3.23}$$

The stationary condition of Π_{mc}^{c} gives:

$$\begin{aligned}\delta\Pi_{mc}^{c} = \sum_n \Big\{ & \delta\Delta\underset{\sim}{\beta}^{AT}\left(\underset{\sim}{H}_n^{A}\Delta\underset{\sim}{\beta}^{A} - \underset{\sim}{G}_n^{A}\underset{\sim}{L}_n^{A}\,\Delta\underset{\sim}{f}^{A*}\right) \\ & + \delta\Delta\underset{\sim}{\beta}^{BT}\left(\underset{\sim}{H}_n^{B}\Delta\underset{\sim}{\beta}^{B} - \underset{\sim}{G}_n^{B}\underset{\sim}{L}_n^{B}\,\Delta\underset{\sim}{f}^{B*}\right) \\ & + \delta\Delta\underset{\sim}{f}^{A*T}\left(-\underset{\sim}{L}_n^{AT}\underset{\sim}{G}_n^{AT}\Delta\underset{\sim}{\beta}^{AT} + \underset{\sim}{L}_n^{BT}\Delta\underset{\sim}{Q}_n^{B} + \underset{\sim}{L}_n^{B}\underset{\sim}{Q}_n^{B}\right. \\ & \left. - \underset{\sim}{L}_n^{BT}\underset{\sim}{R}_{EN}^{\circ B} - \underset{\sim}{L}_n^{BT}\underset{\sim}{F}_n^{BT}\underset{\sim}{L}_n^{t}\underset{\sim}{t}^{*}\right)\end{aligned}$$

$$+ \delta t^{*T} \left(- \underset{\sim}{L}_n^{AT} \underset{\sim}{F}_n^{A} \underset{\sim}{L}_n^{t} \underset{\sim}{\Delta q}^{A*} \right.$$

$$+ \underset{\sim}{L}_n^{BT} \underset{\sim}{F}_n^{B} \underset{\sim}{L}_n^{t} \underset{\sim}{\Delta q}^{B*}$$

$$\left. - \underset{\sim}{L}_n^{tT} \underset{\sim}{R}_{En}^{\circ} \right) \Big\} = 0 \qquad (3.24)$$

Therefore, for arbitrary $\delta\underset{\sim}{\Delta\beta}^{AT}$, $\delta\underset{\sim}{\Delta\beta}^{BT}$, $\delta\underset{\sim}{\Delta q}^{*AT}$, $\delta\underset{\sim}{\Delta q}^{*BT}$, and $\delta\underset{\sim}{t}^{*T}$ not equal to zero, the following equations must be satisfied:

$$\underset{\sim}{H}_n^{A} \underset{\sim}{\Delta\beta}^{A} - \underset{\sim}{G}_n^{A} \underset{\sim}{L}_n^{A} \underset{\sim}{\Delta q}^{A*} = 0$$

$$\underset{\sim}{H}_n^{B} \underset{\sim}{\Delta\beta}^{B} - \underset{\sim}{G}_n^{B} \underset{\sim}{L}_n^{B} \underset{\sim}{\Delta q}^{B*} = 0$$

$$\sum_n \left(- \underset{\sim}{L}_n^{A} \underset{\sim}{G}_n^{AT} \underset{\sim}{\Delta\beta}^{AT} + \underset{\sim}{L}_n^{AT} \underset{\sim}{\Delta Q}_n^{A} \right.$$

$$\left. + \underset{\sim}{L}_n^{AT} \underset{\sim}{Q}_n^{A} - \underset{\sim}{L}_n^{AT} \underset{\sim}{R}_{En}^{A\circ} - \underset{\sim}{L}_n^{AT} \underset{\sim}{F}_n^{AT} \underset{\sim}{L}_n^{t} \underset{\sim}{t}^{*} \right) = 0$$

$$\sum_n \left(- \underset{\sim}{L}_n^{B} \underset{\sim}{G}_n^{BT} \underset{\sim}{\Delta\beta}^{BT} + \underset{\sim}{L}_n^{BT} \underset{\sim}{\Delta Q}_n^{B} \right. \qquad (3.25)$$

$$\left. + \underset{\sim}{L}_n^{BT} \underset{\sim}{Q}_n^{B} - \underset{\sim}{L}_n^{BT} \underset{\sim}{R}_{En}^{B\circ} - \underset{\sim}{L}_n^{BT} \underset{\sim}{F}_n^{BT} \underset{\sim}{L}_n^{t} \underset{\sim}{t}^{*} \right) = 0$$

$$\sum_n \left(-\underset{\sim}{L_n}^{AT}\underset{\sim}{F_n}^{A}\underset{\sim}{L_n}^{t}\underset{\sim}{\Delta q}^{A*} + \underset{\sim}{L_n}^{TB}\underset{\sim}{F_n}^{B}\underset{\sim}{L_n}^{t}\underset{\sim}{\Delta q}^{B*} - \underset{\sim}{L_n}^{tT}\underset{\sim}{R_{cn}}^{\circ}\right) = 0$$

Since $\Delta\beta$ are independent from element to element they can be eliminated on the element level by solving the first of equations (3.25):

$$\underset{\sim}{\Delta\beta}^{A} = \underset{\sim}{H_n}^{A-1}\underset{\sim}{G_n}^{A}\underset{\sim}{L_n}^{A}\underset{\sim}{\Delta q}^{A*}$$

$$\underset{\sim}{\Delta\beta}^{B} = \underset{\sim}{H_n}^{B-1}\underset{\sim}{G_n}^{B}\underset{\sim}{L_n}^{B}\underset{\sim}{\Delta q}^{B*} \qquad (3.26)$$

Substitution of equation (3.26) into the third and fourth of equations (3.25) yields

$$\sum_n \underset{\sim}{L_n}^{AT}\underset{\sim}{k_n}^{A}\underset{\sim}{L_n}^{A}\underset{\sim}{\Delta q}^{A*} + \underset{\sim}{L_n}^{AT}\underset{\sim}{F_n}^{AT}\underset{\sim}{L_n}^{t}\underset{\sim}{t}^{*} = \underset{\sim}{L_n}^{AT}\underset{\sim}{\Delta Q_n}^{A} + \underset{\sim}{L_n}^{AT}\underset{\sim}{Q_n}^{A} - \underset{\sim}{L_n}^{AT}\underset{\sim}{R_{\varepsilon n}}^{\circ A} \qquad (3.27)$$

$$\sum_n \underset{\sim}{L_n}^{BT}\underset{\sim}{k_n}^{B}\underset{\sim}{L_n}^{B}\underset{\sim}{\Delta q}^{B*} - \underset{\sim}{L_n}^{BT}\underset{\sim}{F_n}^{BT}\underset{\sim}{L_n}^{t}\underset{\sim}{t}^{*} = \underset{\sim}{L_n}^{BT}\underset{\sim}{\Delta Q_n}^{B} + \underset{\sim}{L_n}^{BT}\underset{\sim}{Q_n}^{B} - \underset{\sim}{L_n}^{BT}\underset{\sim}{R_{\varepsilon n}}^{\circ B}$$

where

$$\underset{\sim}{k_n}^{A} = \underset{\sim}{G_n}^{AT}\underset{\sim}{H_n}^{A-1}\underset{\sim}{G_n}^{A}$$

$$\underset{\sim}{k_n}^{B} = \underset{\sim}{G_n}^{BT}\underset{\sim}{H_n}^{B-1}\underset{\sim}{G_n}^{B} \qquad (3.28)$$

Equation (3.28) defines the element stiffness matrices. The summation over n in equation (3.27) corresponds to the usual assembly operation. Applying this to equation (3.27) and the last of equations (3.25) gives:

$$K^{*A}\Delta q^{*A} + F^{AT*}t^{*} = \Delta Q^{A*} + Q^{A*} - R_{E}^{A*\circ}$$

$$K^{*B}\Delta q^{*B} + F^{BT*}t^{*} = \Delta Q^{B*} + Q^{B*} - R_{E}^{B*\circ} \qquad (3.29)$$

$$-\underset{\sim}{F}^{A*}\underset{\sim}{\Delta q}^{A*} + \underset{\sim}{F}^{B*}\underset{\sim}{\Delta q}^{B*} - \underset{\sim}{R}_{C}^{*\circ} = 0$$

Equations (3.29) may be collected in matrix form in the following manner:

$$\begin{bmatrix} \underset{\sim}{K}^{*A} & 0 & \underset{\sim}{F}^{*AT} \\ 0 & \underset{\sim}{K}^{*B} & -\underset{\sim}{F}^{*BT} \\ \underset{\sim}{F}^{*A} & -\underset{\sim}{F}^{*B} & \underset{\sim}{0} \end{bmatrix} \begin{Bmatrix} \underset{\sim}{\Delta q}^{A*} \\ \underset{\sim}{\Delta q}^{B*} \\ t^{*} \end{Bmatrix} \qquad (3.30)$$

$$= \begin{Bmatrix} \Delta Q^{*A} + Q^{*A} - R_{E}^{*\circ A} \\ \Delta Q^{*B} + Q^{*B} - R_{E}^{*\circ B} \\ -R_{C}^{*\circ} \end{Bmatrix}$$

For the contacting bodies, $\underset{\sim}{K}^{*A}$, $\underset{\sim}{K}^{*B}$ is assembled and constrained. The only portion of equation (3.31) which must be recomputed for each iteration are the contact stiffnesses, $\underset{\sim}{F}^{*A}$, $\underset{\sim}{F}^{*B}$ the global stiffnesses of A and B remain constant. In practice using the first two of equations (3.29) to solve for $\underset{\sim}{\Delta q}^{*A}$ and $\underset{\sim}{\Delta q}^{*B}$ in terms of $\underset{\sim}{t}^{*}$. $\underset{\sim}{\Delta q}^{*A}$ and $\underset{\sim}{\Delta q}^{*B}$ are substituted into the last of equations (3.29). Once $\underset{\sim}{t}^{*}$ was found, $\underset{\sim}{\Delta q}^{*A}$ and $\underset{\sim}{\Delta q}^{*B}$ were found using back substitution. The assembled contact stiffnesses are very sparce; i.e. only the displacement degrees of freedom which fall on the contact surface will contribute to the contact stiffness. The sparcity is considered in order to minimize the number of multiplications necessary to find a solution.

3.4 THE CONTACT ELEMENT FOR LAMINATE EDGE CONTACT

As described earlier, the first step to begin an increment or iteration is to assume the location of the contact surface, S_c, between the two contacting bodies (Figure 10). The contact surface is divided into contact elements with contact nodes (Figure 11). It was determined that the elements should have three nodes so that they would be compatible with the number of nodes along one side of the multilayer laminated composite plate element (MQH3T) which has been described in the previous chapter.

The normal and tangential tractions are interpolated along the contact surface in terms of their values at the three contact nodes using the quadratic distribution given by: where ξ varies from -1 to 1, as seen in Figure 11, and $\underset{\sim}{t}_n$ and $\underset{\sim}{t}_s$ are the nodal values of the normal and tangential components respectively of the contact tractions.

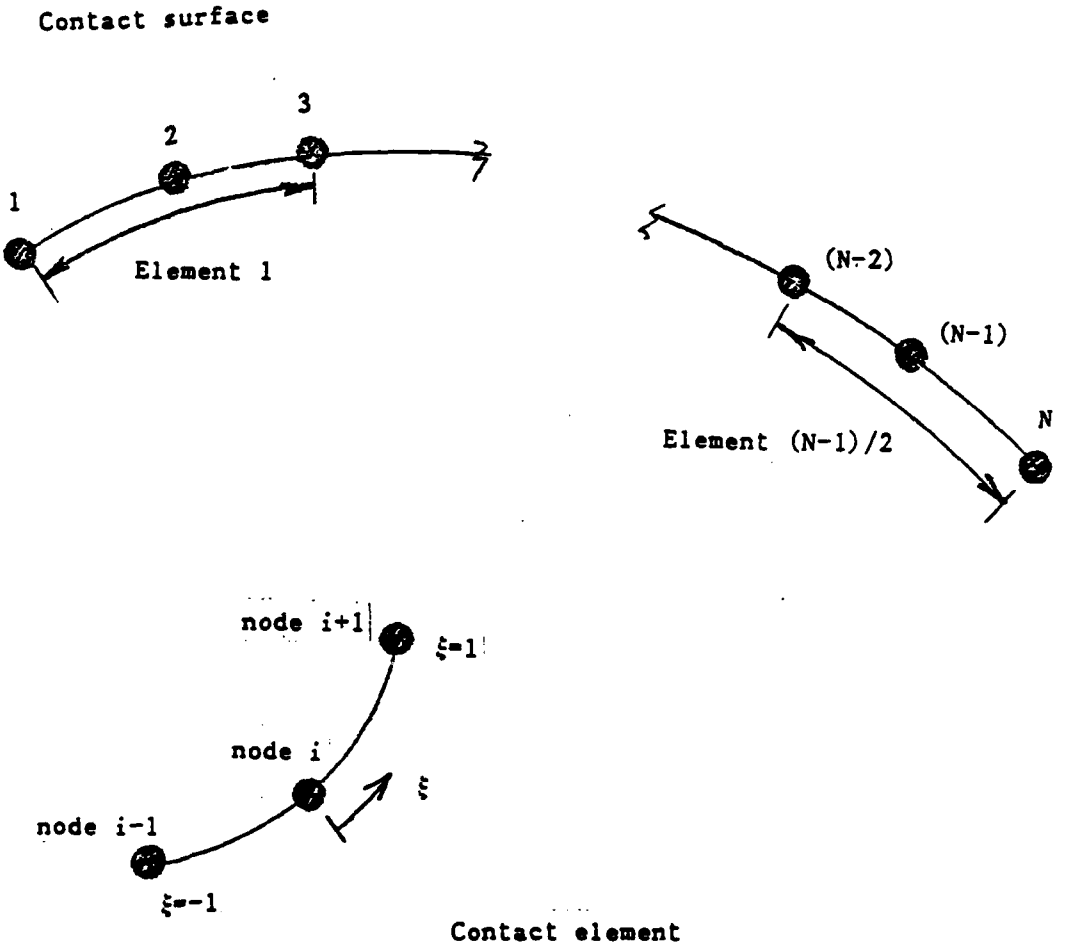

Figure 11 Typical contact surface and description of a single contact element.

$$\tilde{T}_n + \Delta\tilde{T}_n = \frac{1}{2}(\xi^2 - \xi)t_n^{i-1} + (1-\xi^2)t_n^{i} + \frac{1}{2}(\xi^2 + \xi)t_n^{i+1}$$

$$\tilde{T}_s + \Delta\tilde{T}_s = \frac{1}{2}(\xi^2 - \xi)t_s^{i-1} + (1-\xi^2)t_s^{i} + \frac{1}{2}(\xi^2 + \xi)t_s^{i+1} \qquad (3.31)$$

The relationship described in equation (3.31) is stated in matrix form by equation (3.18), and defines the matrix $\underset{\sim}{M}$. The contact element stiffness, $\underset{\sim}{F}_n$, can then be computed by integrating over the contact surface using the last of equations (3.20).

In the present formulation, it is not necessary for the nodes of one elastic body to be in contact with the nodes of the opposing body along the contact surface. Nor is it necessary for the nodes of either elastic body to be in contact with the contact nodes. A contact surface is assumed to be fixed in the coordinate system but not necessarily to the contacting bodies. The contact surface and the contact nodes are assumed to be known in order to perform the integrals along the contact surface, S_c.

In application, the interval of the integral is broken into a sum of integrals each of which is over an area in which one contact element is in contact with one body element. In Figure 12, the interval of the first integral begins at node 1 of contact element A and corresponds to the degrees of freedom at the 3 nodes of body element a and also to the contact tractions at the 3 nodes of contact element A. The interval of the first integral ends at node 3 of the body element a. The second integral begins at the first node of the body element b and ends at the third node of contact element A. The third integral begins at the first

node of contact element B and continues to the third node of body element b.

This process continues until the end of the contact surface is reached. As the integrals are evaluated they are assembled to form the contact stiffness $\underset{\sim}{F}^*$.

AD-A160 453 DEVELOPMENT OF A REDUCED MINDLIN HYBRID STRESS THIN MULTILAYER PLATE ELEM..(U) ILLINOIS UNIV AT CHICAGO CIRCLE DEPT OF CIVIL ENGINEERING MEC..

2/2

UNCLASSIFIED R L SPILKER ET AL. AUG 85 AMMRC-TR-85-23 F/G 4/2 NL

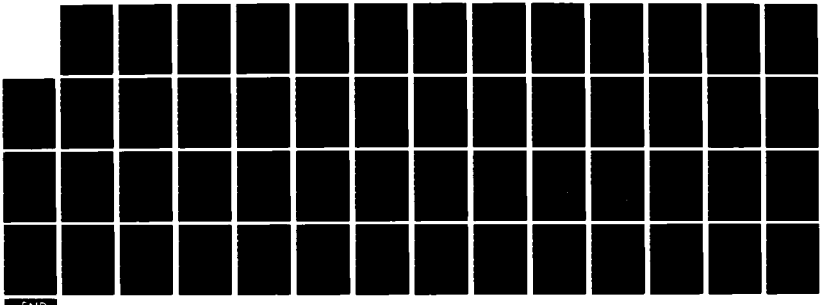

END

FILMED

DTIC

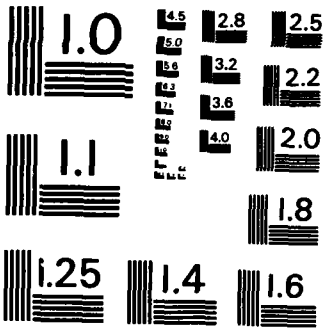

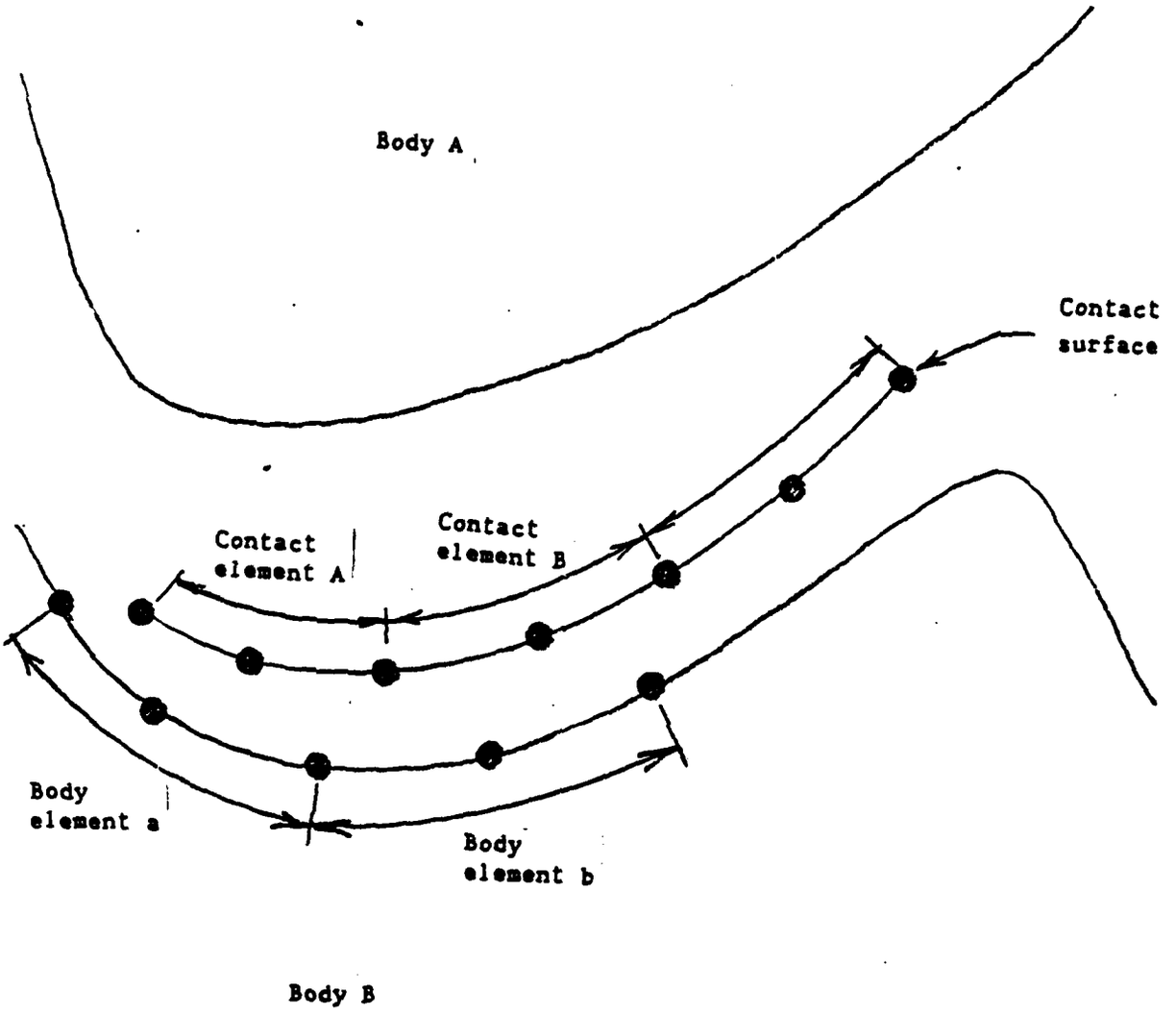

Figure 12 Description of how the integral necessary to compute the contact stiffness is broken up along the contact surface.

3.5 SOLUTION TECHNIQUE

3.5.1 Introduction

Throughout the formulation, the contact surface has been assumed to be known. As the load varies, a major portion of the solution is to vary the contact surface

The overall strategy for solving the contact problem is illustrated in Figure 13, and is briefly summarized as follows (for the Nth increment and the kth node):

1. The Nth increment of external load or prescribed displacement is applied.
2. A contact surface is assumed along with the contact nodes on the contact surface. Each contact node is assumed to be sliding or not sliding.
3. The necessary matrices are calculated and assembled. Then for the i^{th} iteration of the N^{th} load step, incremental displacements ${}^{i}\Delta U_k$, and contact tractions ${}^{i}(\tilde{T}_k+\Delta\tilde{T}_k)$ are solved for from the finite element matrix equation (3.31).
4. Knowing the total displacement ${}^{N-1}U_k$ at the end of the previous loading step (N-1), the total displacements ${}^{N-1}U_k$ + $\Delta^{i}U_k$ on the boundary are checked to determine if the displacements satisfy the condition that there are no gaps and no penetration in the region of contact. The contact tractions ${}^{i}(\tilde{T}_k+\Delta\tilde{T}_k)$ are checked to determine if the normal tractions are compressive and if Coulomb's law of friction, equation (3.2), is satisfied. If any of these conditions are not satisfied, the

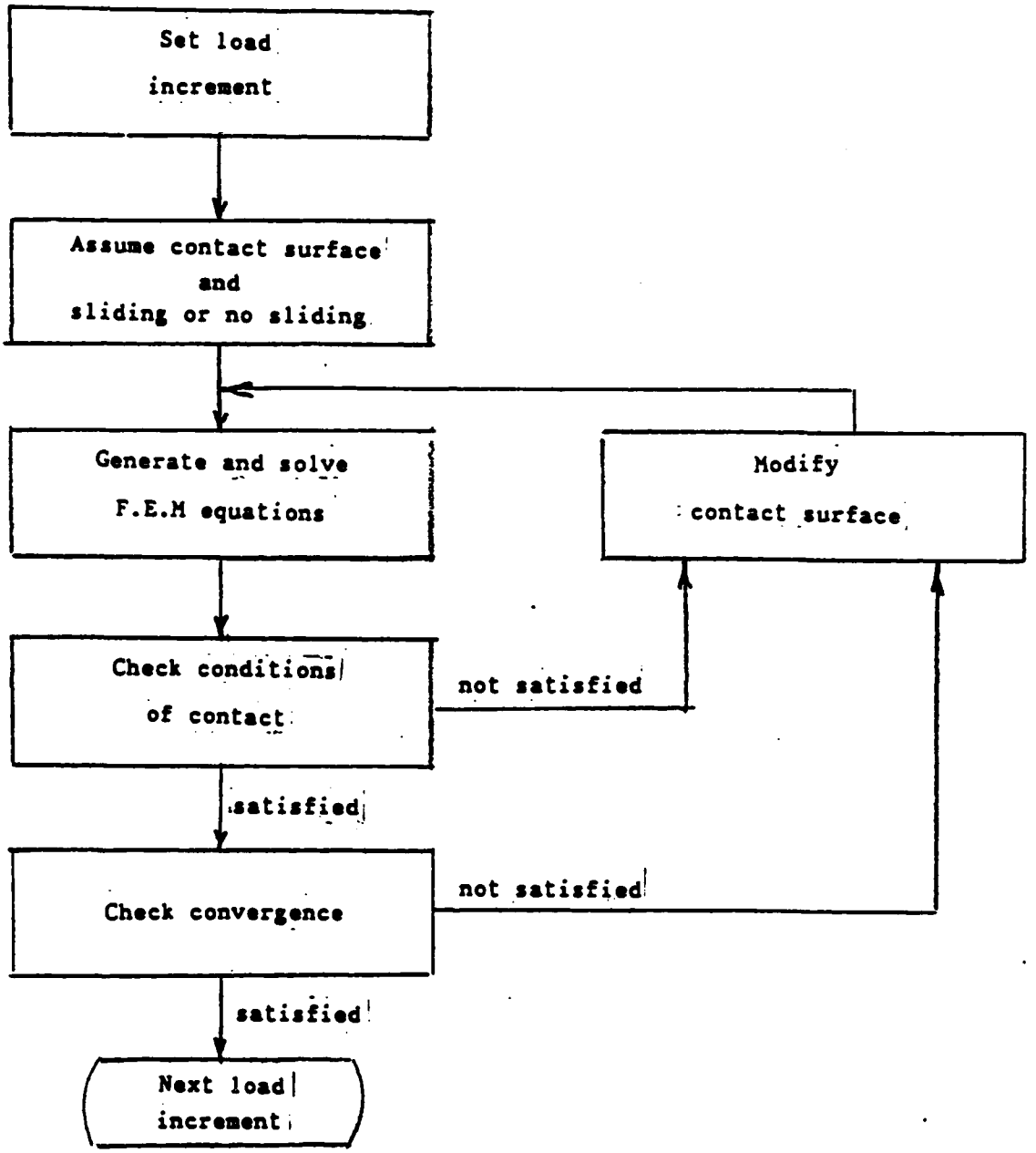

Figure 13 Summary of the solution technique for solving the problem of contact between two elastic bodies using the hybrid stress formulation.

location of the assumed contact surface is modified and steps 3 and 4 are repeated until the conditions of contact are satisfied.

5. Once the conditions described above have been satisfied a convergence check is made. If the solution is not converged steps 3 - 5 are repeated until the solution does converge.

Specifically the conditions of contact are listed below with a brief description of the manner in which the contact surface is modified if the condition of contact is not satisfied.

1. The first condition of contact states that the nodes of one body beyond the last contacting node may not penetrate the other body. If the elastic bodies in contact have overlapped, the contact surface is extended to include the contact nodes that penetrated the opposing body. Subsection 3.5.2 will describe the method used to extend the contact surface.
2. The second condition of contact states that normal tractions along the surface of contact must be compressive. If the normal traction at any two contact nodes within a single contact element are found to be tensile, the contact element is excluded from the contact surface. Subsection 3.5.3 will explain the method used to release contact nodes.
3. The third condition of contact is the relationship between normal and tangential contact tractions:

$$|\tilde{T}_s + \Delta\tilde{T}_s| \leq \mu |\tilde{T}_n + \Delta\tilde{T}_n| \qquad (3.32)$$

If the equation (3.32) is not satisfied then the constraint in equation (3.33) is applied and the contact node is assumed to be sliding. Subsection 3.5.4 will describe the method to satisfy the relationship between normal and tangential contact tractions.

$$|\tilde{T}_s + \Delta\tilde{T}_s| = \mu |\tilde{T}_n + \Delta\tilde{T}_n| \tag{3.33}$$

Subsection 3.5.5 will describe the method employed to check for convergence.

3.5.2 Extension of the contact surface

As previously described the first condition of contact states that nodes of neither body beyond the last contacting node may penetrate the opposing body. Each node outside the zone of contact along the surface of two elastic bodies which may come in contact with the opposing body is checked to determine if it has penetrated the surface of the opposing body.

The method to determine if nodes of one body have penetrated the other is described as follows:

1. The first step is to check if any nodes in body A penetrate body B. The x-coordinate of each node on body A is compared to the x-coordinates of the nodes on the surface of body B to determine between which two nodes on body B the node on body A falls. The

y-coordinate of the surface of body B is computed at the x-coordinate at which the node of body A is located. Thus it can be determined if the node has penetrated the surface.

2. The second step is to check if any nodes on body B penetrate body A in a manner similiar to that which has just been explained. Once it has been determined which nodes have penetrated the opposing body for both elastic bodies, the contact surface is extended to include these nodes.

3. The third step is to extend the contact surface. Figure 14 illustrates before and after the solution for an iteration has been computed. Node 4 and node 5 of each body have penetrated the opposing body. The contact surface is extended to include nodes 4 and 5 of body B. The coordinates of the new node 4 of body B are chosen by constructing a straight line between the locations of node 4 of body B for the solution of the previous iteration and the solution of the present iteration. The new location of node 4 of body B is located along this line midway between the boundary of body A and the boundary of body B. The new location of node 5 on body B is found in a similiar manner.

The nodes of body A which have penetrated body B are then placed on the contact surface in the following manner. A straight line is drawn between the location of node 4 for the previous solution and the present solution. Another straight line is drawn between the new nodes 4 and 5 of body B. The new node 4 of body A is found at the intersection of these two straight lines just mentioned. The nodes of body A which have

converged solution of load increment (I-1)

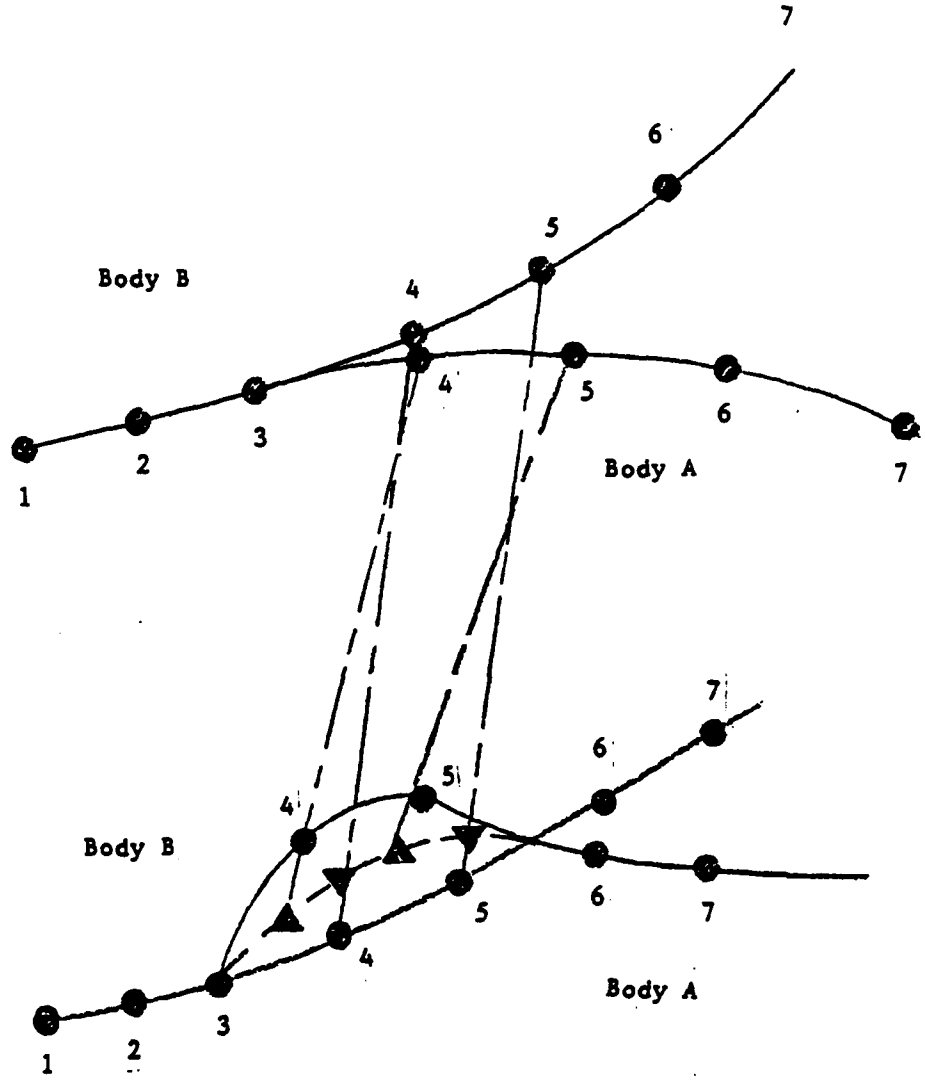

Solution of the ith iteration for load increment I

Figure 14 Description of how the contact surface is extended to include nodes outside the contact surface which have penetrated the opposing body.

penetrated body B beyond the last new node on body B are not added, so that the end node on the contact surface might always be a node on body B.

As a result of nodes 4 and 5 of bodies A and B penetrating the oposing body, the contact surface is extended to include nodes 4 and 5 of body B and node 4 of body A.

3.5.3 Release of Contact Nodes

Once the solution has been calculated for a given iteration, all the contact nodes are checked to determine whether or not the normal traction is compressive. The contact elements used each have three nodes as described previously in Section 3.4. The method used to determine whether or not to exclude a contact element from the contact surface was to drop any element in which the majority of its nodes have tensile normal tractions. In other words, at least two out of three nodes must have tensile normal contact tractions to exclude the contact element from the contact surface.

3.5.4 Satisfaction of the Relationship between Normal and Tangential Contact Tractions

As the load is applied incrementally to one or both of the elastic bodies in contact, the location of the zone of contact will change. It is possible for the locations of the contact nodes to also change as well as the type of contact, i.e. whether or not the contacting bodies are allowed to slide relative to one another at any particular node.

To simplify programming efforts for this problem we have chosen to locate the contact nodes along the contact surface in the same location as the nodes along the surface of body B.

If no sliding occurred during the i^{th} iteration, the location of the nodes on body A are located by maintaining the ratio of $\Delta L/L$ found from the converged solution for the last load increment illustrated in Figure 15 and stated as follows:

$$\frac{\Delta L}{L} = \left| \frac{A_1^{N-1} - B_1^{N-1}}{B_2^{N-1} - B_1^{N-1}} \right| = \left| \frac{{}^{i}A_1^{N} - {}^{i}B_1^{N}}{{}^{i}B_2^{N} - {}^{i}B_1^{N}} \right| \tag{3.34}$$

Therefore ${}^{i}A_1^{N}$ may be located. The following test is made at each contact node.

$$| \tilde{T}_s + \Delta \tilde{T}_s | < \mu | \tilde{T}_n + \Delta \tilde{T}_n | \tag{3.35}$$

If the condition is not satisfied at a contact node the following constraint is introduced:

$$| \tilde{T}_s + \Delta \tilde{T}_s | = \mu | \tilde{T}_n + \Delta \tilde{T}_n | \tag{3.36}$$

The state of the contact node is then changed to sliding.

If sliding has occurred during the ith iteration, the location of the nodes of body A are found by projecting them perpendicularly onto the contact surface. The following test is made at each node on body A to determine whether of not the node will continue to slide.

$$\left| \frac{\Delta L}{L} - \frac{\Delta L'}{L'} \right| < \varepsilon \tag{3.37}$$

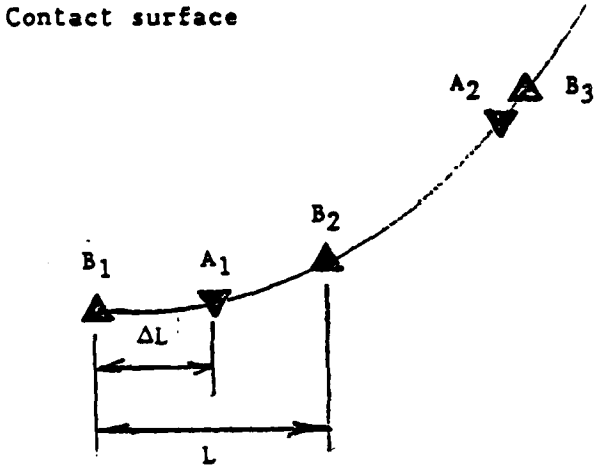

Converged solution for the (N-1)th load increment

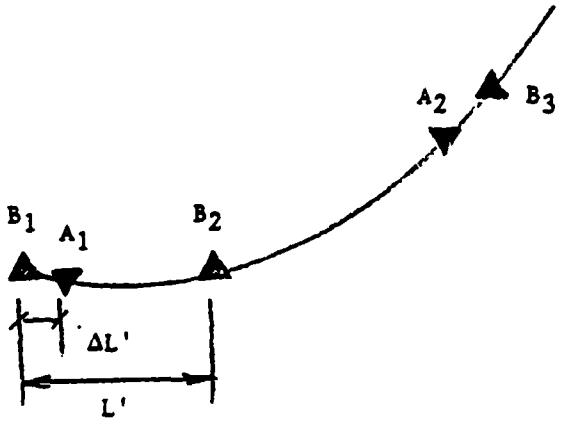

Solution after the ith iteration of the Nth load increment

Figure 15 Description of ratios used to determine whether or not a node is classified as sliding or not sliding.

where ϵ is some prescribed small number and $\Delta L'$, L' are illustrated in Figure 15. If this comparison is satisfied, the node will continue to slide. If this comparison is not satisfied, the sliding condition, equation (3.36), is dropped and the nodes of body A are relocated in the manner previously described for the state of no sliding.

Thus after each iteration the locations of nodes for both of the contacting bodies are found along the zone of contact as well as the state, i.e. sliding or no sliding at each node.

3.5.5 Convergence

Once the conditions of contact are satisfied a test of convergence may be made,

$$R = \left| \frac{{}^{i+1}\Delta U_k - {}^{i}\Delta U_k}{{}^{i+1}\Delta U_k} \right| \tag{3.38}$$

where ΔU_k is the displacement at the k^{th} degree of freedom. If R is less than a prescribed quantity the solution is considered converged.

3.6 EXAMPLE PROBLEMS AND NUMERICAL RESULTS

In this section, the finite element model and solution scheme developed in this chapter is applied to problems of contact between a disk and the edge of a rectangular plate (used to simulate a semi-infinite half-space). This model problem was selected for several practical reasons:

1. For elastic bodies, an analytic solution exists for the problem of frictionless contact between a disk and a semi-infinite half-space.
2. It was determined that a relatively coarse mesh would be required in order to not exceed available core storage. Comparison with an available analytic solution was necessary for identification of an adequate mesh.

The thin multilayer plate element, MQH3T, developed in the previous chapter, has been used to model each of the contacting bodies. Attention is restricted to symmetric laminates (i.e. no bending/stretching coupling) subject to contact by a cylindrical isotropic body. It is assumed that contact varies only in the x-y plane (i.e independent of the plate thickness direction). Thus transverse displacement and cross-section rotations are zero. In order to conserve computer core storage, all transverse displacements and cross-section rotations have been constrained to be zero.

After substantial trial and error, the mesh shown in Figure 16 was selected. The semi-infinite half space is simulated by a finite plate with the same overall dimensions of the disk due to the limitation on the number of elements. There were not enough elments available to make

a transition from the very small elements near the contact zone to the very large elements far away from the contact zone. Note that core storage of 4096k was needed for this mesh even after constraining the transverse displacements and cross-section rotations. (The major storage requirements correspond to the assembled stiffness and the product $H^{-1}G$ stored for each element.)

At this point due to the coarse mesh which was used, there is a necessary lack of automation to find a reasonable solution. For each increment of load it was necessary to make sample runs and compare them to one another in order to find the increment of applied displacement that would bring the desired number of contact elements into contact. This was accomplished by keeping the magnitude of the contact traction at the last node to come into contact as close to zero as possible. If the magnitude of the last contact traction was negative, the magnitude of the increment of applied displacement was manually increased. If the magnitude of the last contact traction was greater than the contact traction at its neighboring node the magnitude of the increment of applied displacement was manually decreased. For a finer mesh this would not be necessary; i.e. load or displacement increments could be imposed automatically.

The following problems were solved:

1. Moderate sliding frictionless contact of a deformable disk with a deformable semi-infinite half-space.
2. Moderate sliding frictionless contact of a nearly rigid disk with a deformable semi-infinite half-space.

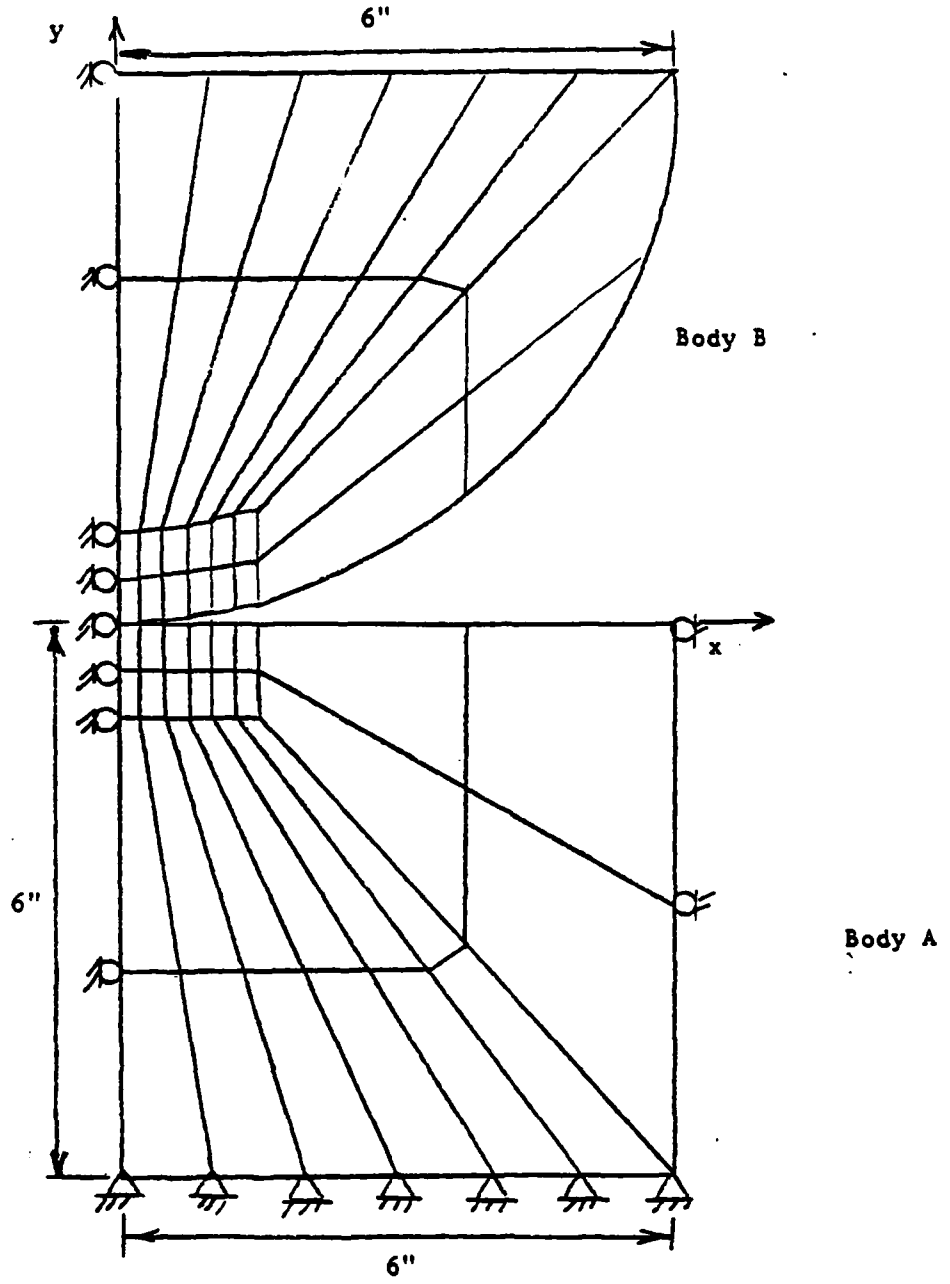

Figure 16 Mesh and boundary conditions for the problem of contact between an elastic disk and an elastic half-space.

3. Moderate sliding frictionless contact of a nearly rigid disk with a symmetric multilayer composite plate.

In the following subsections, the solution of each problem is discussed in detail and compared with independent solutions when available.

3.6.1 Contact between an Elastic Disk and an Elastic Half-space

The problem of frictionless contact between an elastic disk, and an elastic half-space has been solved by Hertz [49]. The problem is also solved in this section by the finite element method and results are compared with the Hertz solution.

The mesh and boundary conditions are shown in Figure 16. The material was isotropic and the material properties for both the disk and the half-space are $E=1x10^3$ psi. and $\nu=.25$. Quantities of interest are the contact tractions, $(T+\Delta T)$ and the distributions of σ_y in the half-space near the boundary (y=0) and near the plane of symmetry (x=0).

The solution is presented for the case of prescribed displacements applied to the top of the disk. The prescribed displacements were applied in three increments. For the first increment equal to -.9698 in. two elements are in contact, the second increment equal to -.148 in. has four elements in contact and the third increment equal to -.0942 in. has five elements in contact.

Figure 17 illustrates the distribution of the contact traction, $(T+\Delta T)$ along the zone of contact as they compare with the Hertz solution. The contact tractions calculated only at 2 point Gauss stations of the contact element are shown in Figure 18. The 2x2 Gauss stations were shown in the previous chapter to be "optimal sampling points". The

magnitudes of the contact tractions calculated at these points agree very closely with the Hertz solution.

The contact surface traction are calculated by a second method using the stress distributions and the stress coefficients $\Delta\beta$'s assumed within each plate element. The distribution of the contact tractions are compared with the Hertz solution in Figure 19. Once again the distribution of contact traction agrees well with the Hertz solution.

Stresses in the half-space near the surface at y=0 are shown in Figure 20. They are calculated from the plate elements at the 2x2 Gauss stations nearest the y=0 boundary. The stresses within the half-space near the surface are only slightly smaller than the tractions on the surface as would be expected. The stress tends toward zero as x increases. Stresses in the half-space near the plane of symmetry are shown in Figure 21. They are also calculated at the 2x2 Gauss stations in the plate elements. The stress is maximum at the surface and decreases to a minimum value as y decreases. The accurate prediction of stress within the half-space for this problem shows the mesh is fine enough so that one may expect good results for problems which have no analytic solution.

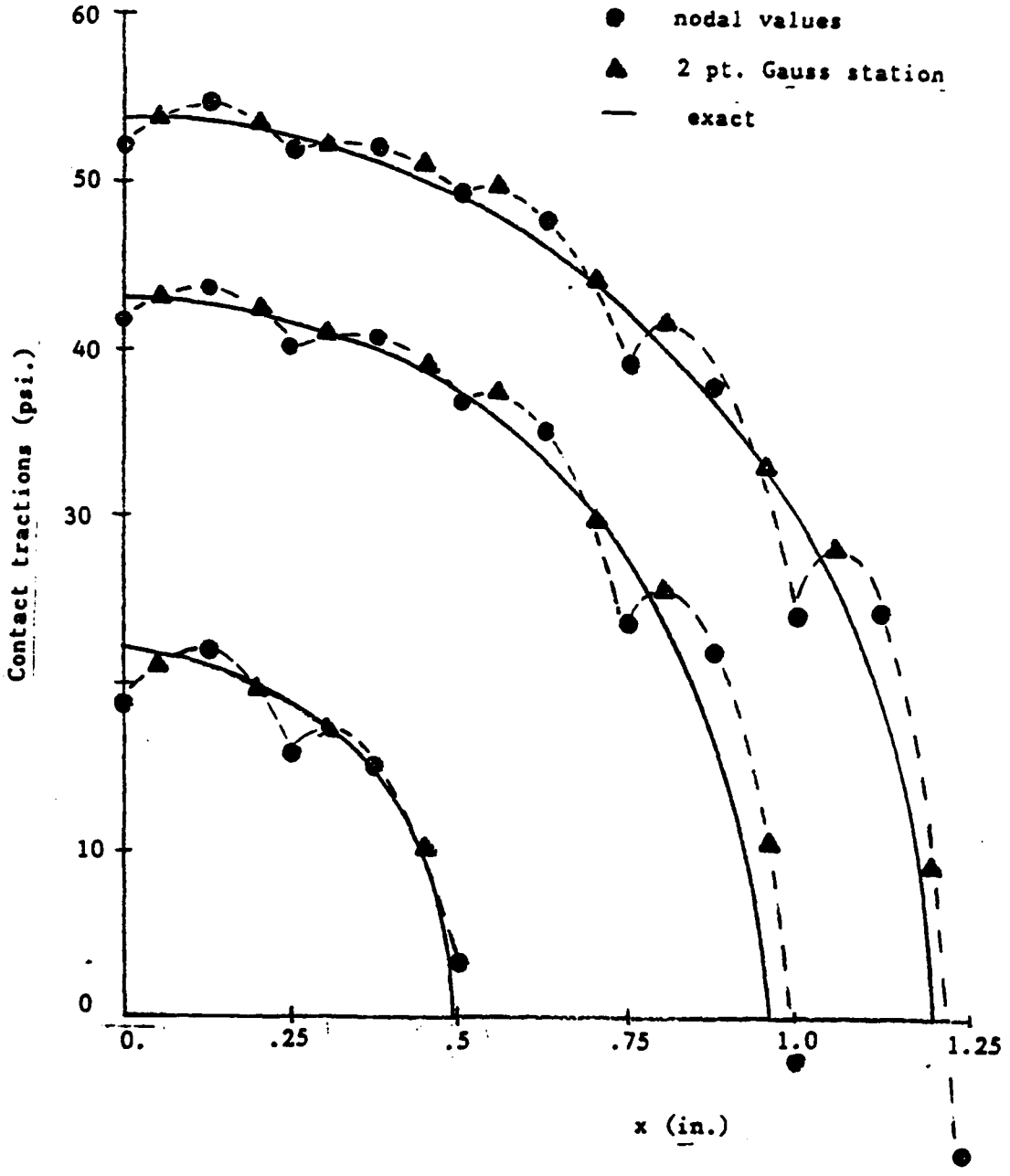

Figure 17 Contact traction (T+ΔT) distribution vs x for contact between a disk and a half-space having identical material properties. The displacements were applied in 3 increments.

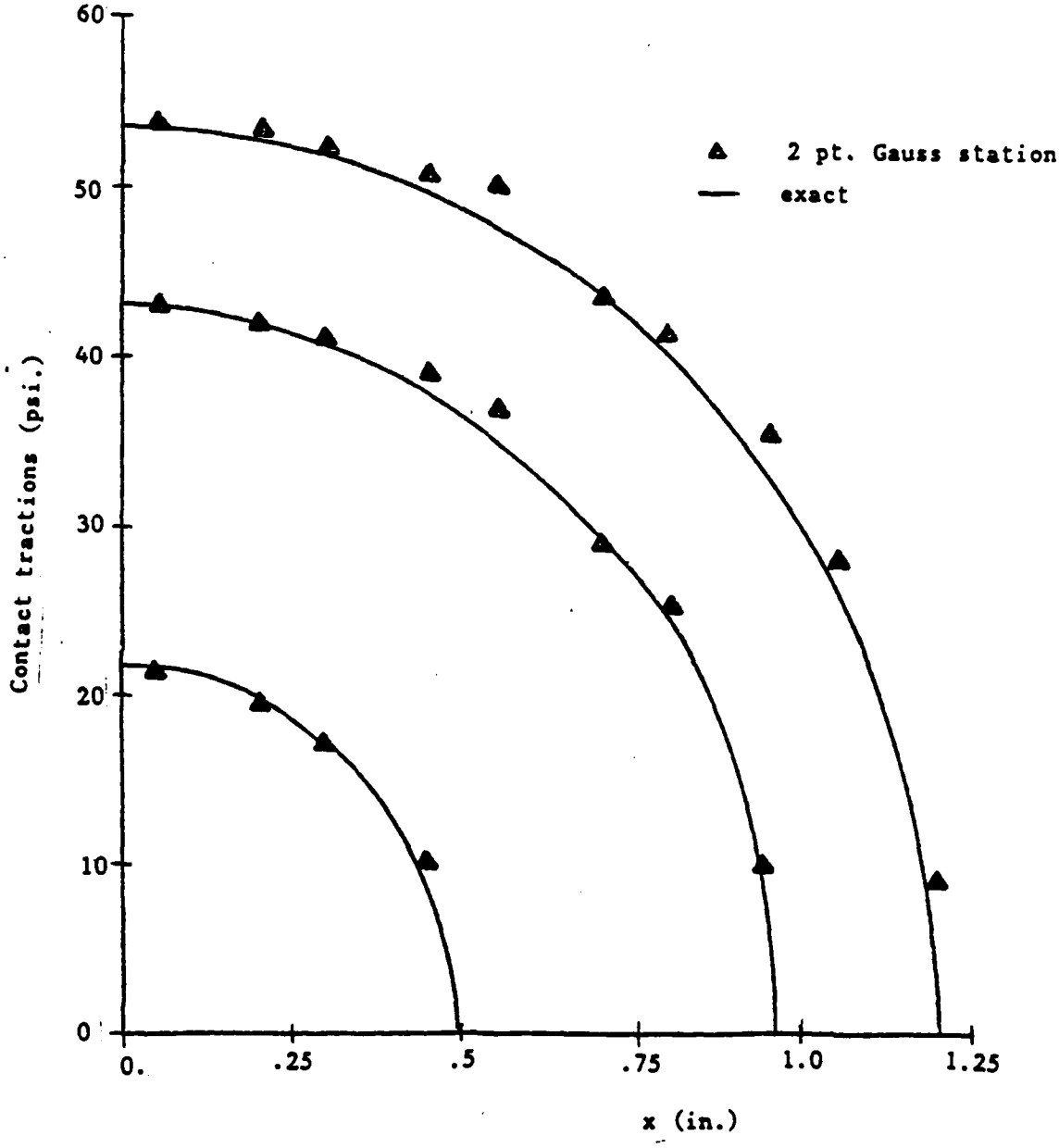

Figure 18 Contact traction (T+ΔT) distribution vs x calculated at the 2 pt. Gauss stations along the contact surface. The displacements were applies in 3 increments. $E_{disk}/E_{half\text{-}space}=1$.

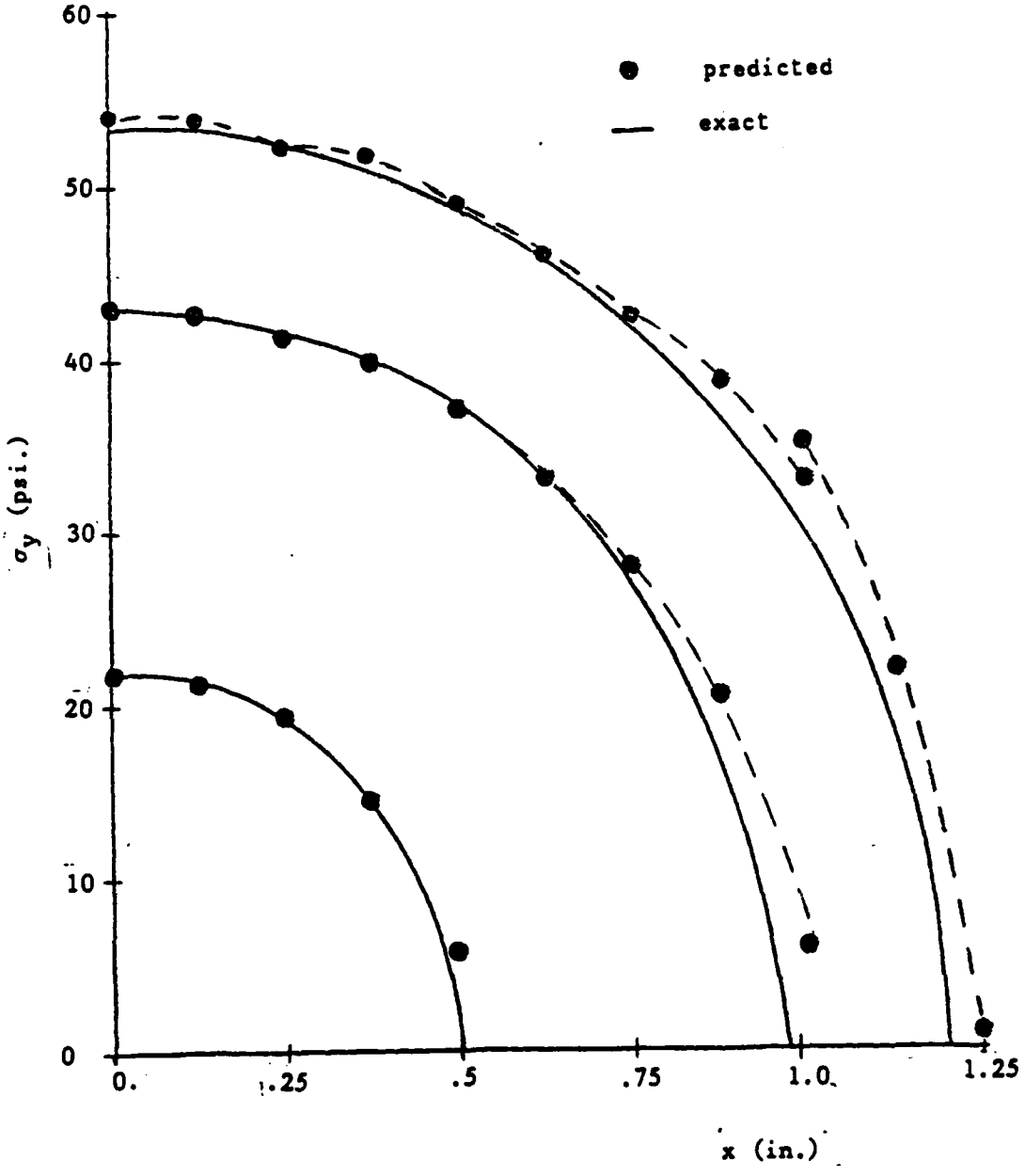

Figure 19 Distribution of the inplane normal stress, σ_y in the half-space calculated along the surface y=0 vs x. The displacements were applied in three increments. $E_{disk}/E_{half\text{-}space}=1$.

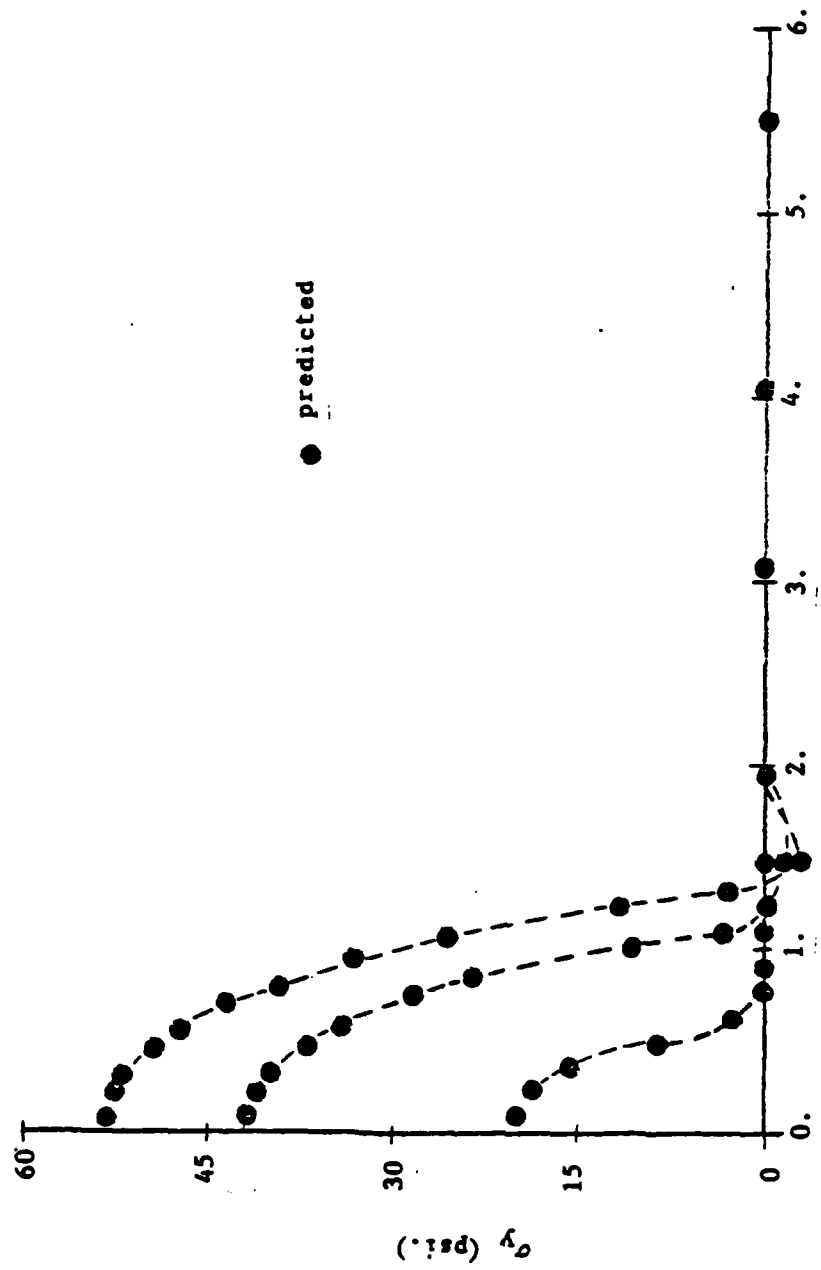

Figure 20 Distribution of the inplane normal stress, σ_y in the half-space calculated through the 2x2 Gauss stations nearest the contact surface vs x. Three increments of applied displacements were used. $E_{disk}/E_{half\text{-}space}=1$.

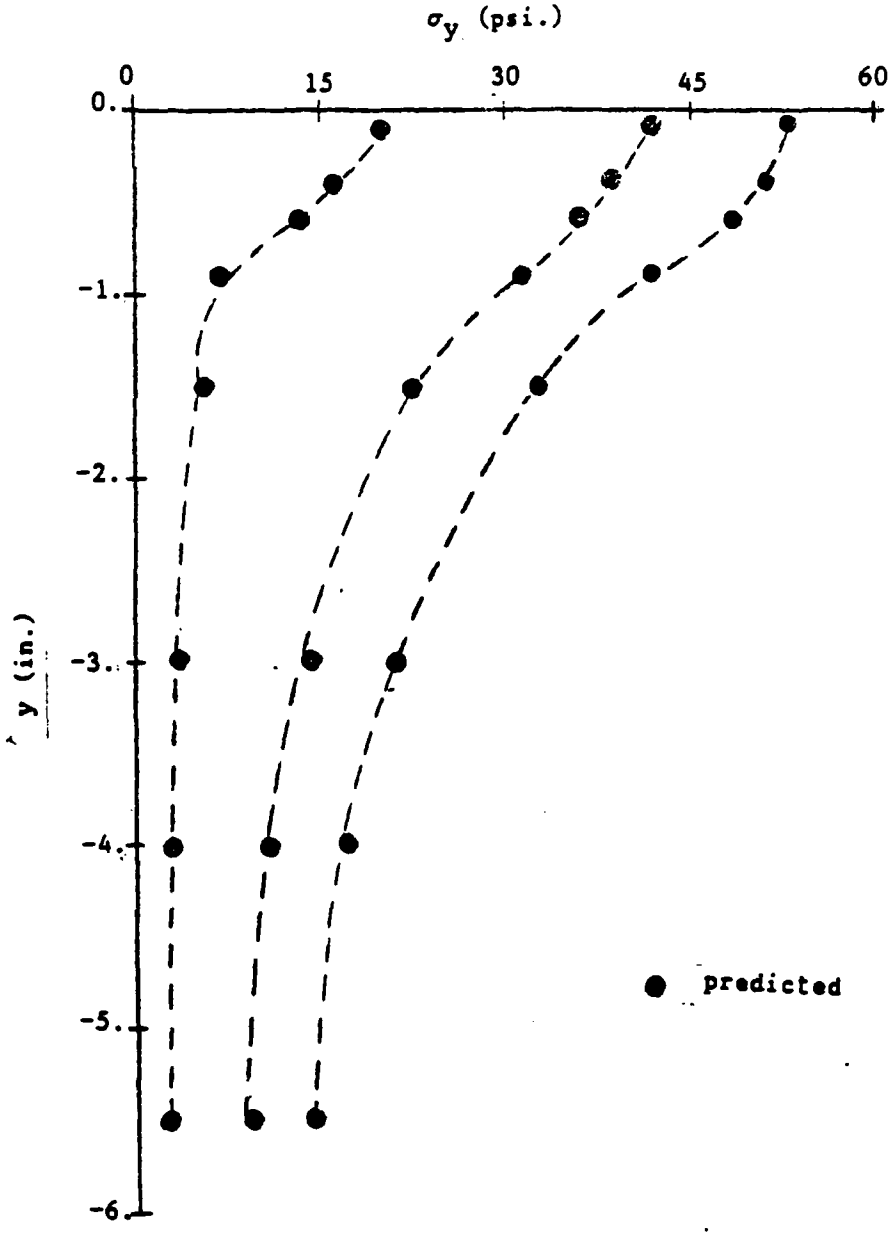

Figure 21 Distribution of the inplane normal stress, σ_y in the half-space calculated through the 2x2 Gauss stations nearest the plane of symmetry vs y. Three increments of applied displacement were used. $E_{disk}/E_{half\text{-}space}=1$.

3.6.2 Contact between a Nearly Rigid Disk and an Elastic Half-space

The problem of frictionless contact between a nearly rigid disk, under an applied load, and an elastic half-space can be solved using the same Hertz solution described in the last subsection.

The mesh and boundary conditions are shown in Figure 16. The materials of the disk and elastic half-space are isotropic and the material properties are $E_{disk}=1.x10^7$ psi., $E_{half-plane}=1.x10^3$ psi. and $\nu_{disk}=\nu_{half-plane}=.25$. The solution presented is for the case of prescribed displacements at the top of the disk in three increments. The magnitudes of the applied displacements were the same as those used in the last example problem. They are -.0698 in., -.148 in., and -.0942 in. for a total of -.312 in. Quantities of interest are the contact tractions, $(T+\Delta T)$ and the distributions of σ_y in the half-plane near the boundary (y=0) and near the center (x=0).

Figure 22 shows the distribution of the contact tractions calculated and the distribution given by the Hertz solution. The pointwise distribution of the contact tractions does not agree as well as the previous example with the Hertz solution although the solution calculated at the 2 point Gauss stations shown in Figure 23 is just as accurate as in the previous example. This serves to point out the importance of using these "optimal sampling points" to calculate contact tractions.

The contact surface tractions are calculated by a second method using the stress distribution and stress coefficients $\Delta\beta$'s assumed within each plate element. The distribution of the contact tractions is compared with the Hertz solution in Figure 24. This time the distribution of the contact tractions agrees well with the Hertz solution.

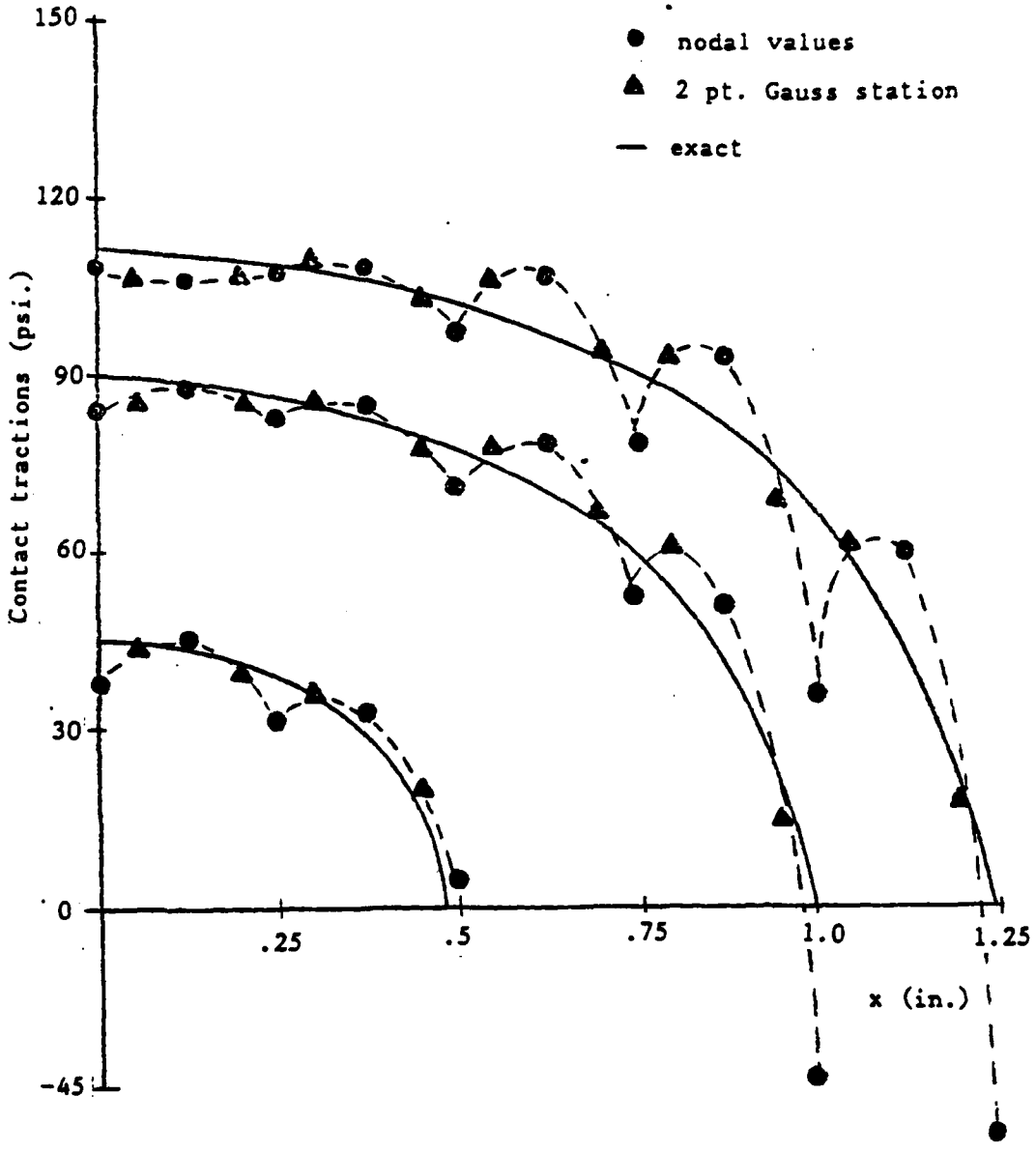

Figure 22 Contact traction, $(T+\Delta T)$ distribution vs x for contact between a nearly rigid disk and an elastic half-space. Three increments of applied displacement were used. $E_{disk}/E_{half\text{-}space}=1000$.

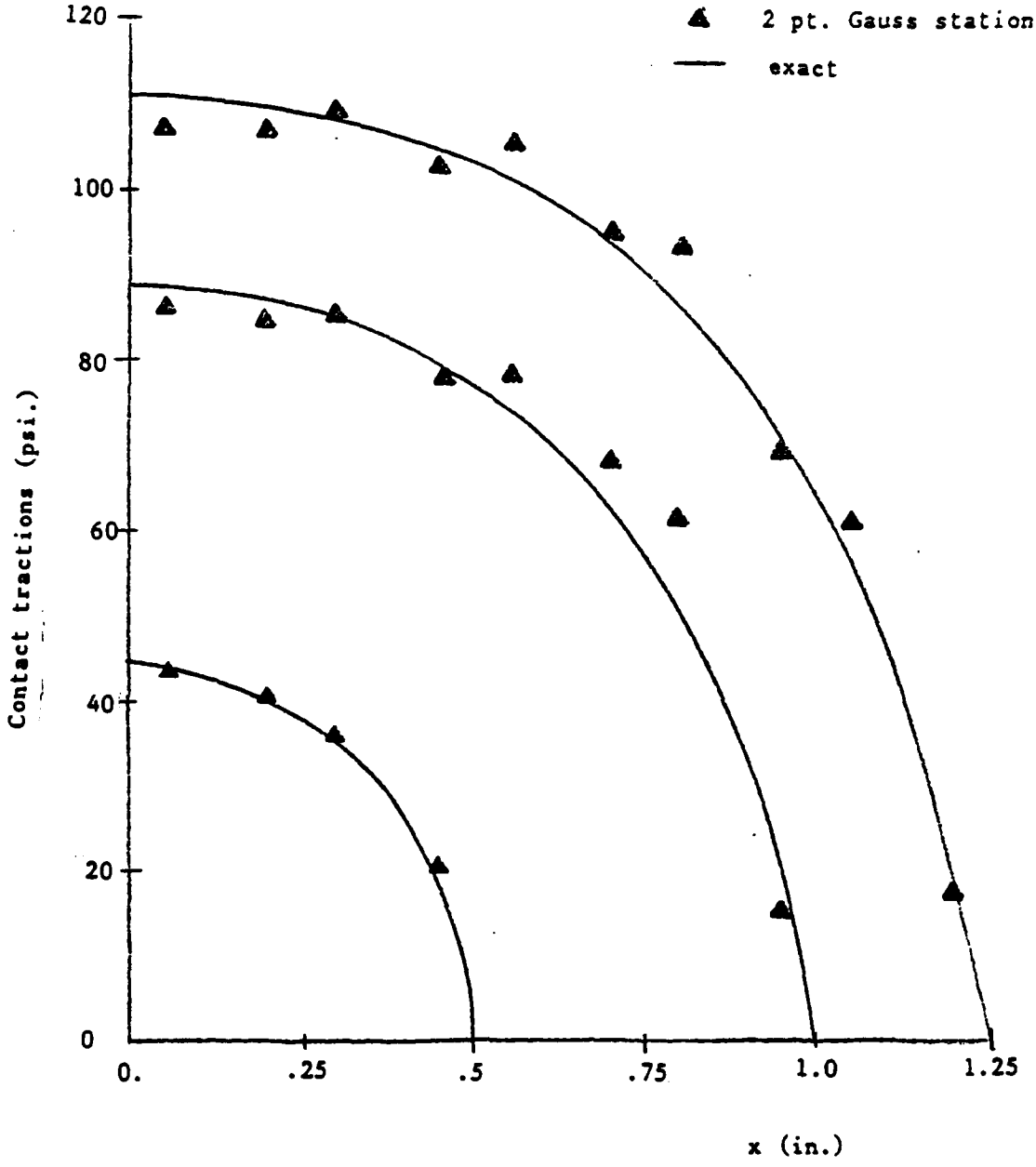

Figure 23 Contact tractions, $(T+\Delta T)$ distribution vs x calculated at the 2 pt. Gauss stations along the contact surface. The displacements were applied in 3 increments. $E_{disk}/E_{half\text{-}space}=1000$.

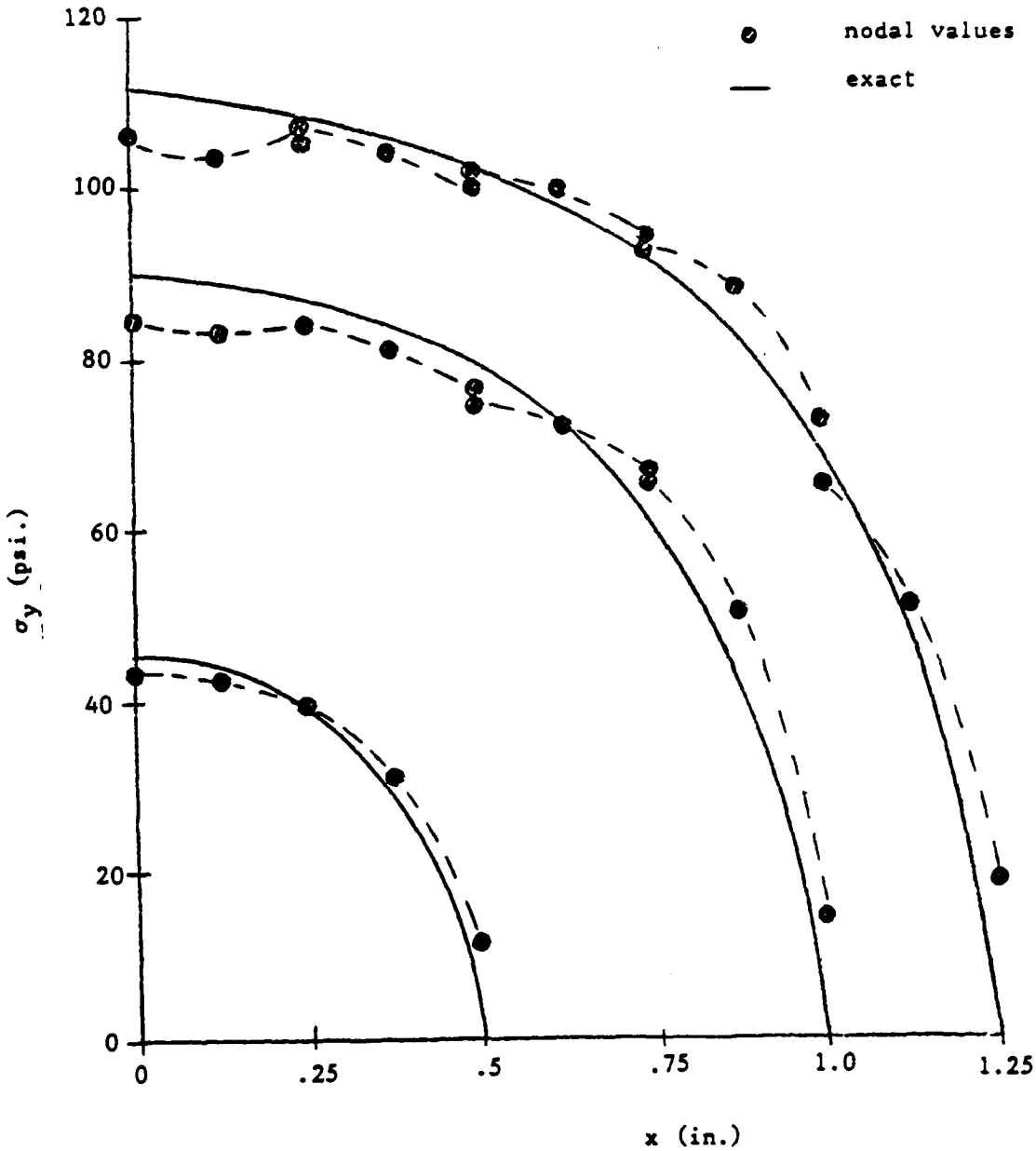

Figure 24 Distribution of the inplane normal stress, σ_y in the half-space calculated along the surface y=0 vs x. The displacements were applied in three increments. $E_{disk}/E_{half\text{-}space}=1000$.

Stresses in the half-plane near the surface at y=0 are shown in Figure 25. They are calculated from the stress coefficients, $\Delta\beta$ at the 2x2 Gauss stations nearest the y=0 boundary. The stresses within the half-space near the surface are only slightly smaller that the tractions on the surface as would be expected. The stress tends toward zero as x increases. Stress in the half-plane near the plane of symmetry are shown in Figure 26. They are also calculated from stress coefficients at the 2x2 Gauss stations. The stress is maximum near the surface and decreases to a minimum value as y decreases.

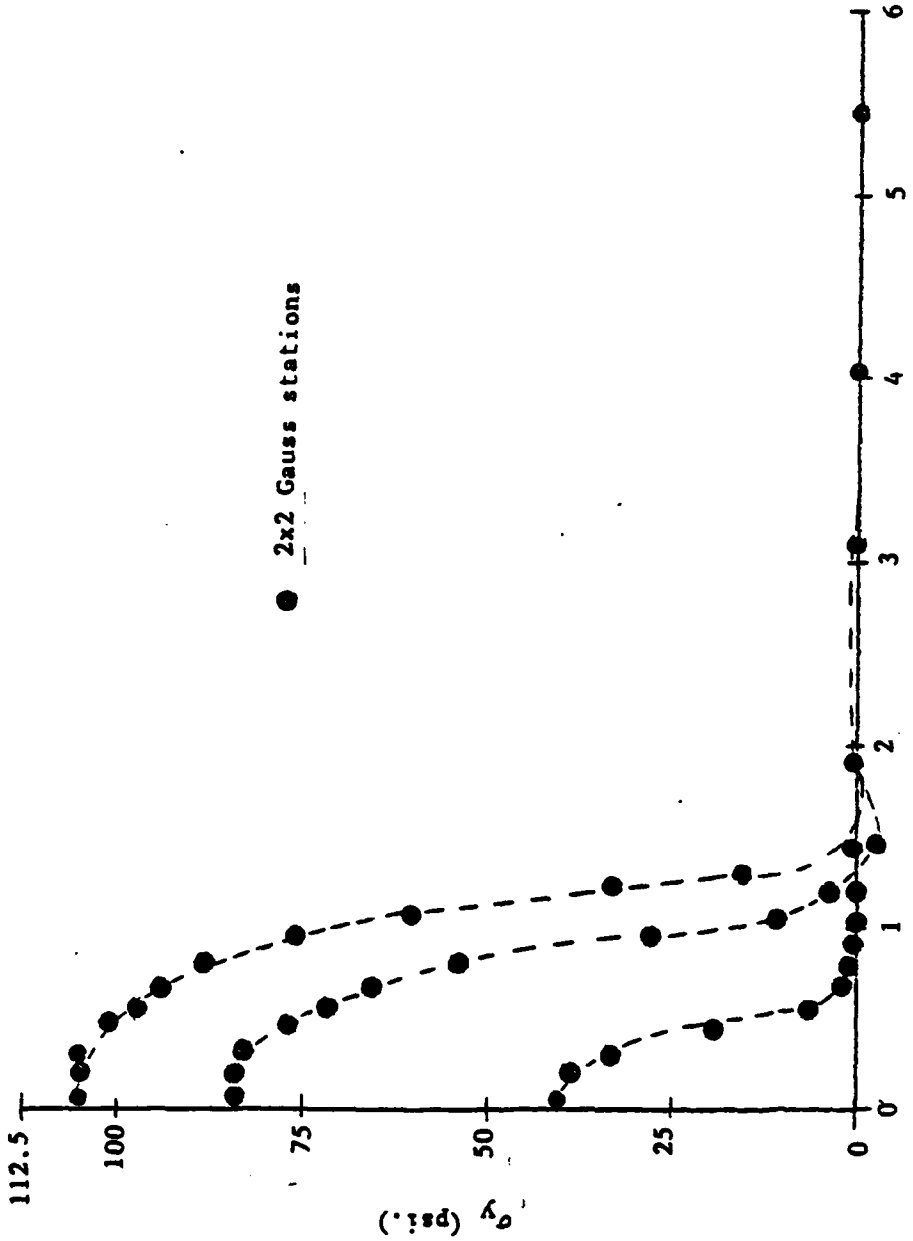

Figure 25 Distribution of the inplane normal stress, σ_y in the half-space calculated through the 2x2 Gauss stations nearest the contact surface vs x. Three increments of applied displacements were used $E_{disk}/E_{half\text{-}space}$=1000.

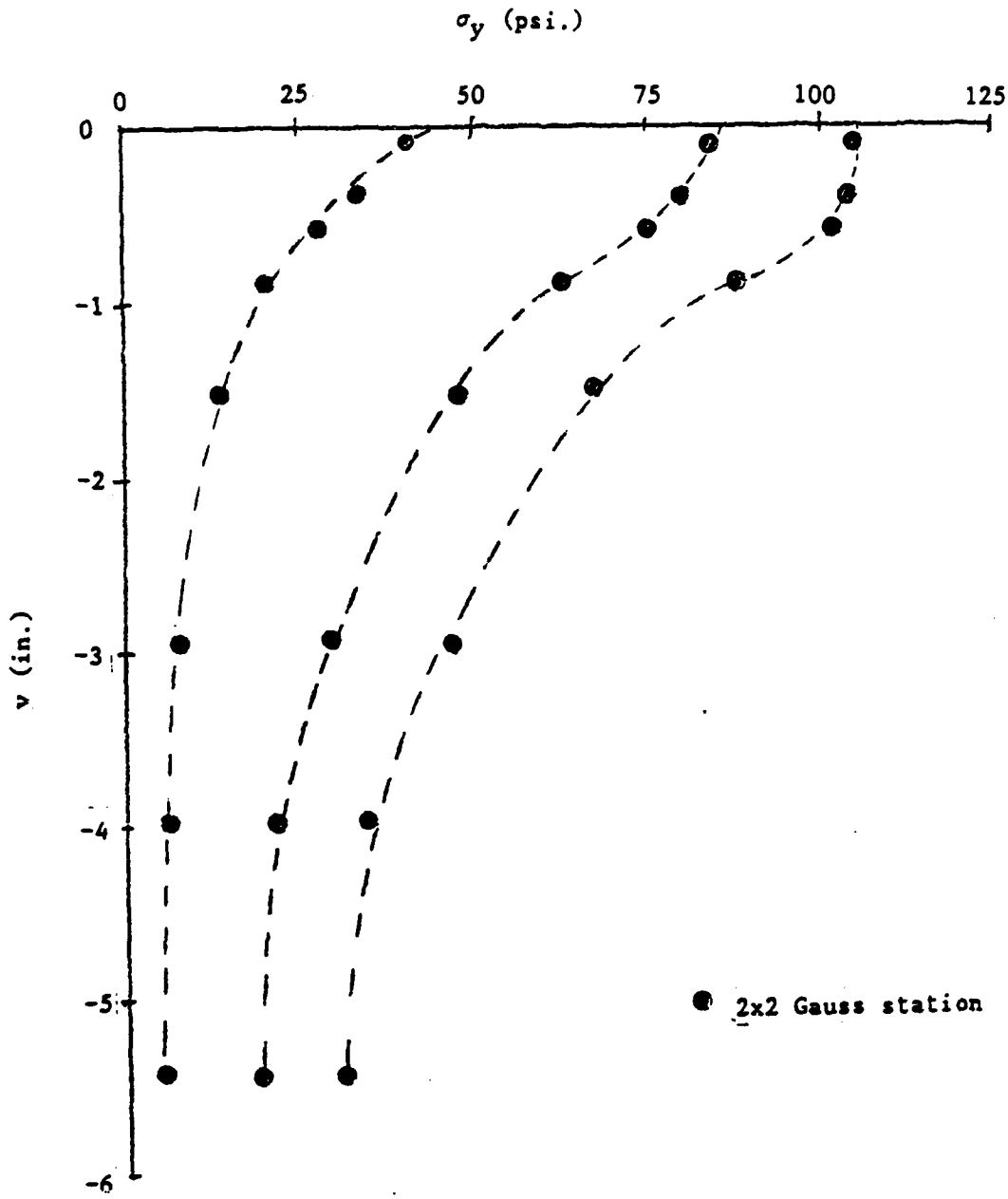

Figure 26 Distribution of the inplane normal stress, σ_y in the half-space calculated through the 2x2 Gauss stations nearest the plane of symmetry vs y. Three increments of applied displacement were used. $E_{disk}/E_{half\text{-}space}=1000$.

3.6.3 Contact between a Nearly Rigid Disk and a Symmetric Multilayer Composite Plate

The problem of frictionless contact between a nearly rigid disk, under an applied displacement, and a symmetric thin multilayer composite plate is solved in this subsection.

The mesh and boundary conditions are shown in Figure 16. The material of the disk is isotropic and the material properties are $E=2.x10^{10}$ psi. and $\nu=.21$. The plate is a 4-layer 90/0/0/90 cross-ply (θ measured from the x-axis). The thickness, h of the plate and the disk is equal to .02 in. Each layer is of equal thickness h/4, and layer material properties are $E_{11}=20x10^6$ psi., $E_{22}=2.1x10^6$ psi., $\nu_{12}=\nu_{23}=.21$, and $G_{12}=.85x10^6$. Magnitudes of the three increments of applied displacement are -.05313 in., -.12009 in., and -.07802 in. (equal to a total applied displacement of -.25124 in.)

Quantities of interest are the contact tractions, $(T+\Delta T)$ and the distributions of σ_y in the plate near the boundary (y=0) and near the plane of symmetry (x=0).

Figure 27 illustrates the distribution of the contact tractions calculated using the finite element program. The solution calculated at the 2 point Gauss stations is shown in Figure 28. Using the experience gained in the last two examples, these are the best locations at which to evaluate the distribution of contact tractions.

A weighted sum of the stress, σ_y in all the layers of the multilayer composite plate have been calculated along y=0 using the stress distibutions assumed within each element. The distribution of stress shown in Figure 29 is very close to the distribution of contact traction calculated at the 2 point Gauss stations in Figure 28, although the

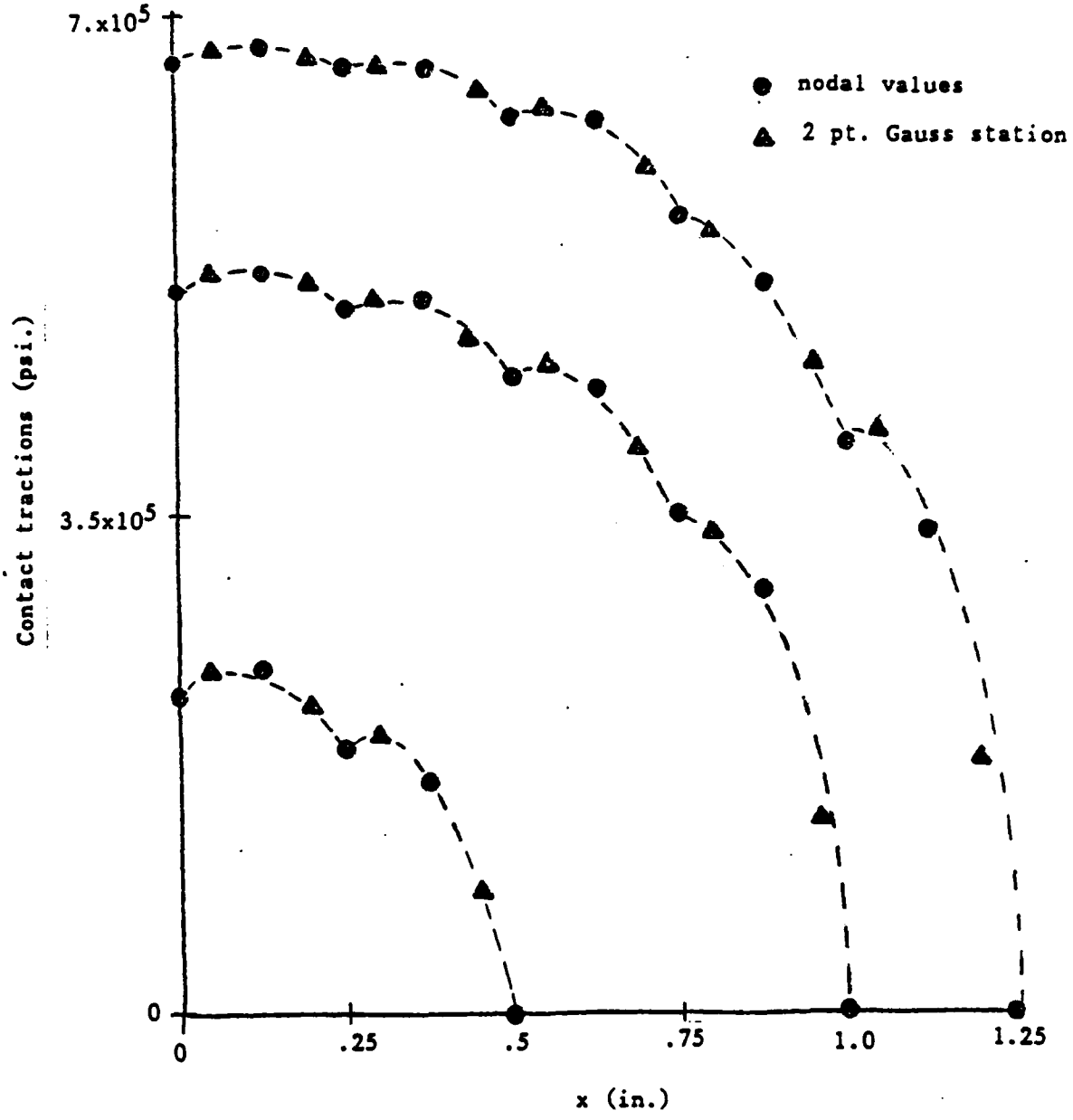

Figure 27 Contact surface tractions, (T+ΔT) distribution vs x for contact between a nearly rigid disk and a symmetric multilayer composite plate. Three increments of applied displacement were used.

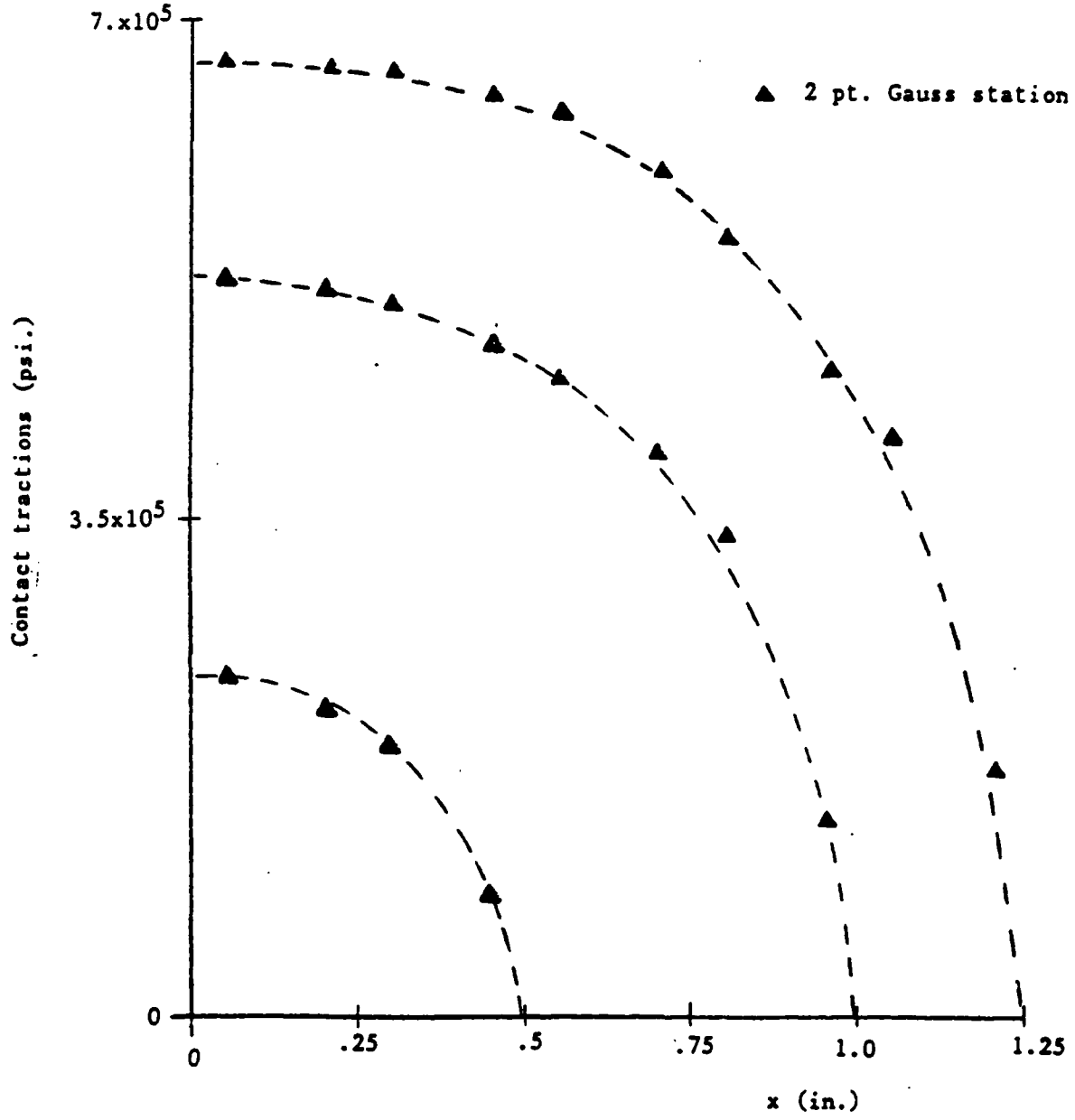

Figure 28 Contact tractions, $(T+\Delta T)$ distribution vs x calculated at the 2 pt. Gauss stations along the contact surface for the problem of contact between a nearly rigid disk and a symmetric multilayer composite plate. The displacments were applied in 3 increments.

stress distribution within the element is discontinuous at interelement boundaries. The stress, σ_y calculated along y=0 using the element stress distribution in each of layers 1 and 2 are shown in Figures 30 and 31 respectively.

A weighted sum of the stress in all the layers of the multilayer composite plate near the surface at y=0 are shown in Figure 32. They are calculated from the stress coefficients, $\Delta\beta$ at the 2x2 Gauss stations nearest the y=0 boundary. The stress, σ_y calculated at the 2x2 Gauss stations nearest the y=0 boundary are shown for layers 1 and 2 separately in Figures 33 and 34. The stress tends toward zero as x increases. Stresses in the multilayer composite plate near the plane of symmetry are shown in Figure 35. They are also calculated from stress coefficients at the 2x2 Gauss stations. The stress, σ_y calculated at the 2x2 Gauss stations nearest the plane of symmetry are shown for layers 1 and 2 separately in Figures 36 and 37. The stress is maximum near the surface and decreases to a minimum value as y decreases.

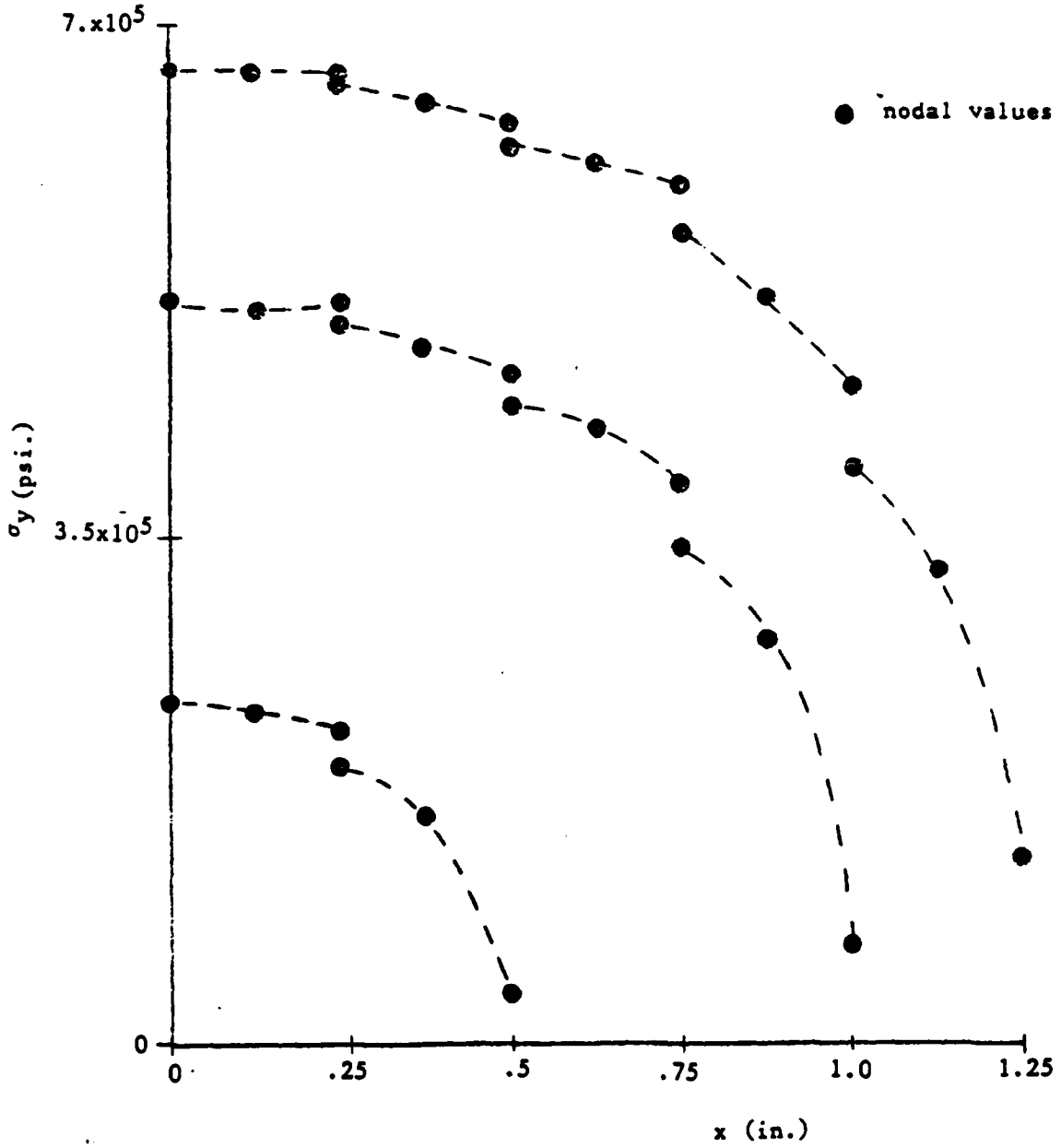

Figure 29 Distribution of the inplane normal stress, σ_y in the multilayer plate calculated along the contact surface (y=0) vs x. The displacments were applied in three increments.

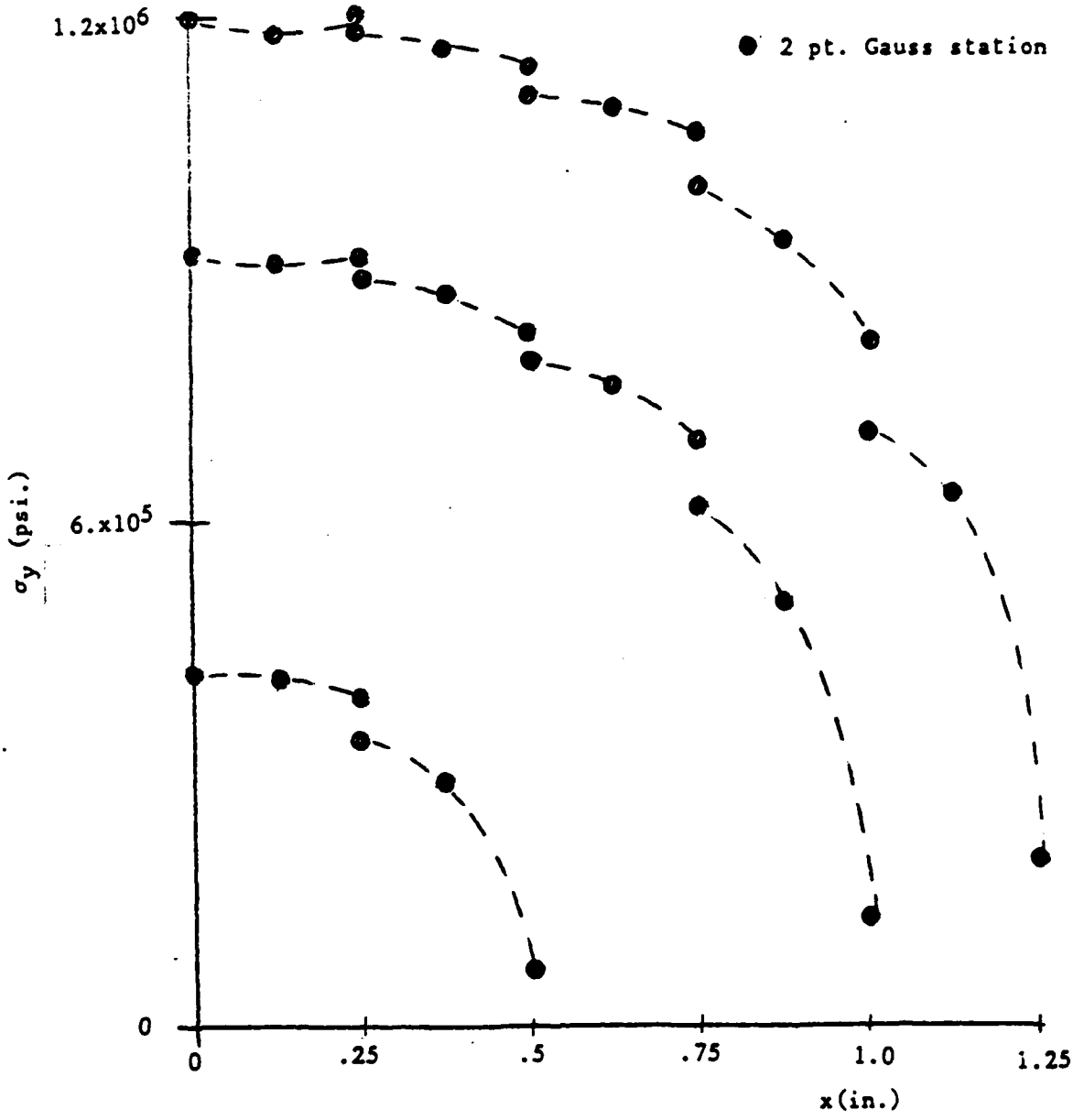

Figure 30 Contact tractions, (T+ΔT) distribution in layer 1 vs x calculated at the 2 pt. Gauss stations along the contact surface for the problem of contact between a nearly rigid disk and a symmetric multilayer composite plate. The displacements were applied in 3 increments.

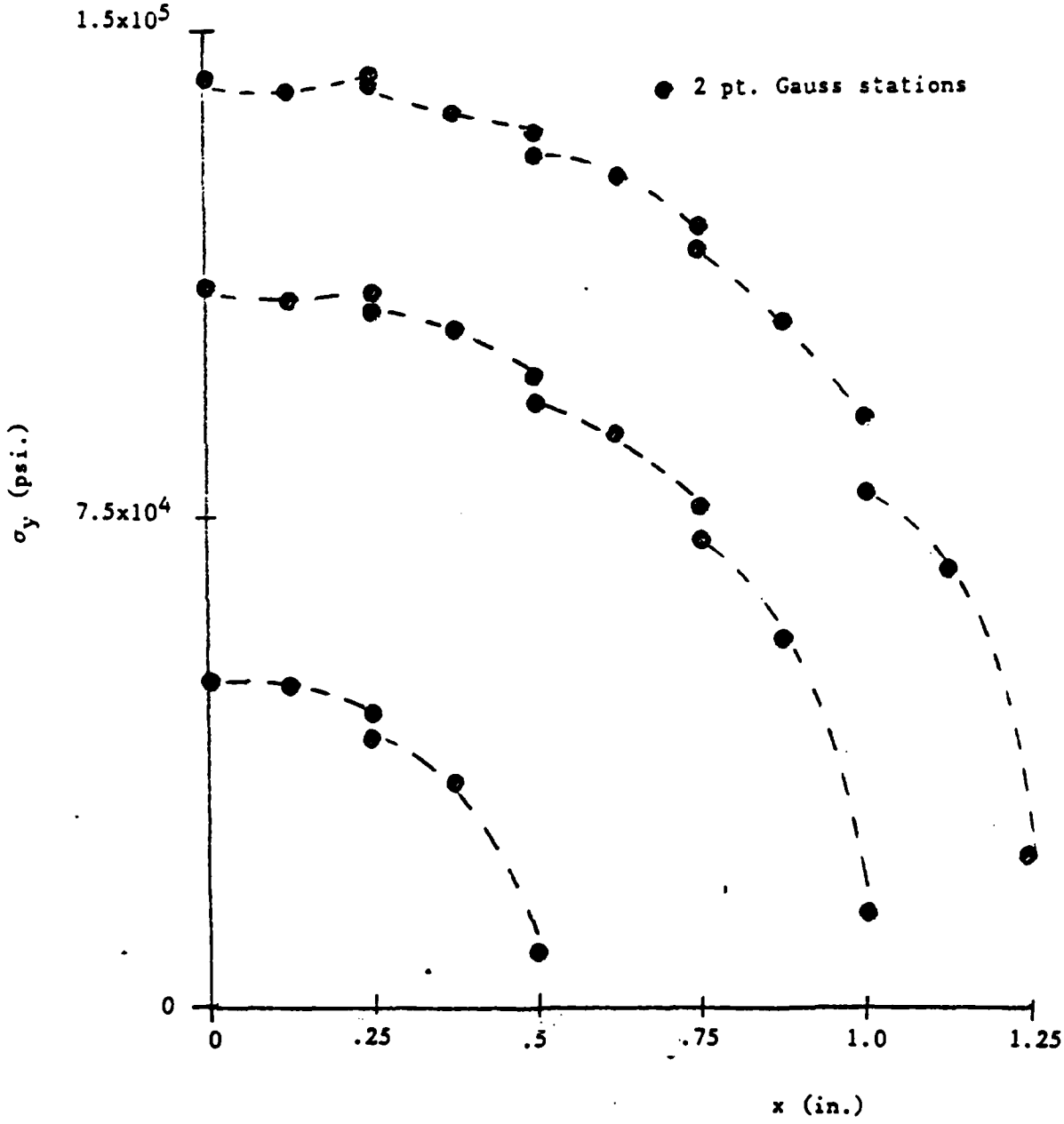

Figure 31 Contact traction, $(T+\Delta T)$ distribution in layer 2 vs x calculated at the 2 pt. Gauss stations along the contact surface for the problem of contact between a nearly rigid disk and a symmetric multilayer plate. The displacements were applied in 3 increments.

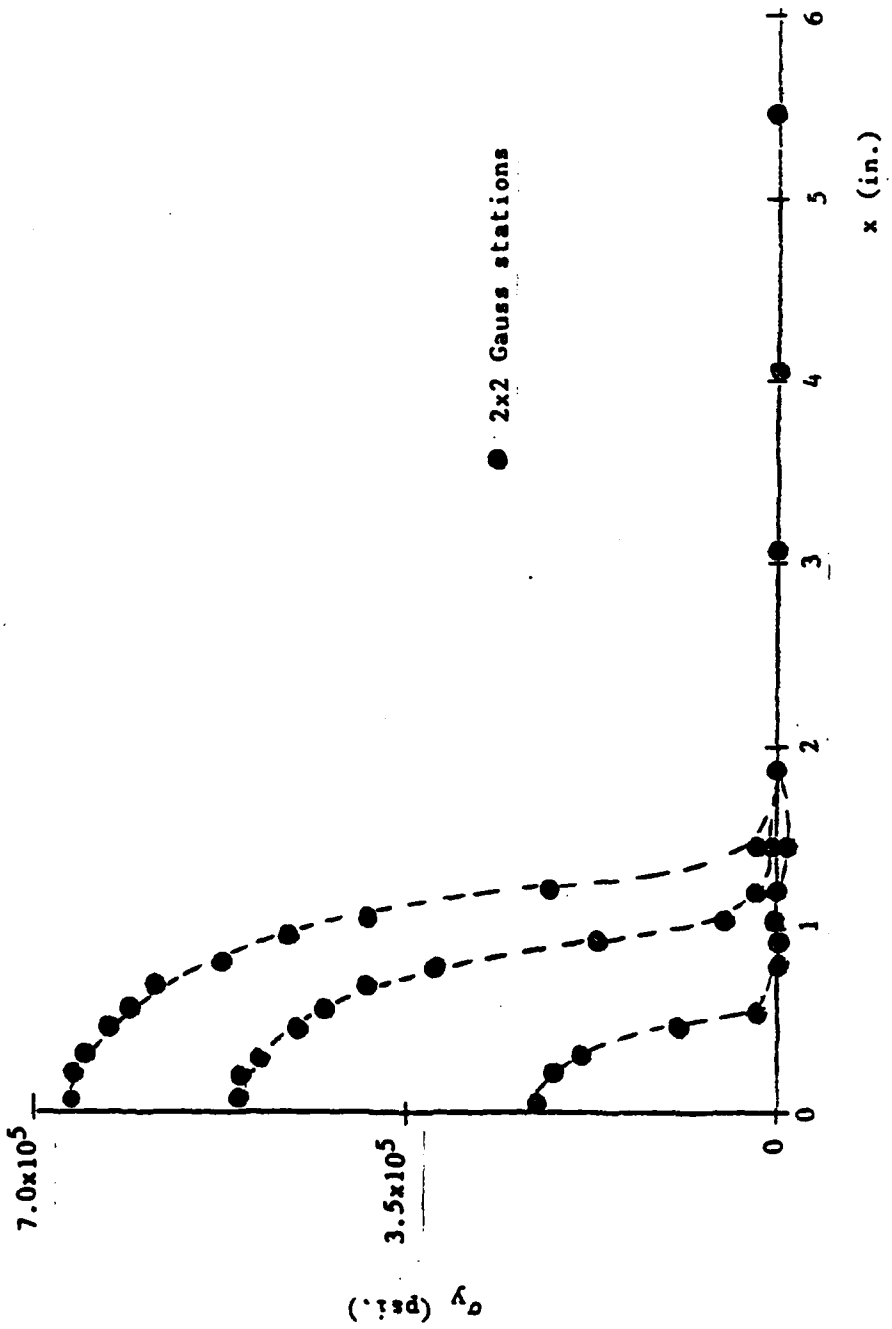

Figure 32 Distribution of the inplane normal stress, σ_y in the multilayer composite plate calculated through the 2x2 Gauss stations nearest the contact surface vs x. Three increments of applied displacement were used.

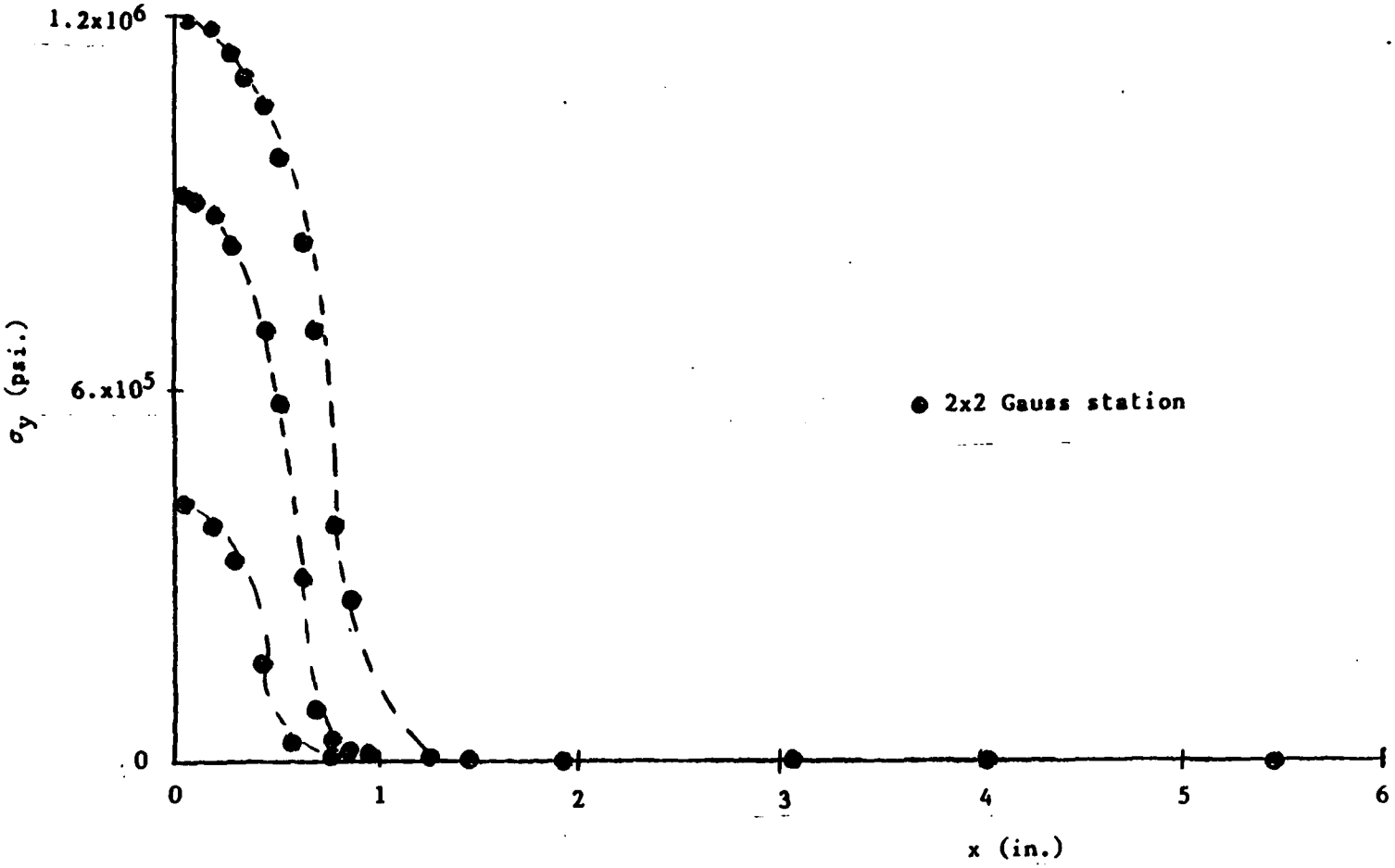

Figure 33 Distribution of the inplane normal stress, σ_y in layer 1 of the multilayer composite plates calculated through the 2x2 Gauss stations nearest the contact surface vs x. Three increments of displacement were applied.

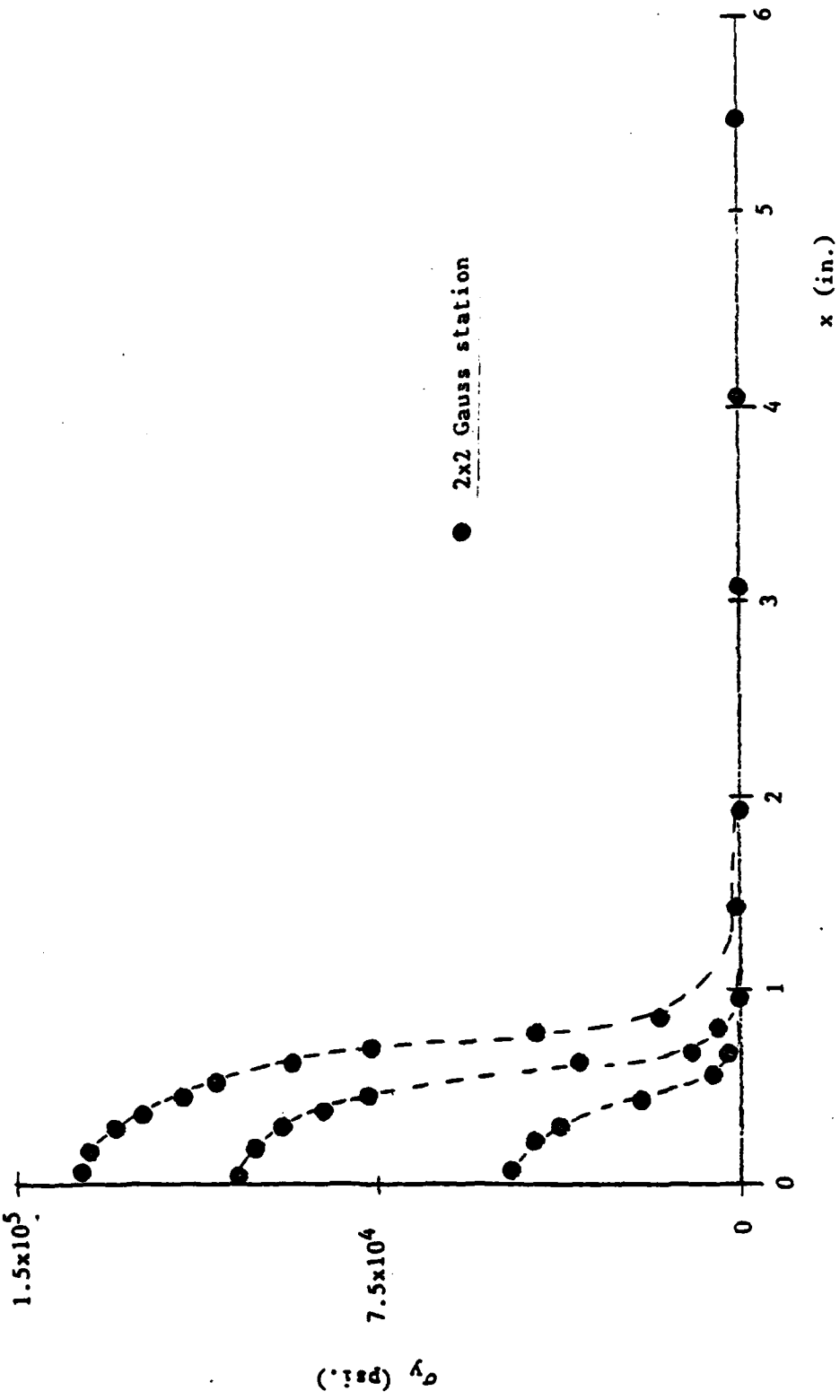

Figure 34 Distribution of the inplane normal stress, σ_y in layer 2 of the multilayer composite plate calculated through the 2x2 Gauss stations nearest the contact surface vs x. Three increments of displacement were applied.

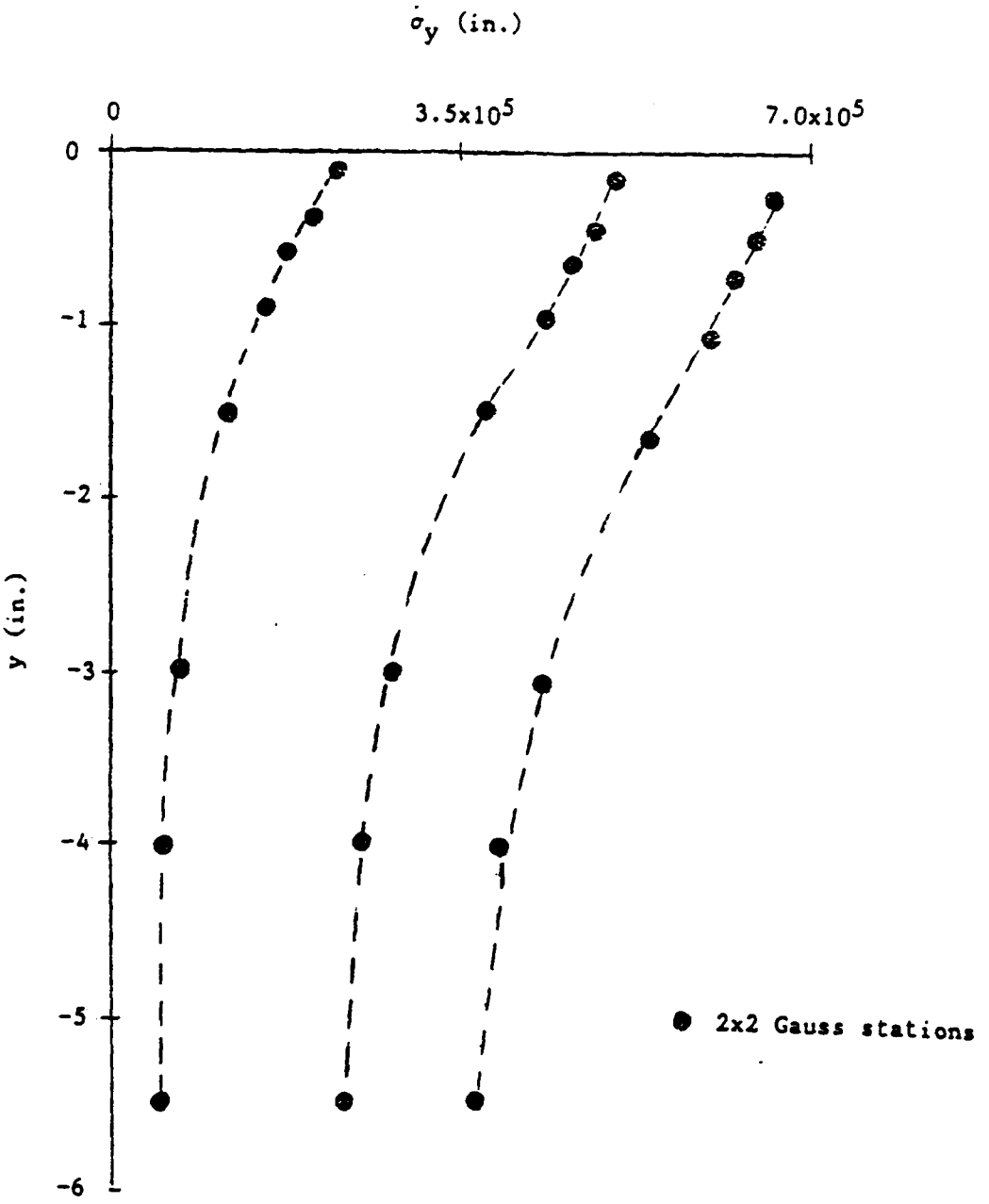

Figure 35 Distribution of the inplane normal stress, σ_y in the multilayer composite plate calculated through the 2x2 Gauss stations nearest to the plane of symmetry vs y. Three increments of applied displacement were used.

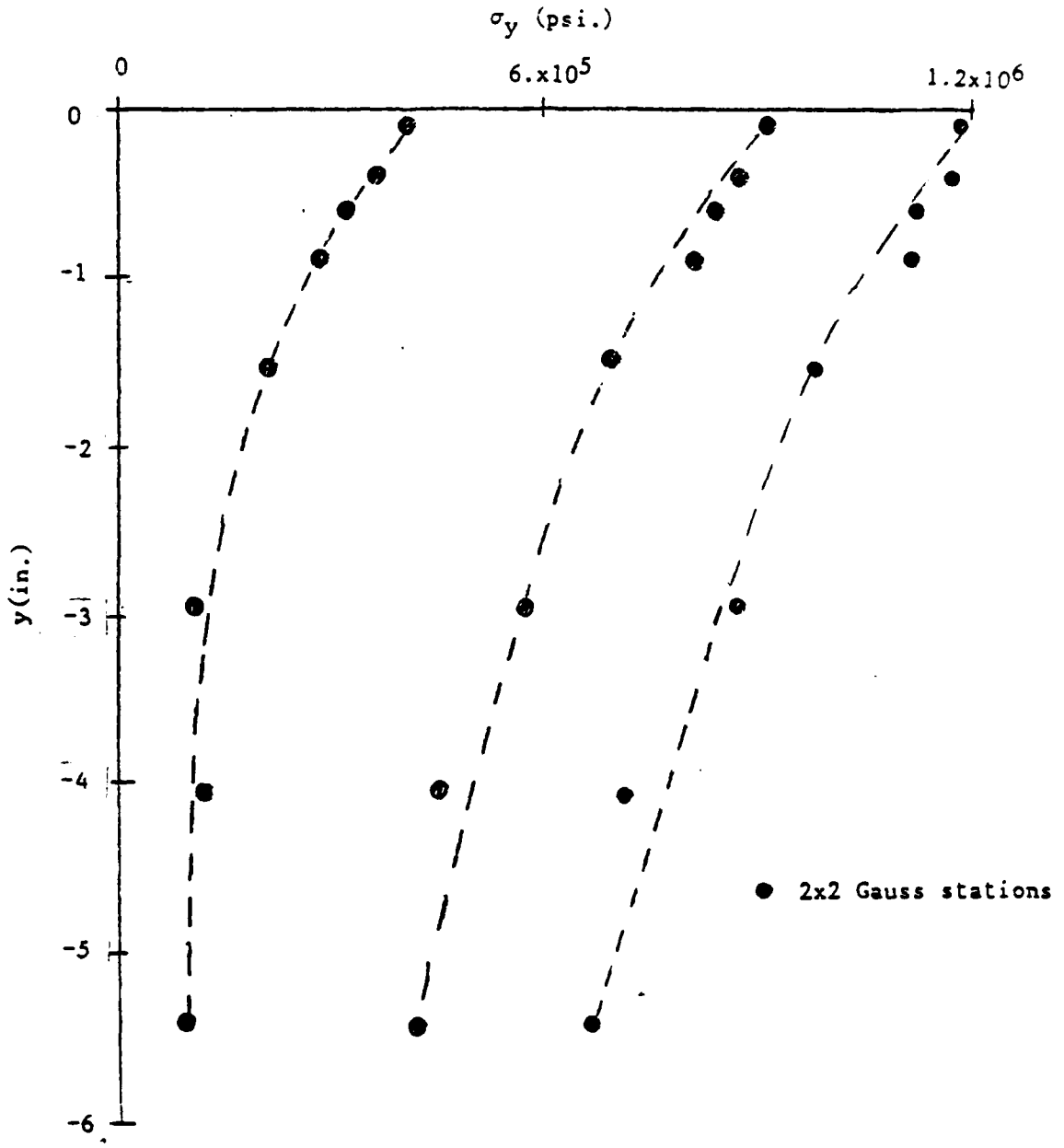

Figure 36 Distribution of the inplane normal stress, σ_y in layer 1 of the multilayer composite plate calculated through the 2x2 Gauss stations nearest to the plane of symmetry vs y. Three increments of applied displacement were used.

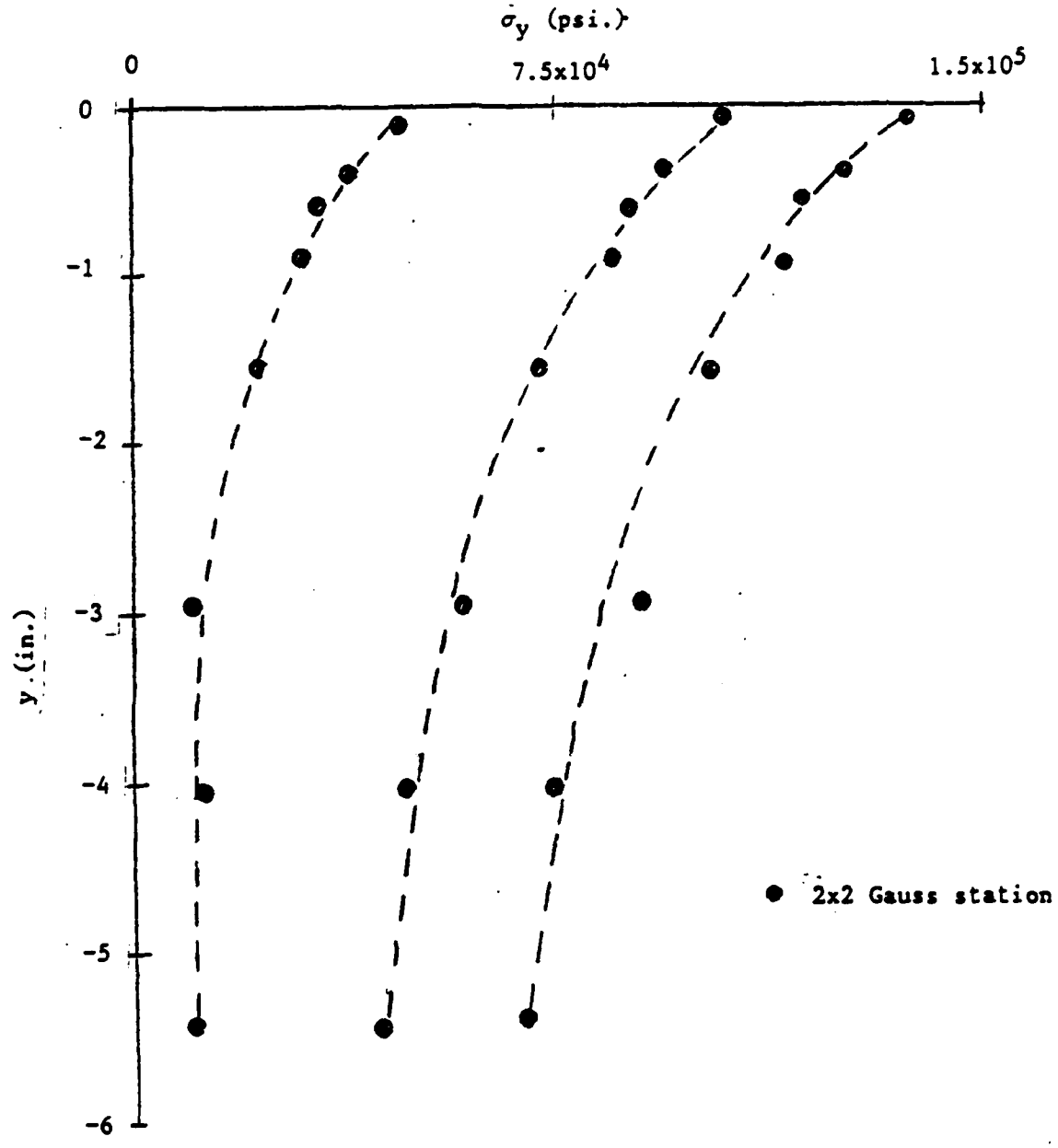

Figure 37 Distribution of the inplane normal stress, σ_y in layer 2 of the multilayer composite plate calculated through the 2x2 Gauss stations nearest to the plane of symmetry. Three increments of displacement were applied.

Chapter IV

CONCLUSIONS AND SUGGESTIONS FOR FURTHER RESEARCH

4.1 CONCLUSIONS

The purpose of this study has been to solve the problem of edge contact between a nearly rigid disk and a multilayer laminated composite plate. A suitable plate element has been formultated for this purpose as well as the method to solve the contact portion of the problem.

The hybrid stress formulation for an isoparametric thin to moderately thick multilayer laminated composite plate element has been presented. The displacement behavior was characterized by laminate reference plane inplane and transverse displacements and laminate non-normal cross-section rotations; as a result, the number of degrees of freedom was independent of the number of layers. All components of stress were included.

A thin to moderately thick multilayer laminated composite plate element (MQH3) was developed. Due to the excessive CPU time necessary to calculate the stiffness of a single element, several unsuccessful schemes were developed to decrease the CPU time . An element formulation for thin laminates was developed as a reduction of the moderately-thick formulation by neglecting the contribution of transverse shear stresses and normal stress to the internal complementary energy. Using the reduced formulation, an algorithm was developed which decreased the CPU time necessary to calculate the stiffness by a significant amount.

CPU time for the reduced element is essentially independent of the number of layers.

For thin laminates the performance of the two elements is essentially identical. For thickness ratios h/L>.01, the more general element is necessary to produce accurate results, but the reduced element results in a large reduction in CPU time. The MQH3T element retains a high degree of accuracy for thin plates having a thickness ratio less than h/L=0.01. For the case of an angle-ply plate which is simply supported on all edges the results are very good and θ has little effect on the accuracy of the predictions. The poor results displayed for small θ in the case of a angle-ply plate which has been clamped on all edges are thought to be due to a type of "material" aspect ratio effect.

The hybrid stress formulation for the analysis of laminate edge contact problems as well as the procedure to locate the surface of contact has been presented. A contact surface was assumed between two contacting bodies and was divided into contact elements. Attention was restricted to cases of inplane displacements and contact which was uniform in the through thickness direction.

Examples considered were the problem of contact between a disk and a half-plane involving both elastic and nearly rigid disks, and isotropic and multilayer composite plates. Results of moderate sliding contact are in very good agreement with Hertz solutions and can be considered good enough to obtain stresses accurately. The problem of moderate sliding frictionless contact of an elastic disk with an elastic semi-infinite half-space agreed very well with the Hertz distribution of contact stress. The best distributions of contact tractions were obtained at the 2 point Gauss stations. The results obtained from the example

problems involving the semi-infinite half-space suggest that the mesh was fine enough to obtain reasonable results for the problem of edge contact between a disk and a thin multilayer composite plate.

4.2 SUGGESTIONS FOR FURTHER RESEARCH

Suggestion for further research include:

1. Efforts should be made to decrease the storage requirements i.e. out-of-core solvers and use of disk storage, so that finer meshes could be used to solve more complicated problems such a curved boundaries.
2. Extension of the present program to include transverse displacements and rotations.
3. Use of more sophisticated multilayer elements near the contact surface which would include the possibility of cross-sectional warping at the edge of the laminate.
4. Inclusion of material and geometric nonlinearities.

BIBLIOGRAPHY

1. Pryor Jr., C.W. and Barker, R.M., 'A finite element analysis including transverse shear effects for applications to laminated paltes', AIAA J., 9 912-917 (1971).

2. Noor, A.K. and Mathers, M.D., 'Anisotropy and shear deformation in laminated composite plates', AIAA J., 14 282-285 (1976).

3. Noor, A.K. and Mathers, M.D., 'Finite element analysis of anisotropic plates', Int. J. Meth. Engng., 11 289-307 (1977).

4. Panda, S.C. and Natarajan, R., 'Finite element analysis of laminate composite plates', Int. J. Num. Meth. Engng., 14 69-79 (1979).

5. Reddy, J.N., 'A penalty plate-bending element for the analysis of laminated anisotropic composite plates', Int. J. Num. Meth. Engng., 15 1187-1206 (1980).

6. Mau, S.T., Tong, P., and Pian, T.H.H., 'Finite element solutions for laminated thick plates', J. Comp. Mats., 6 304-311 (1972).

7. Harris, A., Orringer, O., and Witmer, E.A., 'A multilayer, traction-free edge, quadrilateral warping element for the stress analysis of composite plates and shells', MIT ASML TR 193-1 (1979).

8. Spilker; R.L., 'A hybrid-stress formulation for thick multilayer laminates', Comp. Struct., 11 507-514 (1980).

9. Spilker, R.L., Chou, S.C., and Orringer, O., 'Alternate hybrid-stress elements for analysis of multilayer composite plates', J. Comp. Mats., 11 57-70 (1970).

10. Spilker, R.L., 'Hybrid-stress eight-node elements for thin and thick multilayer laminated plates', Int. J. Num. Meth. Engng., 18 801-828 (1982).

11. Spilker, R.L., 'An invariant 8-node hybrid-stress element for thin and thick multilayer laminated plates', Int. J. Num. Meth. Engng. (to appear).

12. Cook, R.D., 'Two hybrid elements for anaylsis of thick, thin and sandwich plates', Int. J. Num. Meth. Engng., 5 277-288 (1972).

13. Nishioka, T. and Atluri, S.N., 'Assumed stress finite element analysis of through-cracks in angle-ply laminates', AIAA J., 18 1125-1132 (1980).

14. Spilker, R.L. and Munir, N.I., 'The hybrid-stress model for thin plates', Int. J. Num. Meth. Engng., 15 1239-1260 (1980).

15. Spilker, R.L. and Munir, N.I., 'A hybrid-stress quadratic serendipity displacement Mindlin plate bending element', Comp. Struct., 12 11-21 (1980).

16. Spilker, R.L. and Munir, N.I., 'A serendipity cubic-displacement hybrid-stress element for thin and moderately thick plates', Int. J. Num. Meth. Engng., 15 1261-1278 (1980).

17. Spilker, R.L., 'Invariant 8-node hybrid-stress elements for thin and moderately thick plates', Int. J. Num. Meth. Engng., 18 1153-1178 (1982).

18. Spilker, R.L., 'Hybrid-stress reduced Mindlin isparametric elements for the analysis of thin plates', J. Struct. Mech. 11 (1), 49-66 (1983).

19. Pian, T.H.H., 'Finite element methods by variational principles with relaxes continuity requirement, in International Conference of Variational Methods in Engineering Southhampton University, England, Session III, 1972, p. 1-24.

20. Tong, P., 'A family of hybrid plate elements', Int. J. Num. Meth. Engng. (to appear).

21. Pian, T.H.H., Chen, D-P, and Kang, D., 'A new formulation of hybrid/mixed finite element', Comput. Struct. (to appear).

22. Batoz, J.L., Bathe, K.J., Ho, L.W., 'A study of three-node triangular plate bending elements', Int. J. Num. Meth. Engng., 15 1771-1812 (1980).

23. Spilker, R.L., Maskeri, S.M., and Kania, E., 'Plane isoparametric hybrid-stress elements', Int. J. Num. Meth. Engng. (to appear).

24. Pagano, N.J., 'Exact solutions for composite laminates in cylindrical bending', J. Comp. Matls., 3 398-411, (1969).

25. Whitney, J.M., 'The effect of boundary conditions on the response of laminated composites', J. Comp. Matls., 4 192-203, (1970).

26. Yamada, Y., Yokouch, Y. and Sasoka, G., 'Analysis of the contact problem by the finite element method', Proceedings of the Third Conference, Soc. Steel Constr. of Japan 412-421, (1969).

27. White, D.J. and Enderby, L.R., 'Finite-element stress analysis of a non-linear problem: a connecting-rod eye loaded by means of a pin', J. Strain Analy., 5 41-48, (1970).

28. Gaertner, R., 'Investigation of plane elastic contact allowing for friction', Computers and Structures, 7 59-63, (1977).

29. Fredriksson, B., 'Finite element solution of surface nonlinearities in structural mechanics with special emphasis to contact and fracture mechanics problems', Computers and Structures, 6 281-290, (1976).

30. Stadter, J.T. and Weiss, R.O., 'Analysis of contact through finite element gaps', Computers and Structures, 10 867-873, (1979).

31. Okamoto, N. and Nakazawa, M., 'Finite element incremental contact analysis with various frictional conditions', Int. J. Num. Meth. Engng., 14 337-357, (1979).

32. Sachdeva, T.D. and Ramakreshnan, C.V., 'A finite element solution for the two dimensional elastic contact problems with friction', Int. J. Num. Meth. in Engng. 17 1257-1271, (1981).

33. Francavilla, A. and Zienkiewicz, O.C., 'A note on numerical computation of elastic contact problems', Int. J. Num. Meth. Engng., 9 913-924, (1975).

34. Mahmoud, F.F., Salamon, N.J., and Marks, W.R., 'A direct automated procedure for frictionless contact problems', Int. J. Num. Meth. Engng. 18 247-257, (1982).

35. Chan, S.K. and Tuba, I.S., 'A finite element method for contact problems of solid bodies - Part I, Theory and validation. and Part II, Application to turbine blade fastenings', Int. J. Mech. Sci., 13 615-639, (1971).

36. Hughes, T.J.R., Taylor, R.L., Sackman, J.L., Curnier, A. and Kanoknukulchai, W., 'A finite element method for a class of contact-impact problems', Comp. Meth. in Appl. Mech. and Engng., 8 249-276, (1976).

37. Kubomura, K., Solutions of Contact Problems by the Assumed Stress Hybrid Model Ph.D. Thesis, MIT, Dept. of Aeronautics and Astronautics, (1979).

38. Hung, N.D. and Saxce, G., 'Frictionless contact of elastic bodies by finite element method and mathematical programming technique', Computers and Structures, 11 55-67, (1980).

39. Tseng, J. and Olson, M., 'The mixed finite element method applied to two-dimensional elastic contact problems', Int. J. Num. Meth. Engng., 17 991-1014, (1981).

40. Schafer, H., 'A contribution to the solution of contact problems with the aid of bond elements', Comp. Meth. in Appl. Mech. and Engr., 6
,335-354, (1974).

41. Oden, J.T. and Piries, E.B., 'Nonlocal and nonlinear friction laws and variational principles for contact problems in elasticity', Trans. ASME J. Appl. Mech., 50 67-76, (1983).

42. Svec, O.J., 'The unbonded contact problem of a plate on the elastic half space', Comp. Meth. in Appl. Mech. and Engng., 3 105-113, (1974).

43. Mohr, G.A., 'A contact stiffness matrix for finite element problems involving external elastic restraint', Computers and Structures, 12 189-191, (1980).

44. Westbrook, D.R., 'Contact problems for the elastic beam', Computers and Structures, 15 473-479, (1982).

45. Tielking, J.T. and Schapery, R,A., 'A method for shell contact analysis', Comp. Meth. in Appl. Mech. and Engng., 26 181-195, (1981).

46. Paul B. and Hashemi, J., 'Contact pressures on closely conforming elastic bodies', Trans. ASME J. Appl. Mech., 48 543-548, (1981).

47. Singh, K.P. and Paul, B., 'Numerical solution of nonHertzian elastic contact problems', Trans. ASME J. Appl. Mech., 96 (3), 484-490, (1974).

48. Conry, T.F. and Seireg, A., 'A mathematical programming method for design of elastic bodies in contact', J. Appl. Mech., 38 387-392, (1971).

49. Timoshenko, S.P. and Goodier, J.N., Theory of Elasticity, Third Edition McGraw-Hill Book Company.

DISTRIBUTION LIST

	No. of Copies
Office of Deputy Under Secretary of Defense for Research and Engineering (ET) ATTN: Mr. J. Persh, Staff Specialist for Materials and Structures (Room 3D1089) The Pentagon Washington, DC 20301	1
Office of Deputy Chief of Research Development and Acquisition ATTN: DAMA-CSS The Pentagon Washington, DC 20301	1
Commander U.S. Army Materiel Command ATTN: AMCLD, R. Vitali, Office of Laboratory Management 5001 Eisenhower Avenue Alexandria, VA 22333	1
Director Ballistic Missile Defense Systems Command ATTN: BMDSC-TEN, N. J. Hurst BMDSC-HE, J. Katechis BMDSC-HNS, R. Buckelew BMDSC-AOLIB P.O. Box 1500 Huntsville, AL 35807	1 1 1 1
Director Ballistic Missile Defense Advanced Technology Center ATTN: ATC-X, D. Russ ATC-X, COL K. Kawano ATC-M, D. Harmon ATC-M, J. Papadopoulos ATC-M, S. Brockway P.O. Box 1500 Huntsville, AL 35807-3801	1 1 1 1 1
Director Defense Nuclear Agency ATTN: SPAS, MAJ D. K. Apo SPLH, J. W. Somers SPLH, Dr. B. Steverding Washington, DC 20305-1000	1 1 1

	No. of Copies
Director Army Ballistic Research Laboratories ATTN: DRDAR-BLT, Dr. N. J. Huffington, Jr. DRDAR-BLT, Dr. T. W. Wright DRDAR-BLT, Dr. G. L. Moss Aberdeen Proving Ground, MD 21005	 1 1 1
Commander Harry Diamond Laboratories ATTN: DRXDO-NP, Dr. F. Wimenitz 2800 Powder Mill Road Adelphi, MD 20783	 1
Commander Air Force Materials Laboratory Air Force Systems Command ATTN: LNC, Dr. D. Schmidt Wright Patterson Air Force Base Dayton, OH 45433	 1
Commander BMO/ABRES Office ATTN: BMO/MNRT, COL R. Smith Norton Air Force Base, CA 92409	 1
Commander Air Force Materials Laboratory ATTN: AFML/MBM, Dr. S. W. Tsai Wright-Patterson Air Force Base Dayton, OH 45433	 1
Dommander Naval Ordinance Systems Command ATTN: ORD-03331, Mr. M. Kinna Washingron, DC 20360	 1
Naval Postgraduate School ATTN: Code NC4(67WT), Professor E. M. Wu Monterey, CA 93943	 1
Commander Naval Surface Weapons Center ATTN: C. Lyons C. Rowe Silver Springs, MD 20910	 1 1

	No. of Copies
Lawrence Livermore Laboratory ATTN: Dr. W. W. Feng P.O. Box 808 (L-342) Livermore, CA 94550	1
Sandia Laboratories ATTN: Dr. W. Alzheimer Dr. M. Forrestal Div. 1524 Dr. E. P. Chen P.O. Box 5800 Albuquerque, NM 87115	1 1 1
Aerospace Corporation ATTN: Dr. R. Cooper P.O. Box 92957 Los Angeles, CA 90009	1
AVCO Corporation Government Products Group ATTN: Dr. W. Reinecke P. Rolincik 201 Lowell Street Wilmington, MA 01997	1 1
ETA Corporation ATTN: D. L. Mykkanen P.O. Box 6625 Orange, CA 92667	1
Fiber Materials, Inc. ATTN: M. Subilia, Jr. L. Landers R. Burns Biddeford Industrial Park Biddeford, ME 04005	1 1 1
General Electric Company Advanced Materials Development Laboratory ATTN: K. Hall J. Brazel 3198 Chestnut Street Philadelphia, PA 19101	1 1
General Dynamics Corporation Convair Division ATTN: J. Hertz 5001 Kearny Villa Road San Diego, CA 92138	1

	No. of Copies
General Research Corporation	
ATTN: Dr. R. Wengler	1
Dr. R. Parisse	1
J. Green	1
5383 Hollister Avenue	
Santa Barbara, CA 93111	
Kaman Sciences Corporation	
ATTN: Dr. D. C. Williams	1
P.O. Box 7463	
Colorado Springs, CO 80933	
Ktech	
ATTN: Dr. D. Keller	1
911 Pennsylvania Avenue, N.E.	
Albuquerque, NM 87110	
Lehigh University	
Institute of Fracture and Solid Mechanics	
ATTN: Dr. George C. Sih	1
Bldg. 39, Packard Lab	
Bethlehem, PA 18015	
Los Alamos National Laboratory	
ATTN: Dr. W. D. Birchler	1
Mail Stop G787	
Los Alamos, NM 87545	
Martin Marietta Aerospace	
ATTN V. Hewitt	1
Frank H. Koo	1
P.O. Box 5837	
Orlando, FL 32805	
Massachusetts Institute of Technology	
Department of Aeronautics and Astronautics	
ATTN: Prof. T. H. H. Pian	1
Cambridge, MA 02139	
Pacifica Technology, Inc.	
ATTN: Dr. Ponsford	1
P.O. Box 148	
Del Mar, CA 92014	
University of Illinois at Chicago	
Dept. of Civil Eng., Mech. & Metallurgy	
ATTN: Dr. R. L. Spilker	1
Dr. T. C. T. Ting	1
Box 4348, Chicago, IL 60680	

	No. of Copies
Rohr Industries, Inc. ATTN: Dr. T. H. Tsiang MZ-19T P.O. Box 878 Chula Vista, CA 92012-0878	1
Radkowski Associates ATTN: Dr. P. Radkowski P.O. Box 5474 Riverside, CA 92507	1
Southwest Research Institute ATTN: A. Wenzel 8500 Culebra Road San Antonio, TX 78206	1
SPARTA Inc. ATTN: G. Wonacott 1055 Wall Street Suite 200 P.O. Box 1354 La Jolla, CA 92038	1
Terra Tek, Inc. ATTN: Dr. A. H. Jones 420 Wakara Way Salt Lake City, UT 84108	1
Defense Documentation Center Cameron Station, Bldg. 5 5010 Duke Station Alexandria, VA 22314	2
Director Army Materials and Mechanics Research Center ATTN: AMXMR-B, J. F. Dignam AMXMR-B, Dr. S. C. Chou AMXMR-B, L. R. Aronin AMXMR-B, Dr. D. P. Dandekar AMXMR-K AMXMR-PL Watertown, MA 02172	 1 5 1 1 1 2

Army Materials and Mechanics Research Center
Watertown, Massachusetts 02172
DEVELOPMENT OF A REDUCED MINDLIN HYBRID STRESS THIN MULTILAYER PLATE ELEMENT WITH APPLICATION TO EDGE CONTACT PROBLEMS
R. L. Spilker and D. M. Jakobs
Department of Civil Engineering, Mechanics and Metallurgy
University of Illinois at Chicago
Chicago, Illinois 60680
Technical Report AMMRC TR 85-23, August 1985, 146 pp
Illus.-tables, Contract DAAG46-82-K-0004
D/A Project: 8X363304D215
AMCMS Code: 693000.2156
Final Report, 15 August 1981 - 15 June 1983

AD
Unclassified
Unlimited Distribution

Key Words
Finite elements
Hybrid stress
Multilayer plate
Composite materials
Elastic shells
Contact problem
Stress concentration

A hybrid-stress formulation of isoparametric elements for the analysis of thin multilayer laminated composite plates is presented, and is applied to edge contact analyses. The element displacement behavior is characterized by laminate reference surface inplane and transverse displacements and laminate non-normal cross-section rotations; as a result, the number of degrees of freedom is independent of the number of layers. All components of stress are included and are related to a set of laminate stress parameters, the number of which is independent of the number of layers. Attention is restricted here to thin laminates: for thin laminates it is shown that the contributions of transverse shear stress and transverse normal stress to the internal complementary strain energy can be neglected. As a result, a modified stiffness-formation-algorithm can be used which provides a significant improvement in computation efficiency. The formulation is used to develop an 8-node isoparametric thin multilayer plate element. The resulting element is naturally invariant, of correct rank, and non-locking in the thin plate limit. Element performance is documented here for several illustrative examples.

Army Materials and Mechanics Research Center
Watertown, Massachusetts 02172
DEVELOPMENT OF A REDUCED MINDLIN HYBRID STRESS THIN MULTILAYER PLATE ELEMENT WITH APPLICATION TO EDGE CONTACT PROBLEMS
R. L. Spilker and D. M. Jakobs
Department of Civil Engineering, Mechanics and Metallurgy
University of Illinois at Chicago
Chicago, Illinois 60680
Technical Report AMMRC TR 85-23, August 1985, 146 pp
Illus.-tables, Contract DAAG46-82-K-0004
D/A Project: 8X363304D215
AMCMS Code: 693000.2156
Final Report, 15 August 1981 - 15 June 1983

AD
Unclassified
Unlimited Distribution

Key Words
Finite elements
Hybrid stress
Multilayer plate
Composite materials
Elastic shells
Contact problem
Stress concentration

A hybrid-stress formulation of isoparametric elements for the analysis of thin multilayer laminated composite plates is presented, and is applied to edge contact analyses. The element displacement behavior is characterized by laminate reference surface inplane and transverse displacements and laminate non-normal cross-section rotations; as a result, the number of degrees of freedom is independent of the number of layers. All components of stress are included and are related to a set of laminate stress parameters, the number of which is independent of the number of layers. Attention is restricted here to thin laminates: for thin laminates it is shown that the contributions of transverse shear stress and transverse normal stress to the internal complementary strain energy can be neglected. As a result, a modified stiffness-formation-algorithm can be used which provides a significant improvement in computation efficiency. The formulation is used to develop an 8-node isoparametric thin multilayer plate element. The resulting element is naturally invariant, of correct rank, and non-locking in the thin plate limit. Element performance is documented here for several illustrative examples.

Army Materials and Mechanics Research Center
Watertown, Massachusetts 02172
DEVELOPMENT OF A REDUCED MINDLIN HYBRID STRESS THIN MULTILAYER PLATE ELEMENT WITH APPLICATION TO EDGE CONTACT PROBLEMS
R. L. Spilker and D. M. Jakobs
Department of Civil Engineering, Mechanics and Metallurgy
University of Illinois at Chicago
Chicago, Illinois 60680
Technical Report AMMRC TR 85-23, August 1985, 146 pp
Illus.-tables, Contract DAAG46-82-K-0004
D/A Project: 8X363304D215
AMCMS Code: 693000.2156
Final Report, 15 August 1981 - 15 June 1983

AD
Unclassified
Unlimited Distribution

Key Words
Finite elements
Hybrid stress
Multilayer plate
Composite materials
Elastic shells
Contact problem
Stress concentration

A hybrid-stress formulation of isoparametric elements for the analysis of thin multilayer laminated composite plates is presented, and is applied to edge contact analyses. The element displacement behavior is characterized by laminate reference surface inplane and transverse displacements and laminate non-normal cross-section rotations; as a result, the number of degrees of freedom is independent of the number of layers. All components of stress are included and are related to a set of laminate stress parameters, the number of which is independent of the number of layers. Attention is restricted here to thin laminates: for thin laminates it is shown that the contributions of transverse shear stress and transverse normal stress to the internal complementary strain energy can be neglected. As a result, a modified stiffness-formation-algorithm can be used which provides a significant improvement in computation efficiency. The formulation is used to develop an 8-node isoparametric thin multilayer plate element. The resulting element is naturally invariant, of correct rank, and non-locking in the thin plate limit. Element performance is documented here for several illustrative examples.

Army Materials and Mechanics Research Center
Watertown, Massachusetts 02172
DEVELOPMENT OF A REDUCED MINDLIN HYBRID STRESS THIN MULTILAYER PLATE ELEMENT WITH APPLICATION TO EDGE CONTACT PROBLEMS
R. L. Spilker and D. M. Jakobs
Department of Civil Engineering, Mechanics and Metallurgy
University of Illinois at Chicago
Chicago, Illinois 60680
Technical Report AMMRC TR 85-23, August 1985, 146 pp
Illus.-tables, Contract DAAG46-82-K-0004
D/A Project: 8X363304D215
AMCMS Code: 693000.2156
Final Report, 15 August 1981 - 15 June 1983

AD
U. .lfied
Unlim .d Distribution

Key Words
Finite elements
Hybrid stress
Multilayer plate
Composite materials
Elastic shells
Contact problem
Stress concentration

A hybrid-stress formulation of isoparametric elements for the analysis of thin multilayer laminated composite plates is presented, and is applied to edge contact analyses. The element displacement behavior is characterized by laminate reference surface inplane and transverse displacements and laminate non-normal cross-section rotations; as a result, the number of degrees of freedom is independent of the number of layers. All components of stress are included and are related to a set of laminate stress parameters, the number of which is independent of the number of layers. Attention is restricted here to thin laminates: for thin laminates it is shown that the contributions of transverse shear stress and transverse normal stress to the internal complementary strain energy can be neglected. As a result, a modified stiffness-formation-algorithm can be used which provides a significant improvement in computation efficiency. The formulation is used to develop an 8-node isoparametric thin multilayer plate element. The resulting element is naturally invariant, of correct rank, and non-locking in the thin plate limit. Element performance is documented here for several illustrative examples.

END

FILMED

12-85

DTIC